July 2019

Solar Thermal Geothermal Hybrid System With a Bottoming Supercritical Organic Rankine Cycle

Francesca Moloney
University of South Florida, flmoloney2@gmail.com

Solar Thermal Geothermal Hybrid System

With a Bottoming Supercritical Organic Rankine Cycle

by

Francesca Moloney

A dissertation submitted in partial fulfillment
of the requirements for the degree of
Doctor of Philosophy
Department of Mechanical Engineering
College of Engineering
University of South Florida

Major Professor: Dharendra Yogi Goswami, Ph.D.
Elias Stefanakos, Ph.D.
Rasim Guldiken, Ph.D.
Babu Joseph, Ph.D.
George Philippidis, Ph.D.

Date of Approval:
April 26, 2019

Keywords: supercritical carbon dioxide, sCO_2, ORC, transient, combined cycle

DEDICATION

To my sister whose endless support and encouragement made this work possible.

ACKNOWLEDGMENTS

I would like to thank my family and friends for all their support they have shown during this work. Special thanks to my advisor, Dr. Yogi Goswami, for his expertise and guidance. I would also like to thank my committee members, Dr. Elias Stefanakos, Dr. Rasim Guldiken, Dr. Babu Joseph, and Dr. George Philippidis, who helped me during my research. Thank you also to Bernard Batson and Dr. Claude Villiers for their support and mentorship.

I would like to extend my gratitude to the Clean Energy Research Center (CERC) staff, Barbara Graham, Dr. Chand Jotshi, and Carol Blair. I am forever grateful for my friends at CERC for their professional help and their personal support: Rajeev Kamal, Chatura Wickramaratne, Eydhah Almatrafi, Arun Kumar Narasimhan, Kelly Osterman, Diego Guillen Perez, Ying Zhang, and Martina Leveni.

TABLE OF CONTENTS

LIST OF TABLES

LIST OF FIGURES

ABSTRACT

Climate change has spurred an interest in renewable energy. Many renewable energy technologies are intermittent, such as solar energy, or are dependent on transient conditions such as the ambient temperature in the case of geothermal energy. While solar thermal energy is able to achieve high temperatures and efficiencies, geothermal energy is limited by its lower temperatures which results in low conversion efficiency. There is an opportunity to create a hybrid system using both solar thermal and geothermal energy to improve their stand-alone performance.

In the literature, solar-geothermal hybrid systems are limited by the temperature of the solar field and the cycles and fluids used. In this study, a hybrid solar thermal-geothermal system is studied with a combined cycle operating from two temperature sources: the high temperature source is provided by solar power tower (SPT) and geothermal provides the lower temperature. The innovation lies in the implementation of the geothermal source into the combined cycle and the inclusion of a recuperative supercritical organic Rankine cycle (ORC) as the bottoming cycle to further enhance the system and also capable of operating with the geothermal source only.

First, an ORC is optimized for geothermal reservoirs with temperatures between 170 and 240°C. It was found that the optimized parameters result in wet fluids achieving lower expansion ratios. Only two fluids were optimized with a subcritical configuration due to proximity to the critical point.

Next, the combined cycle was developed and optimized. This analysis was performed assuming only one heat source, such as solar energy, being introduced to the topping cycle. Based on the literature review, a recuperative supercritical carbon dioxide Brayton cycle was chosen as

the topping cycle. The pressures of both cycles were optimized as well as the approach temperature difference between the two cycles. The same fluids considered in the first analysis were considered in the bottoming recuperative ORC cycle except ethane and carbon dioxide which performed the worst. The optimized conditions were used for the hybrid analysis.

Three hybrid configurations were analyzed where the geothermal source was introduced to the combined cycle in various locations. In the literature, the most common solar-geothermal hybrid system analyzed was where the solar energy through parabolic troughs was used to add additional heat to either the geothermal source or directly to the working fluid to increase the cycle temperature and efficiency. In one hybrid configuration, the geothermal source was used to superheat the organic Rankine cycle. The two other configurations used geothermal energy to preheat the carbon dioxide after recompression or to reheat it after recuperation and before being introduced to the ORC. The incremental effectiveness due to geothermal heat, i.e., the additional work that is converted from the additional heat added from the geothermal source, was analyzed.

Finally, the best performing hybrid system for a maximum cycle temperature of 500°C was selected and analyzed transiently with thermal storage. The superheat hybrid configuration with acetone as the working fluid with a recompression topping cycle was chosen. When solar energy and thermal storage was not available, the ORC was run with geothermal energy. As the acetone has a critical temperature above the temperature considered for the geothermal source, it resulted in a subcritical ORC. Subsequently, the power ratio between the sCO_2 cycle and ORC was very low. For this configuration, thermal storage was very beneficial to extend the time of high-power production.

viii

CHAPTER 1: INTRODUCTION

1.1 General Background

There are three main concerns that the power industry is currently facing. The burning of fossil fuels contributes to the first one: rising carbon dioxide levels from emissions which cause climate change. To combat climate change, there is pressure across the globe to pursue renewable energy sources. Many renewable sources, such as wind and solar, are intermittent and do not provide constant, uninterrupted power. Finally, as renewables begin to penetrate more of the market, there is a challenge to meet the energy demand with their fluctuating supply.

According the 2019 Energy Outlook report by the U.S. Energy Information Administration, the U.S. electricity generation is expected to increase almost 40% by 2050 [1]. The increase in capacity will be met with solar and natural gas. Renewable energy generation is projected to increase from a share of 18% to 31% of the market in the United States [1,2]. Globally, some reports project renewable energy to account for almost half of the electricity generation [3]. Solar currently accounts for 13% of the U.S. renewable electricity generation but has the potential to increase about 6 times to a total share of almost half of the total renewable electricity generation. Photovoltaic (PV) panels and combined cycles powered by gas or solar are expected to be the most cost effective in terms of the plant level levelized cost of electricity (LCOE) [1]. Additionally, carbon emissions will likely remain constant during the next 30 years, continually contributing to climate change.

Renewable energy is broken down into the following main categories [2]:

- Wind energy: onshore and offshore

1

- Solar energy: photovoltaics (PV), solar heating, concentrating solar power (CSP)

- Geothermal energy

- Hydro energy

- Bioenergy

The global renewable energy breakdown and outlook is shown in Figure 1-1 [2]. Geothermal and CSP have a very high potential to increase more than 4 and 100 times, respectively. This is partly due to reduced costs and renewable energy directives. Further reducing the cost or increasing the conversion efficiency is crucial to improving the capacity of renewable energy. As of 2010 the production cost of CSP was over five times the cost of fossil fuels (Table 1-1) [4].
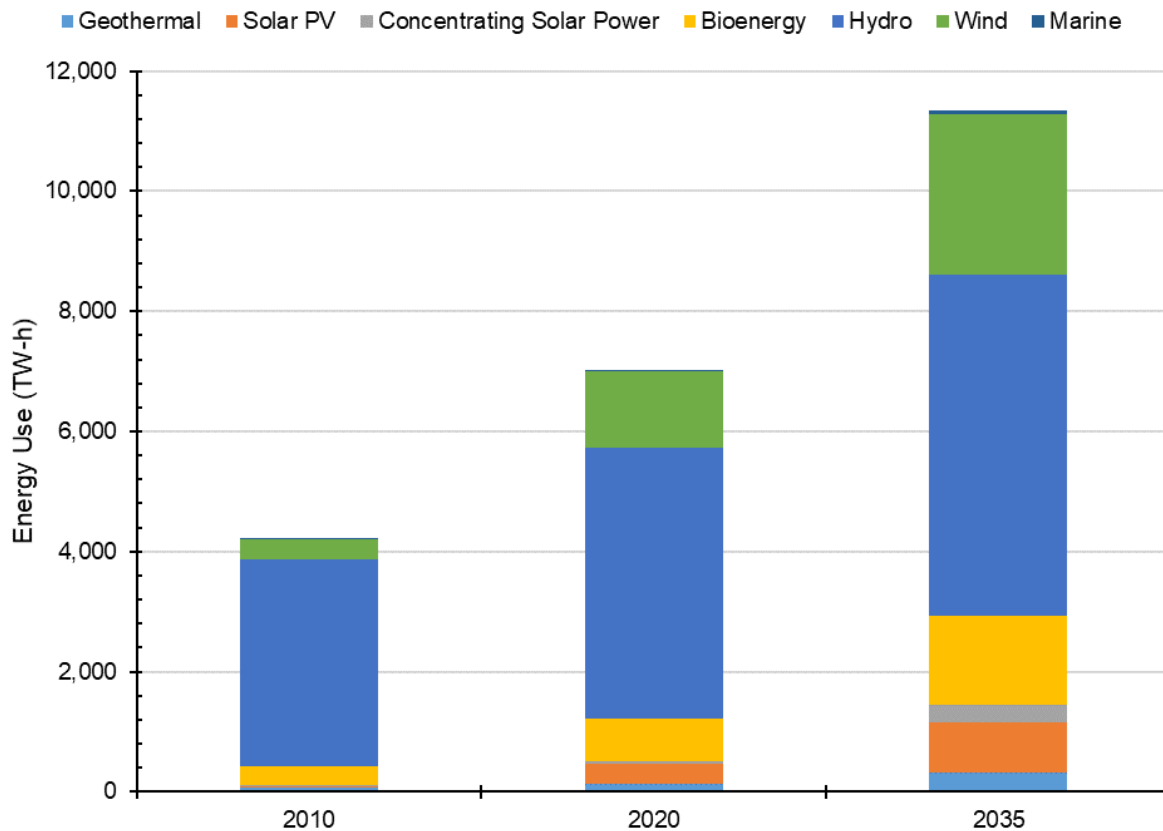
Figure 1-1. Global renewable energy breakdown [2]

Table 1-1. Cost for electricity generation [4]

Source	Production cost (US₵/kW-h)
Coal	3 – 6
Oil	3 – 6
Gas	4 – 6
Nuclear fusion	3 – 7
Biomass	3 – 9
Geothermal	6 – 8
Hydro (large scale)	4 – 10
Hydro (small scale)	4 – 20
Marine	15 – 25
Solar (PV)	10 – 20
Solar (CSP)	15 – 25
Wind	3 – 7

There is a drive in the literature to pursue adaptive yet cost effective and efficient renewable energy systems. As the penetration of renewables increase, intermittency creates a larger impact on utilities. California is trying to reduce greenhouse gas emissions down to at least 1990 levels while providing 50% of retail electricity from renewable sources [5]. As they increase their reliance on solar energy, the typical net load peak in the evening is increased as the availability of solar drops off. Figure 1-2 displays the net load in January for California [5]. This figure is commonly known as the duck curve due to its shape. Between 3pm and 6pm, the utilities must rely on expensive and inefficient peaking plants to ramp up quickly to jump to the peak generation.

Solar radiation is converted into electricity directly with PV or through heat collection in thermal power plants. PV panels use semiconductors that are excited by solar radiation to produce electricity. In solar thermal power plants, a heat transfer fluid is used to collect energy and transfer it to a power cycle. Photovoltaics operate at an efficiency of 6-20% and are negatively impacted by an increase in temperature [6].

There are many types of solar collectors used for solar thermal power. Concentrated solar power (CSP) use mirrors to focus sunlight onto pipes to heat fluids to very high temperatures. The Carnot efficiency is the maximum theoretical efficiency that can be obtained with constant

3
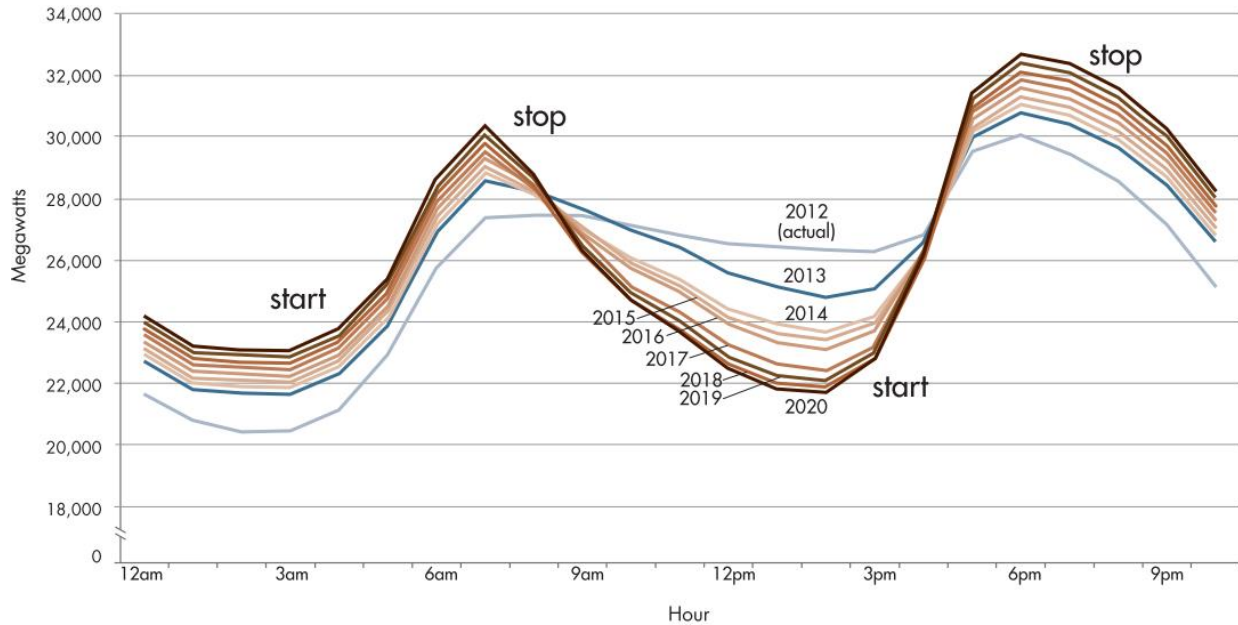
Figure 1-2. California net load generation for January 11, also known as the duck curve [5]

temperature heat rejection and heat addition. The Lorenz efficiency for a triangular cycle is the maximum theoretical efficiency for a constant temperature heat rejection and variable temperature heat addition. The Lorenz efficiency is higher than the Carnot efficiency. Both of these efficiencies increase as the maximum temperature of the cycle increases. Correspondingly, the real efficiency of a plant increases as the maximum temperature increases. CSP plants achieve much higher efficiencies than PV. The solar radiation across the United States is shown in Figure 1-3. Solar power tower plants consist of a field of mirrors, also known as heliostats, that focus acres of sunlight on the top of a tower to heat molten salt. The molten salt transfers heat to thermal power cycle such as a Brayton cycle or a Rankine cycle that can convert heat into electricity at an efficiency around 30-40%.

1.1.1 Power Cycles

For CSP applications, various cycles can be used depending on the temperatures of the solar field. The two most commonly used collectors in the solar industry are parabolic trough collectors (PTC), making up 82% of the market, and solar power tower (SPT), accounting for 13%

4

of the market [7]. For PTC, the solar concentration ratio varies from 70-100 times, and the temperature of the working fluid can reach up to 450°C [7]. Organic Rankine cycles (ORC) and steam Rankine cycles are used with PTC. For lower working temperatures, ORC can achieve higher efficiencies than steam Rankine cycles due to the higher molecular mass of the organic fluid compared to water. For SPT, steam Rankine cycles are typically used with an upper cycle temperature above 500°C. There are many studies on the solar receiver and heat transfer fluids to increase the temperature of SPT. Currently molten salts are used as the heat transfer fluid but corrosion becomes a challenge well over 800°C [8]. With better and more cost-effective materials, SPT power cycles will easily be able to operate at temperatures up to 800°C.

There is a large focus in the literature on supercritical carbon dioxide (sCO$_2$) Brayton cycles. A sCO$_2$ Brayton cycle can achieve higher efficiencies than a traditional air Brayton cycle
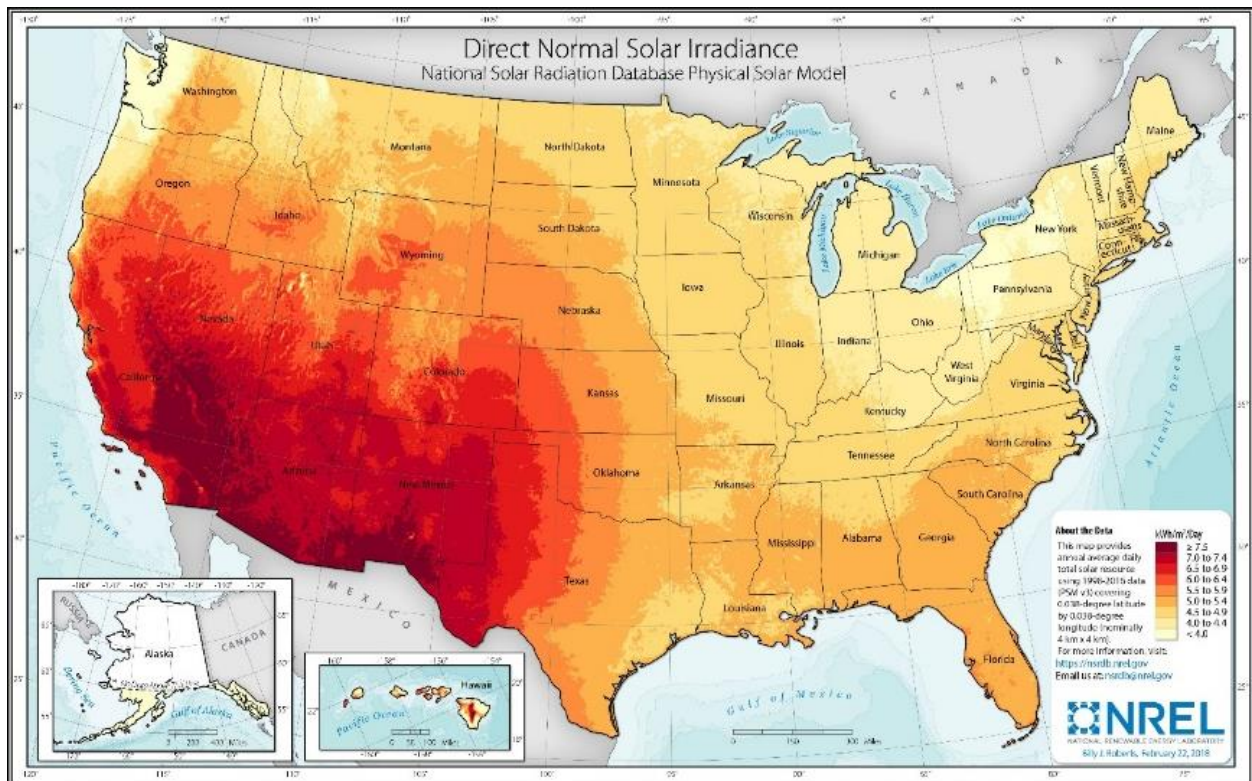
This map was created by the National Renewable Energy Laboratory for the U.S. Department of Energy.
Figure 1-3. Direct normal solar irradiance in the United States [106]

due to the lower work requirements of compressing the supercritical fluid. Additionally, there is no risk of corrosion which is a problem for air at high temperatures. For maximum operating temperatures above 450°C in the power cycle, it is much more efficient to use a supercritical carbon dioxide cycle (sCO_2) than a steam Rankine cycle as shown in Figure 1-4 [9,10].
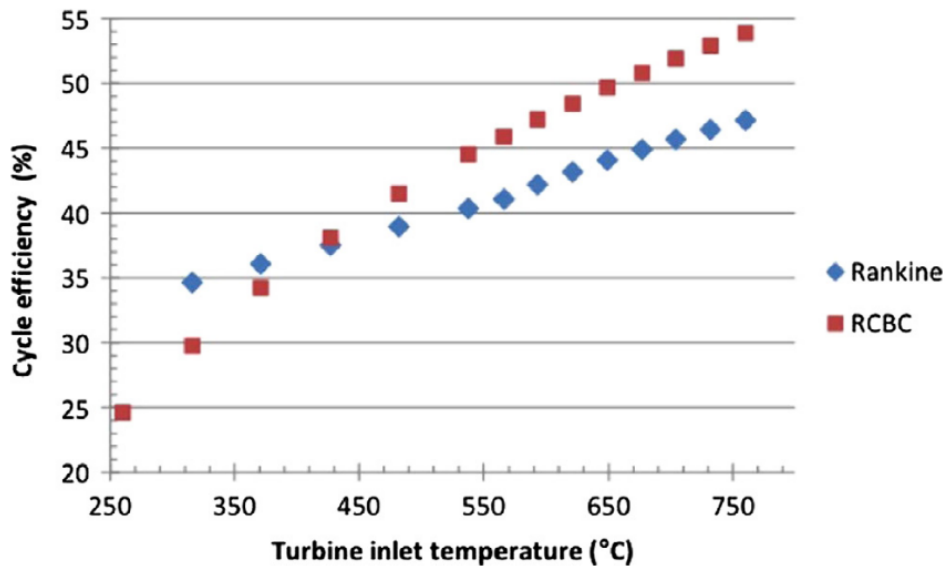
Figure 1-4. Cycle efficiency comparison between steam Rankine and recompression sCO_2 Brayton cycles [9]

Combined cycles are used to improve the efficiency of a cycle by utilizing some of the waste heat in a lower temperature cycle. These are used in gas fired plants as well as solar power plants. Depending on the temperatures of the cycle, various cycles can be used as the bottoming cycle, such as steam Rankine cycle, Kalina cycle, or an organic Rankine cycle. While a Kalina cycle can theoretically achieve higher efficiencies than a steam Rankine, the cost is very high and the system is limited by a very high condensing pressure [11]. As mentioned above, ORCs perform better at low temperatures than steam Rankine cycles. Besarati et al. studied a combined cycle configuration of a sCO_2 cycle with a bottoming ORC for solar applications [12]. However, supercritical ORCs can have a higher performance than standard subcritical ORCs. In a supercritical ORC, the heat addition occurs without passing through the mixture state. This allows

6

the fluid to have a better thermal match with the heat source, improving the thermal and exergetic efficiencies. A more in-depth review of ORCs is contained in Chapter 2.

1.1.2 Solar Energy Shortcomings

The largest shortcoming of solar energy is its intermittency. To address this, storage, such as thermal or electrical storage, can be added or the system can be integrated with another source of energy in a hybrid system.

1.2 Geothermal Energy

Geothermal energy, heat transferred through the ground from the earth's core, can be utilized for heating and cooling or power generation. Geothermal energy can be accessed by numerous ways. One way is to bury pipes in the ground to transfer heat in or out into a specific fluid. To access higher temperatures, wells can be bored. Areas that have water content are called hydrothermal sites. In contrast, areas without water are called hot dry rock (HDR). The heat from hot dry rock can be removed by drilling down below the earth's surface and creating a fractured area in a rock feature, often times with explosives [13]. A heat transfer fluid, such as water or carbon dioxide, is pumped through the HDR and extracted at the surface to be utilized. HDR also has the capacity to reach higher temperatures than hydrothermal sites.

There are three primary geothermal plant configurations: dry steam, flash, and binary. Dry steam uses superheated and pressurized steam from a well to directly run a steam turbine. A flash steam plant takes pressurized heated geothermal brine and flashes it to a lower pressure, separates the steam, and runs a steam turbine. A binary geothermal plant takes the geothermal brine and transfers the heat to another fluid to run a cycle such as an organic Rankine cycle.

Geothermal reservoirs are classified by either low, medium, or high enthalpy. As some areas can be under pressure, there are conflicting definitions across the literature for the

7

corresponding temperature ranges of these classifications. However, medium temperature resources generally fall in the range of 100–220 °C, which describes the most commonly available geothermal sources [14].

Areas suitable for geothermal energy are places that receive high heat flow through the earth's crust and are thus able to access and use heat relatively close to the surface. Figure 1-5 shows the heat flow through the continental United States. Favorable states include Nevada, Utah, California, Colorado, Arizona, New Mexico, Oregon, and Idaho. Geothermal has the capacity to increase substantially in these areas. There are many current plants under development with capacities up to 300 MW as shown in Figure 1-6.

SMU Geothermal Laboratory Heat Flow Map of the Conterminous United States, 2011
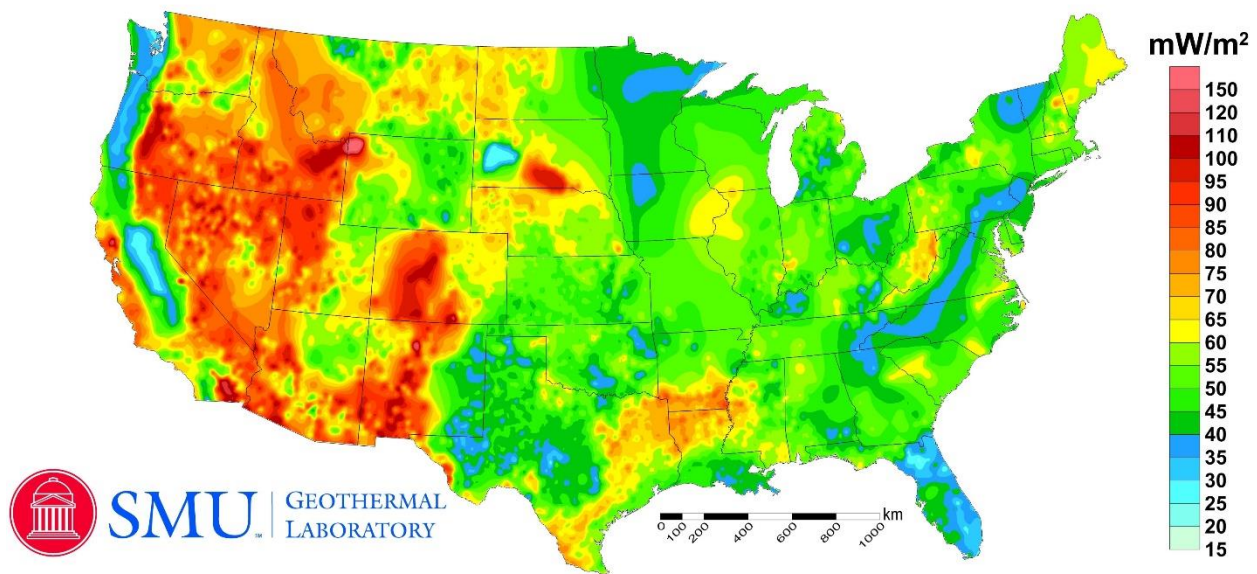
Reference: Blackwell, D.D., Richards, M.C., Frone, Z.S., Batir, J.F., Williams, M.A., Ruzo, A.A., and Dingwall, R.K., 2011, "SMU Geothermal Laboratory Heat Flow Map of the Conterminous United States, 2011". Supported by Google.org. Available at http://www.smu.edu/geothermal.

Figure 1-5. Geothermal heat flow through the continental United States [107]

1.2.1 Shortcomings

Many geothermal plants rely on air cooled condensers. Although geothermal is not intermittent in its supply, daily transients affect the condenser efficiencies which affect the overall plant performance. The performance can vary around 20% across the day [15].
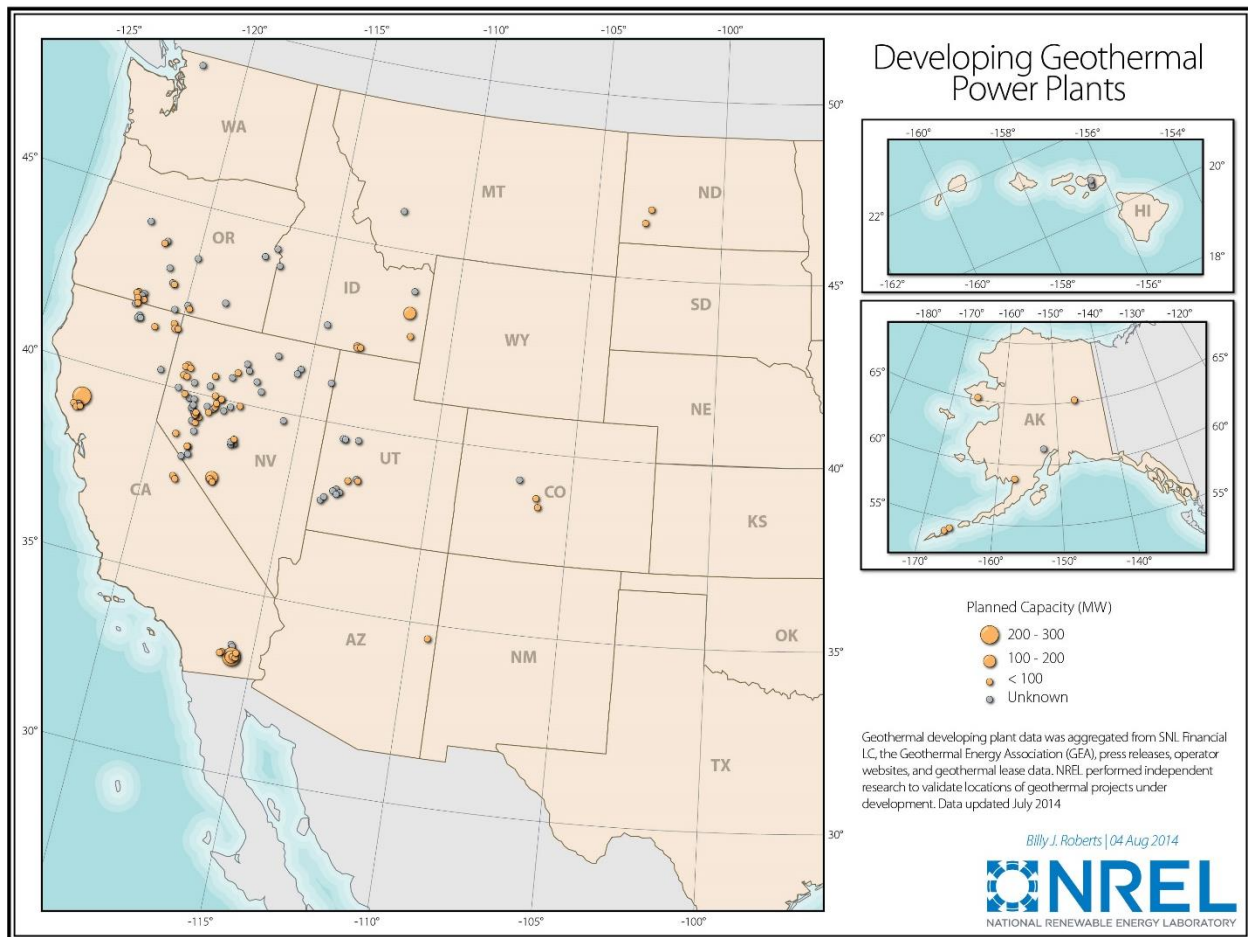
8

This map was created by the National Renewable Energy Laboratory for the U.S. Department of Energy.

Figure 1-6. Geothermal plants currently under development in the United States [106]

1.3 Hybrid Systems

A hybrid system is a combination of any two or more separate systems. Synergy is a concept where the combination of two systems is greater than the stand-alone systems. DiPippo argued that a hybrid plant needs synergy in order to make sense from a thermodynamic sense [6]. A synergistic hybrid plant is a hybrid plant that produces more work from the input and energy sources than the two systems separately. However, cost is also a factor. Even if the output is similar, there can be synergy present in the cost savings [7]. Peterseim et al. analyzed numerous hybrid plants for CSP to enhance their cost synergy [7]. Solar energy can increase the efficiency of geothermal systems when geothermal power systems decline during the day. Geothermal energy

9

can supplement solar energy systems by providing a consistent heat source throughout the day, specifically providing power during nighttime and during periods of cloud cover.

In the United States, locations with high solar irradiance also coincide with geothermal suitable sites as evident in Figure 1-3 and Figure 1-5. There have been a few studies in the literature exploring various configurations of solar thermal geothermal hybrid systems. Table 1-2 summarizes the systems that have been studied numerically and experimentally. There is only one solar geothermal and solar hybrid plant in operation; it is located in Stillwater, Nevada [8]. The plant comprises of a 33 MW binary geothermal system which has been in operation since 2009. This plant uses an air-cooled condenser. As the ambient temperature increases during the day, the performance of the geothermal plant degrades. A PV plant with a peak capacity of 26 MW was added to supplement the degradation [16]. In addition, a 17 MWth parabolic trough collector system was installed to boost the electricity generation by 2 MW [16,17].

Most of the studies focus on mildly supplementing the geothermal system with solar or thermal storage to add heat to the geothermal fluid or directly to the cycle to improve the system efficiency and increase the net work. Many of the hybrid configurations were combined heating and power (CHP) or CHP with cooling. While this yields a higher system efficiency since the wasted heat from the power cycles is being used for cooling and heating, the applications for cooling and heating are site specific and limited in range. There was only one study on a geothermal solar hybrid plant with SPT. Carbon dioxide was used as the ground heat transfer fluid as well as the working fluid. SPT with a bottoming cycle would allow the bottoming cycle to be run by geothermal heat when solar energy is not available. There is an opportunity to use state of the art solar power systems in a combined cycle with a supercritical bottoming organic Rankine cycle to improve the performance of both solar thermal energy and geothermal energy.

10

Table 1-2. Review of the studies on solar-geothermal hybrid systems

	Multi-Gen	Simulation/ Experiment	Solar System	Geothermal System	Geothermal Well Temperature	Storage	System Efficiency	Solar-Geothermal Integration
[16]	-	Plant	PTC	Binary	-	-	-	PV for increased electricity Solar thermal to superheat geothermal brine
[18]		Experiment	PTC	Flash	160°C	TES	-	Solar to superheat brine before steam turbine
[19]	-	Experiment	PTC	Flash	225°C	TES	-	Solar to increase steam content in brine
[20]	Water heating Space heating Space cooling	Experiment	Flat plate	-	-	-	Heating 3 Cooling 4.8 (COP)	Geothermal heat pump for cooling; heat pump heat rejection and solar (gas backup) for heating
[21,22]	-	Simulation	PTC	Flash	198°C (1566 kJ/kg enthalpy, 15 bar)	-	-	Solar to superheat brine before steam turbine
[23]	-	Simulation	PTC	Binary	150°C	-	17% (additional)	Solar to superheat working fluid in supercritical ORC
[24]	-	Simulation		Flash	300°C	-	-	Solar/nuclear used to heat a fluid to store heat rock (geothermal)
[25,26]	-	Simulation	PTC	Binary	150°C	-	11%	Solar to superheat working fluid (supercritical and subcritical)
[27]	-	Simulation	PTC	Binary	145°C	-	18% (additional)	Parallel solar and geothermal heating
[28]	-	Simulation	-		60 - 180°C	-	32%	Geothermal as preheat
[29]	-	Simulation		Flash	205 - 240°C	-	-	Solar to superheat steam to turbine and reheat separated saturated liquid brine
[30]	-	Simulation	PTC	Binary	160°C	-	12%	Solar to superheat working fluid (supercritical)
[31]	-	Simulation	PTC	Binary	170°C	-	15%	Solar to superheat working fluid
[32]	-	Simulation	PTC	Binary	150°C	-	12.2% (additional)	Solar to Rankine cycle; geothermal to power ORC and condense steam Rankine cycle
[33]	-	Simulation	PTC	Binary	-	-	-	Solar to supplement heat to ORC
[34]	-	Simulation	PTC	Flash	250°C	-	-	Solar to superheat and reheat geothermal steam
[35]	-	Simulation	PTC	Binary	150°C	-	-	Solar to preheat working fluid
[36,37]	-	Simulation	PTC	Binary	150°C	TES	18%	Solar to superheat working fluid
[10]	-	Simulation	PTC	Binary (steam)	150°C	TES	30%	Solar to superheat and reheat working fluid (steam)
[38]	-	Simulation	PTC	Binary	135°C	TES	8% (additional)	Parallel solar and geothermal heating
[39]	-	Simulation	SPT	HDR	115 - 295°C	TES	22%	Geothermal to produce heated CO_2 directly to turbines and to preheat and add CO2 to solar CO_2 cycle
[40]	-	Simulation	PTC	Binary	155°C	TES	-	Solar to superheat working fluid

11

Table 1-2 (Continued)

	Multi-Gen	Simulation/ Experiment	Solar System	Geothermal System	Geothermal Well Temperature	Storage	System Efficiency	Solar-Geothermal Integration
[41]	-	Simulation	CPV/T	Condenser		Electrolyser Fuel cell	-	Geothermal as condenser
[42]	Electricity Cooling Heating	Simulation	PTC	Flash	190°C	-	16.4% (single-gen) 78% (multi-gen)	Solar used to reheat some of geothermal steam turbine exit to heat a separate ORC
[43,44]	CHP	Simulation	PTC	Binary	80 - 100°C	-	13%	Solar to superheat working fluid
[45]	CHP	Simulation	Evacuated tube	Binary	95°C	-	-	Solar to superheat working fluid
[46]	Electricity Drying Desalination	Simulation	PTC	Flash	500 kPa	-	-	Solar to run steam Rankine cycle and superheat flashed geothermal steam; wind and ORC work to power desalination
[47]	Electricity Heating Cooling	Simulation	Flat plate	Binary	121°C	-	-	Solar and geothermal to simultaneously heat working fluid (Kalina)
[48]	Electricity Heating Cooling Desalination	Simulation	PTC	Binary	160°C	TES	12% (ORC)	Geothermal and solar in series to heat transfer fluid to ORC
[49]	CHP	Simulation	Flat plate	Binary	90°C	TES	40% (system, thermal)	Solar to superheat working fluid
[50]	Electricity Heating Cooling	Simulation	PTC	Binary	95°C	TES	7%	Geothermal and solar in series to heat transfer fluid (diathermic oil) to ORC
[51]	Electricity Cooling Heating Hydrogen production	Simulation	PV/T	Binary	210°C	TES	11%	Very integrated cycle; geothermal and solar not directly linked
[52]	Electricity Cooling Heating Drying	Simulation	PTC	Binary	167 - 187°C	TES	51%	Geothermal and solar thermal not directly linked One ORC loop, two subsequent cycles: one heated from geothermal, one heated from solar
[53]	Electricity Heating Cooling	Simulation	Flat plate	Binary	90°C	TES	-	Solar to superheat working fluid

12

1.4 Research Objectives

The objectives analyzed in this work are:

1. Determine the suitable operating conditions of a supercritical ORC using geothermal heat

2. Model and analyze the performance of a combined cycle with a supercritical ORC

3. Model and analyze the performance of a solar-geothermal hybrid plant performance

4. Determine the impact of thermal energy storage (TES) during transient conditions on the hybrid system

13

CHAPTER 2: DESIGN OF A SUPERCRITICAL ORGANIC RANKINE CYCLE FOR GEOTHERMAL APPLICATIONS[1]

2.1 Introduction

To mitigate climate change, it is important to support the penetration of renewables and to improve the cycle efficiencies of renewable and non-renewable technologies. Heat engines using low-temperature resources have inherently low conversion efficiencies. At temperatures below 400 °C, organic Rankine cycles (ORC) are the most effective at extracting power from low temperature sources such as geothermal, waste heat, and biomass sources. ORC had an installed capacity of 2.7 GWe at the end of 2016, 75% of which was provided by geothermal sources, while waste heat and biomass had a 14% and 11% share of the market, respectively [54].

Currently, geothermal energy provides a total of 12.7 GW of electric power and has the potential and the resource to grow exponentially, as it has done since 2010 [55,56]. The Americas have the largest amount of installed geothermal power with another 3.2 GWe, or 62% more, planned by 2020 (Figure 2-1) [56]. For high temperature reservoirs above 220 °C, the geothermal brine is flashed into steam to be used directly for power generation [14]. For dry steam, single flash, and double flash plants, the efficiency ranges from around 6 to 15% on average for heat reservoirs with an enthalpy between 900 and 2900 kJ/kg [57]. The downside of flash steam plants

---

[1] This chapter has been previously published (Moloney, F., Almatrafi, E., and Goswami, D. Y., 2017, "Working Fluid Parametric Analysis for Regenerative Supercritical Organic Rankine Cycles for Medium Geothermal Reservoir Temperatures," *Energy Procedia*, pp. 599–606.)

is that non-condensable gases and salt content add corrosion to the system and reduce turbine efficiency [57]. Hot dry rocks (HDR) are geothermal resources that do not have water. They can be fractured to allow a fluid to be pumped through to extract the heat. In Japan, projects have been aimed to achieve temperatures up to 250 °C at depths less than 2.5 km [58]. In Larderello, Italy, temperatures in HDR can reach up to 400 °C [58]. In a binary system, the geothermal brine, or heat transfer fluid in the case of HDR, exchanges heat with an organic fluid which is used to run a cycle, such as an ORC [14]. Medium temperature resources, ranging from around 100–220 °C, are the most common available geothermal sources [14]. The breakdown of installed capacity of geothermal energy as of 2015 is displayed in Figure 2-1 [56]. The seven megawatts from the hybrid category are contributed from the solar PV and thermal and geothermal hybrid plant in Stillwater, Nevada (additional 2 MWe) and the biomass geothermal hybrid plant in Italy (5 MWe additional) [56]. While binary plants make up almost half of the total market by number of installed units, they only represent 14% of the installed electric capacity of geothermal plants as of 2015 (Figure 2-1b) [56]. Additionally, current binary plants have efficiencies below 10% for heat sources up to
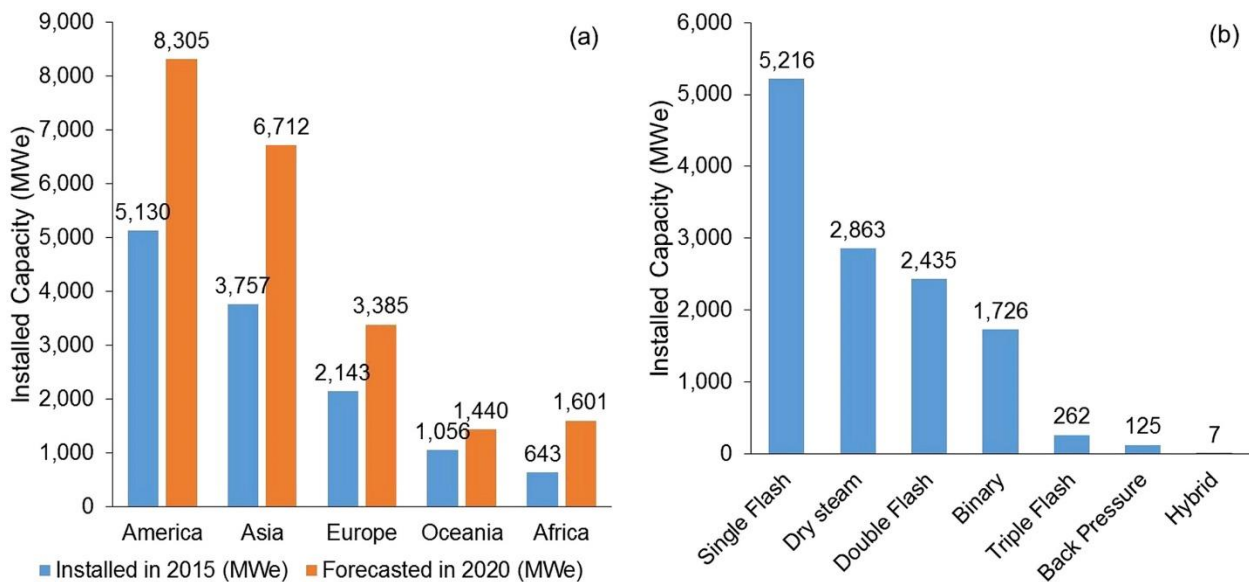
Figure 2-1. Geothermal plants installed capacity by: (a) continent and (b) plant type [56]

15

253 °C [57]. For geothermal energy to be utilized to its fullest capacity, its conversion efficiency needs to be improved.

Many studies have explored the optimization of ORCs. However, supercritical ORCs can achieve higher efficiencies than subcritical ORCs at low-temperatures [59–63]. Supercritical ORCs are also advantageous over subcritical cycles as they have a better thermal match (thermal glide) between the working fluid and the heat source. Li et al. found supercritical ORCs performed better for once through heat sources such as geothermal reservoirs [64].

A recuperative cycle can further improve the efficiency of the system over a simple cycle. A few analyses have compared a recuperative supercritical ORC to a simple supercritical ORC. Glover et al. analyzed fluid performance with a turbine inlet temperature between 100 and 350 °C with a maximum cycle pressure of 5 bar greater than the critical point. The best performance was found when the critical temperature of the fluid was just below the temperature of the heat source. Fluids with high critical temperatures were also more tolerant of temperature and pressure changes in the condenser [65]. Le et al. used a genetic algorithm to maximize the first law and system efficiency for various fluids at a turbine inlet temperature of 139 °C. Carbon dioxide performed the worst at the analyzed conditions. A recuperative cycle was also found to achieve higher efficiencies than a simple cycle [66].

Toffolo et al. studied various supercritical configurations of supercritical ORCs including a recuperative cycle for isobutane and R134a with turbine inlet temperatures between 130 and 180 °C. It was found that for the tested range, isobutane performed better in a subcritical cycle while R134a performed better in a supercritical cycle [67]. Astolfi et al. analyzed supercritical and subcritical ORCs for medium-low temperature geothermal sources (120–180 °C) to optimize system performance in relation to cost [68].

16

To support the penetration of renewables and considering the capacity and exponential growth rate of geothermal energy, organic Rankine cycles must be analyzed on a plant perspective. The system must be optimized to achieve a plant efficiency greater than the current geothermal binary plant maximum of 10% to take advantage of medium to high geothermal heat sources. Supercritical ORC studies have focused on turbine inlet temperatures of 80 °C to 130 °C. Supercritical ORCs with carbon dioxide cycles have been analyzed up to 800 °C. The effect of the cycle high pressure on the plant performance has not been explored for recuperative supercritical ORCs for medium to high geothermal reservoirs (180–250 °C) corresponding to turbine inlet temperatures between 170 and 240 °C. This chapter studies environmental fluids in a recuperative supercritical ORCs to improve the conversion efficiency of geothermal energy. For a comprehensive exergy analysis, the best performing fluid and conditions were compared against a single flash plant. This chapter was previously published, the permission to reuse is included in Appendix B [69]. This article expanded a previous study with an exergy analysis [70]. A discussion on the expander considerations was added in this chapter.

2.2 Methodology

The study was split into two parts: an analysis of a recuperative supercritical ORC and an exergy comparison of the best performing configuration with a single flash geothermal plant. The binary cycle analysis began with a fluid selection (Section 2.1), followed by a parametric study and optimization of the turbine inlet pressure.

2.2.1 Fluid Selection

A model of a recuperative supercritical ORC was created in MATLAB. The model was validated with the models of supercritical ORCs and recuperative cycles of Le et al. and Wang et

17

al. [66,71]. A schematic of the cycle with a recuperator is shown in Figure 2-2a. The corresponding

temperature-entropy (T-s) diagram is shown in Figure 2-2b.
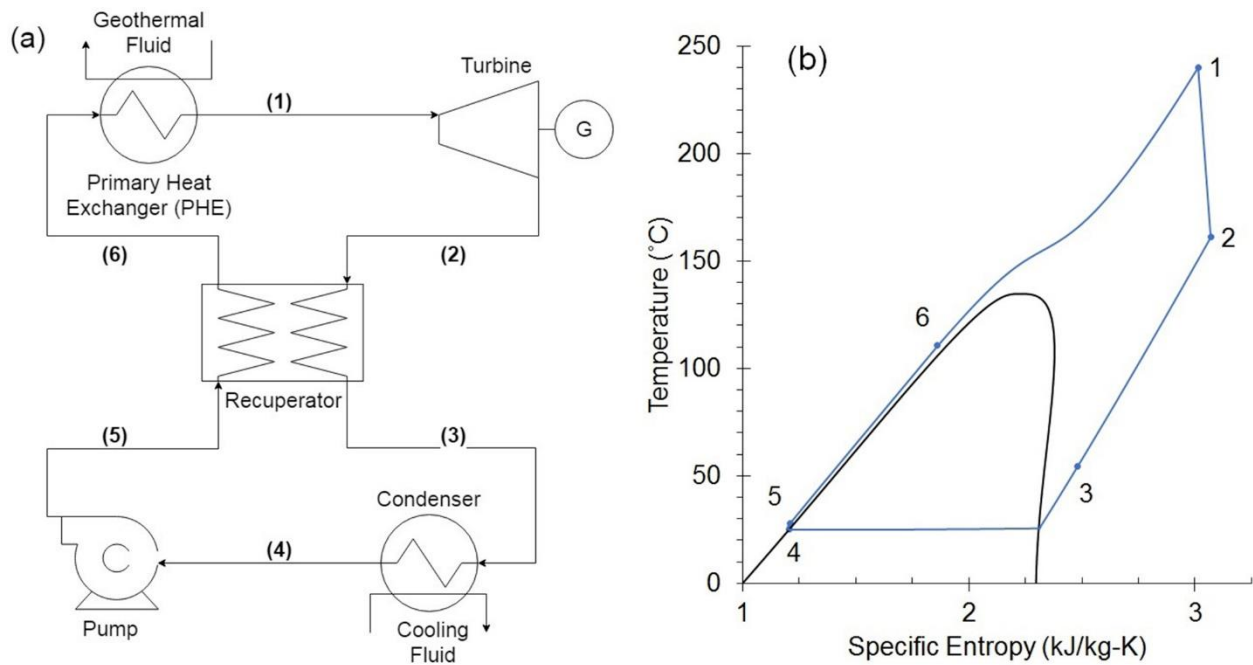
Figure 2-2. (a) Recuperative supercritical ORC schematic; (b) T-S diagram of a recuperative supercritical ORC (isobutane)

To select appropriate fluids for the analysis, various properties were analyzed including

global warming potential (GWP), ozone depleting potential (ODP), thermal stability, toxicity and

critical point. Fluids with high GWP, such as hydrochlorofluorocarbons (HCFC), and fluids with

high ODP, such as chlorofluorocarbons (CFCs), were omitted from the analysis. The ODP was

limited to less than 1. The GWP was limited to less than 150 as limited by directives such as those

by the European Union [72]. No toxic fluids were included in the analysis. NIST REFPROP was

used to calculate fluid properties [73]. The auto-ignition temperature was checked to verify that it

did not fall within the tested range [74]. To analyze a supercritical cycle, the cycle high temperature

and pressure should exceed the critical point. The critical and maximum temperatures for acetone,

cyclopentane, pentane (R601), and isopentane (R601a) fell in the turbine inlet temperature range

(170–240 °C). Therefore, the analysis of these fluids was limited for turbine inlet temperatures

18

between their critical and maximum temperatures. The fluids chosen were hydrocarbons (HC), hydrofluoroolefins (HFO), and hydrofluorocarbons (HFC). The properties of these and other fluids that met the selection criteria are listed in Table 2-1. Fluid properties and displayed in Figure 2-3. A variety of mixtures were tested but they did not outperform any of the pure fluids and were thus omitted from the analysis.

Table 2-1. Fluid properties

Fluid	Alternate Name	Critical Pressure (MPa)	Critical Temperature (°C)	Auto-Ignition Point (°C)	100 year GWP	ODP	Chemical Group	Behavior
acetone	–	4.70	235	465	0.5	–	HC	wet
butane	R600	3.80	152	365	20	0	HC	dry
butene	–	4.01	146	385	–	–	HC	dry
carbon dioxide	R744	7.38	31	–	1	0		wet
cis-butene	–	4.22	163	324	–	–	HC	isentropic
cyclopentane	–	4.57	239	361	11	0	HC	dry
cyclopropane	RC270	5.58	125	495	20	0	HC	wet
dme	RE170; dimethyl ether	5.34	127	235	–	0	HC	wet
ethane	R170	4.87	32	515	–	–	HC	wet
isobutene	–	4.01	145	465	–	0	HC	dry
isobutane	R600a	3.63	135	460	20	0	HC	dry
isopentane	R601a	3.38	187	420	20	0	HC	dry
neopentane	R601b; 2,2-dimethylpropane	3.20	161	450	20	–	HC	dry
pentane	R601	3.37	197	309	11	0	HC	dry
propane	R290	4.25	97	450	20	0	HC	wet
propylene	propene; R1270	4.56	91	480	20	0	HC	wet
propyne	–	5.63	129	455	–	0	HC	wet
transbutene	–	4.03	155	324	–	0	HC	dry
R1233zd(E)	–	3.62	166	–	–	0	HFO	dry
R152a	–	4.52	113	454	133	0	HFC	wet

19
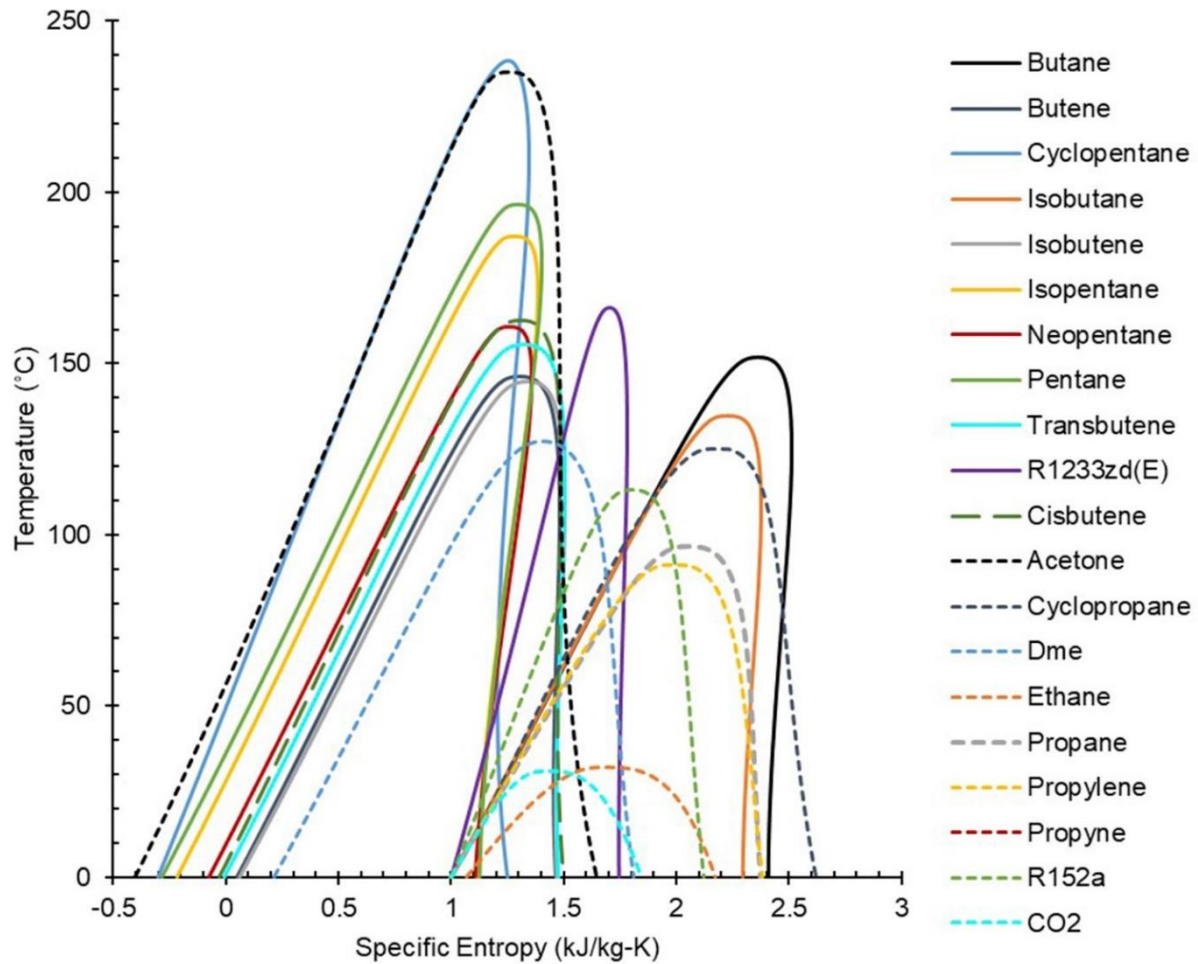
Figure 2-3. T-S diagram of selected fluids (dry, wet, and isentropic fluids are indicated by solid, dashed, and long dashed lines, respectively)

2.2.2 ORC Performance Analysis

Four key performance factors were chosen for the study: first law efficiency, plant efficiency, second law efficiency and the net power. The pump and turbine power are calculated by Eqs. (1) and (2). The first law, or cycle, efficiency measures how much power is produced in relation to the heat absorbed by the working fluid (Eq. (3)). The plant efficiency measures how much net work is produced in the cycle in comparison to the potential heat that can be provided by the geothermal resource (Eq. (4)). In this case, the maximum heat supplied by the geothermal source is defined by the amount of heat that can be released by the geofluid using the ambient

20

temperature as a reference. The ideal cycle for a supercritical ORC is a triangular Lorenz cycle. The heat addition is performed at a variable temperature while the heat removal is performed isothermally. The maximum reversible efficiency for a triangular Lorenz cycle, defined in Eq. (5), compares the entropic average temperatures of the heat sink to the heat source [75]. The second law efficiency compares the plant efficiency to the maximum theoretical of triangular cycles (Eq. (6)). The recuperator was considered with an effectiveness as defined in Eq. (7). A pinch point was considered in the primary heat exchanger (PHE) and the condenser to limit heat exchanger exergy losses. The mass flow of the geofluid was held constant. To satisfy the pinch point conditions, the mass flows of the working fluid and cooling water were iterated until the resulting pinch point matched the constraint within 10^{-10}.

$$\dot{W}_t = \dot{m}_{WF}\eta_{t,m}(h_1 - h_2) = \dot{m}_{WF}\eta_{t,m}\eta_{t,s}(h_1 - h_{2s}) \tag{2-1}$$

$$\dot{W}_p = \dot{m}_{WF}\frac{h_5-h_4}{\eta_{p,m}} = \dot{m}_{WF}\frac{h_{5s}-h_4}{\eta_{p,m}\eta_{p,s}} \tag{2-2}$$

$$\eta_I = \frac{\dot{W}_{net}}{\dot{Q}_{in}} = \frac{\dot{W}_t-\dot{W}_p}{\dot{m}_{WF}(h_1-h_6)} \tag{2-3}$$

$$\eta_{plant} = \frac{\dot{W}_{net}}{\dot{Q}_{max}} = \frac{\dot{W}_t-\dot{W}_p}{\dot{m}_{hs}(h_{hs,in}-h_{hs,a})} \tag{2-4}$$

$$\eta_{rev,max} = 1 - \frac{(T_{hr,out}-T_{hr,in})/ln(T_{hr,out}/T_{hr,in})}{(T_{hs,in}-T_{hs,out})/ln(T_{hs,in}/T_{hs,out})} \tag{2-5}$$

$$\eta_{II} = \frac{\eta_{plant}}{\eta_{rev,max}} \tag{2-6}$$

$$\varepsilon_{recuperator} = \frac{T_2-T_3}{T_2-T_5} \tag{2-7}$$

2.2.3 ORC Turbine Inlet Pressure Parametric Analysis

The pressure was varied over the range of turbine inlet temperatures, starting with a pressure larger than the critical point. Then, the optimum pressure was calculated for each fluid to maximize the plant and subsequently the second law efficiency and the net power. This analysis

21

was performed for all fluids to ultimately determine which fluids and conditions perform the best for medium temperature geothermal reservoirs. The simulation parameters are listed in Table 2-2. Cycle operating conditions. The geofluid entering the PHE was set at 11 °C higher than the turbine inlet temperature. The assumptions used in the model include:

- The geothermal fluid from the reservoir is pure water and saturated liquid

- Pressure is constant in the heat exchangers

- There is no air leakage into the working fluid system

- Power consumption of auxiliary components is negligible

- There are no heat losses in the heat exchangers

Table 2-2. Cycle operating conditions

Parameter	Value
Heat source mass flow	1 kg/s
Condensing temperature	25 °C
Cooling water inlet temperature	20 °C
Cooling water pressure	5 bar
Pump and turbine isentropic efficiency	85%
Pump and turbine mechanical efficiency	90%
Recuperator effectiveness	0.80
PHE pinch point	10 °C
Condenser pinch point	3 °C
Dead state temperature	20 °C
Dead state pressure	100 kPa

The reinjection temperature was not limited in the analysis. The minimum reinjection temperature is site specific, dependent on the concentration of dissolved solids, such as silicates. The minimum reinjection temperature ranges from 50 to 70 °C [76]. In this study, the reinjection temperature of the brine remained above 50 °C for the specified evaporator conditions. This was

22

not a focus of the study, so this was sufficient to provide a comparison of performance factors across a range of turbine inlet temperatures. In practice, the primary heat exchanger can be designed and optimized for the appropriate site specific geothermal reinjection temperature, taking into account the dissolved solids as well as the lifetime of the geothermal reservoir.

2.3 Exergy Analysis

For further comparison, a single flash geothermal plant, shown in Figure 2-4, was also modeled in MATLAB, The model was validated with the work of Yari et al. [77]. From state 1 to 2, the pressure is dropped to flash the geofluid into a mixture. Then the steam passes through a separator where the saturated liquid (state 6) is separated from saturated vapor (state 3). The saturated liquid is sent to a reinjection well. The saturated vapor passes through a turbine (state 3 to 4) and then is condensed (state 4 to 5) before being reinjected.
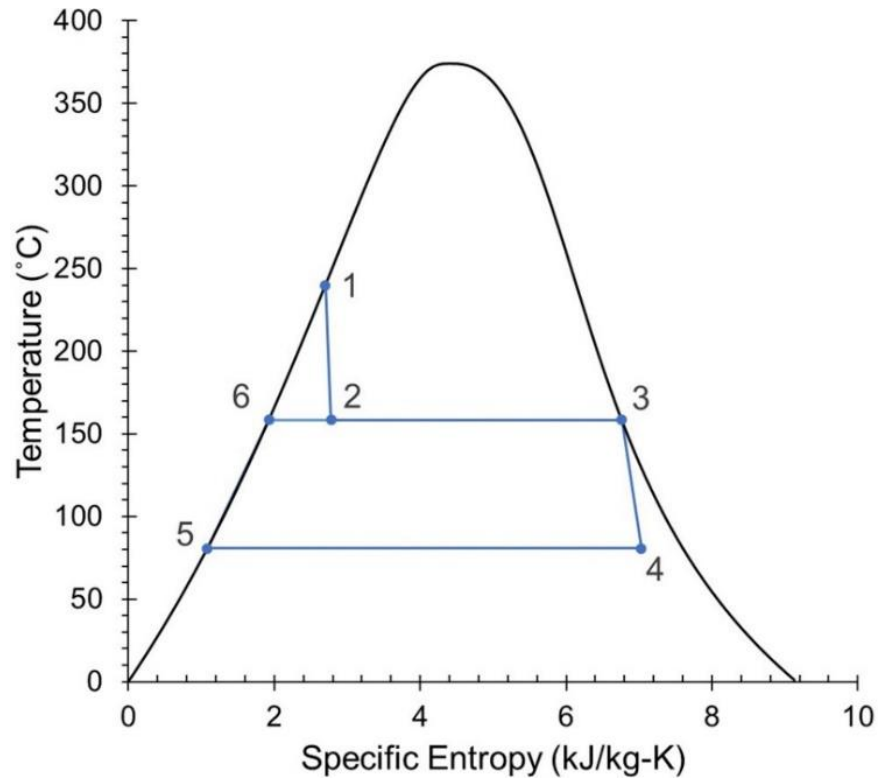
Figure 2-4. Temperature-entropy (T-s) diagram of a single flash plant

It is assumed that the system operates at steady state, the flashing process occurs at constant enthalpy, there is no pressure drop, the properties of the geofluid are equivalent to those of pure water, and the auxiliary power of the condenser and geothermal well pumps is negligible. The single flash plant was compared with the best system from the recuperative supercritical organic Rankine cycle analysis. The input exergy to the system, the exergy destruction through each component, and the exergy loss in the reinjection and from the condenser were calculated by the equations below:

The equations for the single flash plant are:

$$\dot{I}_t = \dot{m}_3 T_o(s_4 - s_3) \tag{2-8}$$

$$\dot{I}_f = \dot{m}_1 T_o(s_2 - s_1) \tag{2-9}$$

$$\dot{I}_c = \dot{m}_{hr}\left(h_{hr,in} - h_{hr,out} - T_o(s_{hr,in} - s_{hr,out})\right) + \dot{m}_3(h_4 - h_5 - T_o(s_4 - s_5)) \tag{2-10}$$

$$\dot{Ex}_{loss,ri} = \dot{m}_3(h_5 - h_o - T_o(s_5 - s_o)) + \dot{m}_6(h_6 - h_o - T_o(s_6 - s_o)) \tag{2-11}$$

The equations for the binary ORC plant are:

$$\dot{I}_t = \dot{m}_{WF} T_o(s_2 - s_1) \tag{2-12}$$

$$\dot{I}_p = \dot{m}_{WF} T_o(s_5 - s_4) \tag{2-13}$$

$$\dot{I}_c = \dot{m}_{hr}\left(h_{hr,in} - h_{hr,out} - T_o(s_{hr,in} - s_{hr,out})\right) + \dot{m}_{WF}(h_3 - h_4 - T_o(s_3 - s_4)) \tag{2-14}$$

$$\dot{I}_{PHE} = \dot{m}_{hs}\left(h_{hs,in} - h_{hs,out} - T_o(s_{hs,in} - s_{hs,out})\right) + \dot{m}_{WF}(h_6 - h_1 - T_o(s_6 - s_1)) \tag{2-15}$$

$$\dot{I}_{IHE} = \dot{m}_{WF} * T_o(s_3 - s_2 + s_6 - s_5) \tag{2-16}$$

$$\dot{Ex}_{loss,ri} = \dot{m}_{hs}\left(h_{hs,out} - h_o - T_o(s_{hs,out} - s_o)\right) \tag{2-17}$$

The equations that apply to both plants are:

$$\dot{Ex}_{in} = \dot{m}_{hs}\left(h_{hs,in} - h_o - T_o(s_{hs,in} - s_o)\right) \tag{2-18}$$

$$\dot{Ex}_{loss,c} = \dot{m}_{hr}\left(h_{hr,out} - h_o - T_o(s_{hr,out} - s_o)\right) \tag{2-19}$$

24

2.4 Results and Discussion

2.4.1 ORC Turbine Inlet Pressure Parametric Analysis

The turbine inlet pressure (greater than critical pressure) was varied for each fluid. The performance of isobutane is shown in Figure 2-5. In some cases, with high pressures and low temperatures at the turbine inlet, the fluid passed through the liquid-vapor mixture state. These instances were removed from the analysis if the fluid exiting the turbine was a mixture as it is not ideal for most expanders to deal with vapor droplets during expansion. However, cases where expansion only passed through the saturation dome, as possible with dry and isentropic fluids, were included in the results. It has been proven that as long as the exit of the turbine is not a mixture, then there is not enough residence time in the turbine for the phase change to occur and for droplets to damage the turbine or expander [78]. Generally, the first law and plant efficiency increase with turbine inlet temperature. As the turbine inlet temperature increases, the total enthalpy added to the working fluid increases as does the net work, increasing the cycle efficiency. The plant efficiency compares the net work to the maximum heat that could be provided by the geothermal fluid, using the ambient temperature (20°C) as a reference. The plant efficiency was almost constant for high pressures. The maximum plant efficiency for isobutane increases from
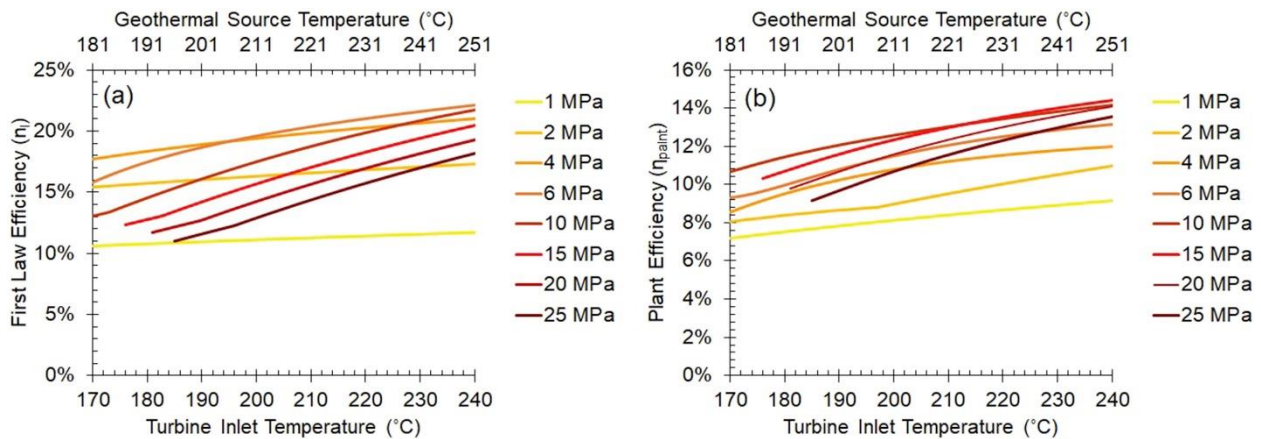
Figure 2-5. Isobutane results for varying turbine inlet temperature and pressure for: (a) first law efficiency; (b) plant efficiency.

25

around 10 to 16% for turbine inlet temperatures from 170 to 240 °C. Generally, lower pressures were more optimum at lower turbine inlet temperatures to maximize the efficiency.

2.4.2 ORC Turbine Inlet Pressure Optimization

Three parameters were selected for optimization: plant efficiency, second law efficiency, and the net power. Based on their definitions, maximizing the plant efficiency also resulted in the maximum net work. The results are shown in Figure 2-6. The analyses for acetone, cyclopentane, cyclopropane, R152a, pentane, and isopentane were limited due to their critical temperatures and maximum REFPROP temperatures. In some cases, the maximum plant efficiency occurred numerically where the turbine exit was a mixture. To prevent this, the upper pressure limit of the cycle needs to be reduced, significantly decreasing the cycle efficiency but protecting the turbine from vapor droplets. These instances were removed from the analysis to show clear correlations of the results. Carbon dioxide performed the worst in first law efficiency as Le et al. likewise found for a turbine inlet temperature of 139°C [14]. Vidhi et al. studied R32 and carbon dioxide in a supercritical ORC for heat sources below 200°C and also found CO_2 to not perform as effectively as R32 [79]. The first law efficiency is described as the ratio of the net power produced in comparison to the amount of heat received by the cycle. Although propyne, cyclopropane, neopentane, acetone, and cyclopentane performed the best in cycle efficiency across the tested geothermal heat source conditions and converted heat to power the most effectively, they did not utilize the heat source effectively leading to high reinjection exergy losses. R1233zd(E), butane, isopentane, pentane, and neopentane performed among the best in plant efficiency, exergy efficiency, and net power. To improve the plant efficiency of the fluids that achieved higher first law efficiencies, the pinch point conditions of the evaporator and the effectiveness of the recuperator need be optimized.

26
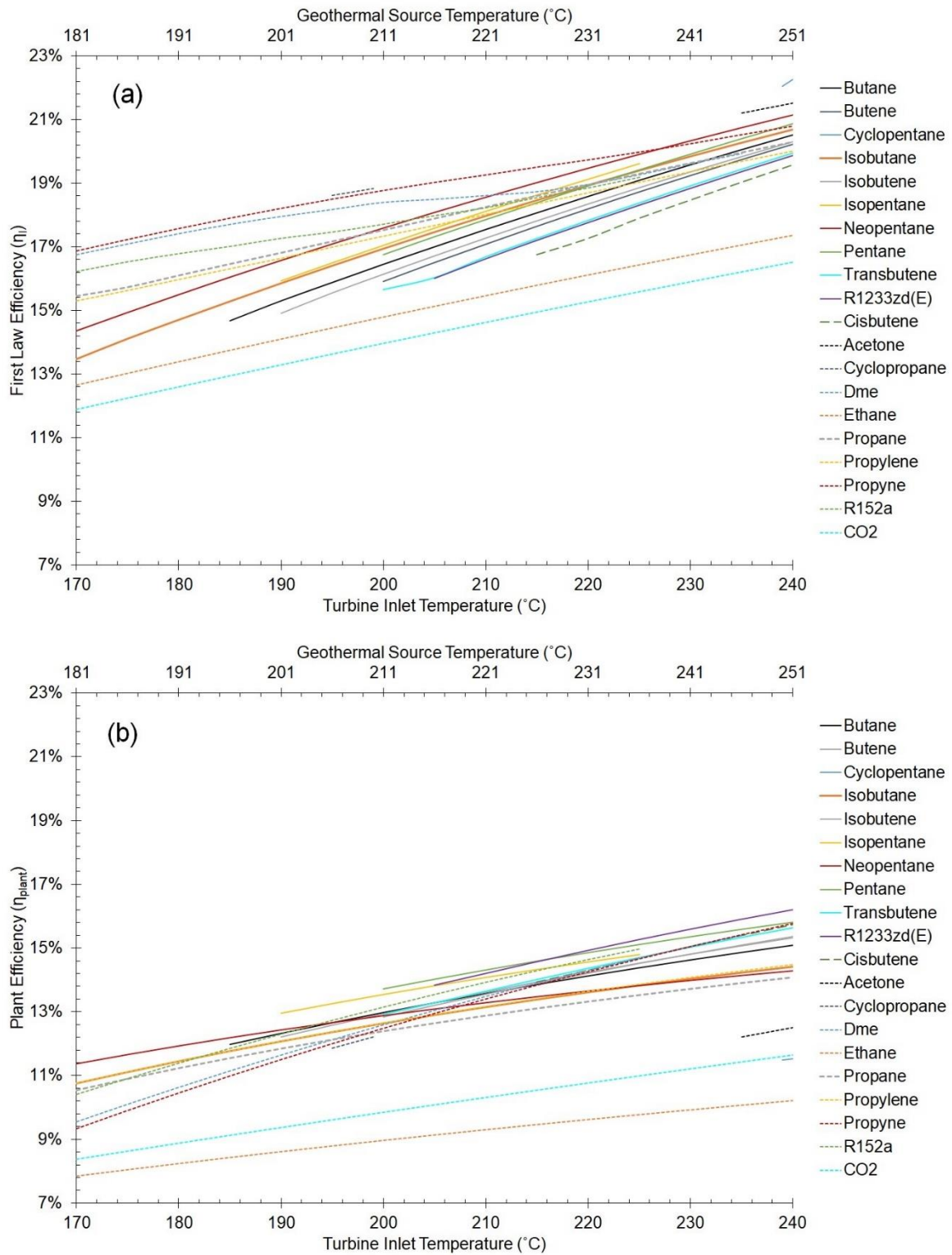
Figure 2-6. Optimized conditions for maximum plant efficiency: (a) cycle efficiency; (b) plant efficiency; (c) exergy efficiency; (d) net power (dry, wet, and isentropic fluids are indicated by solid, dashed, and long dashed lines, respectively).
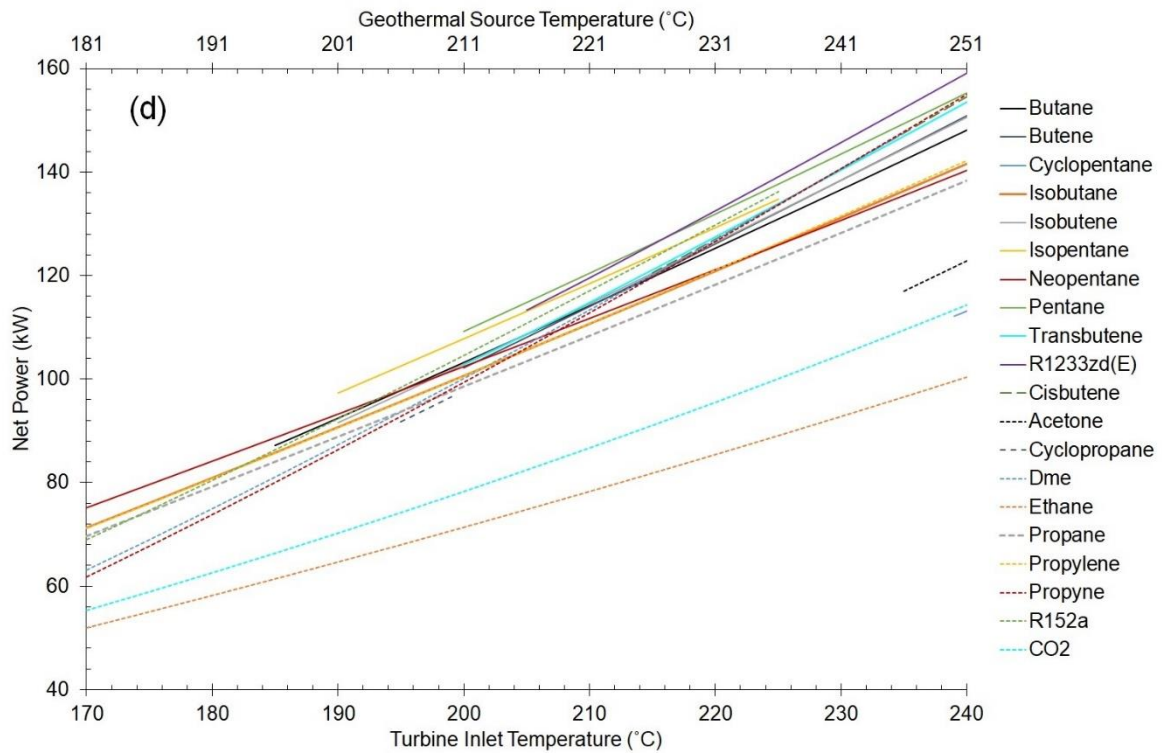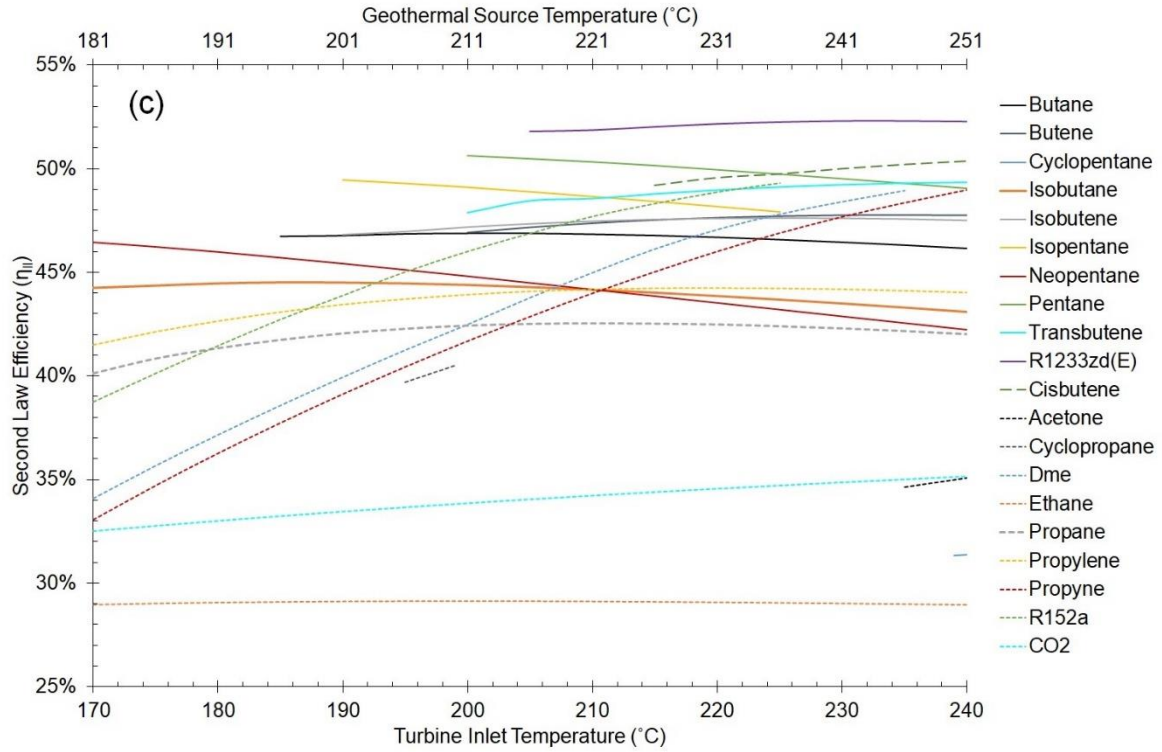
Figure 2-6 (Continued)
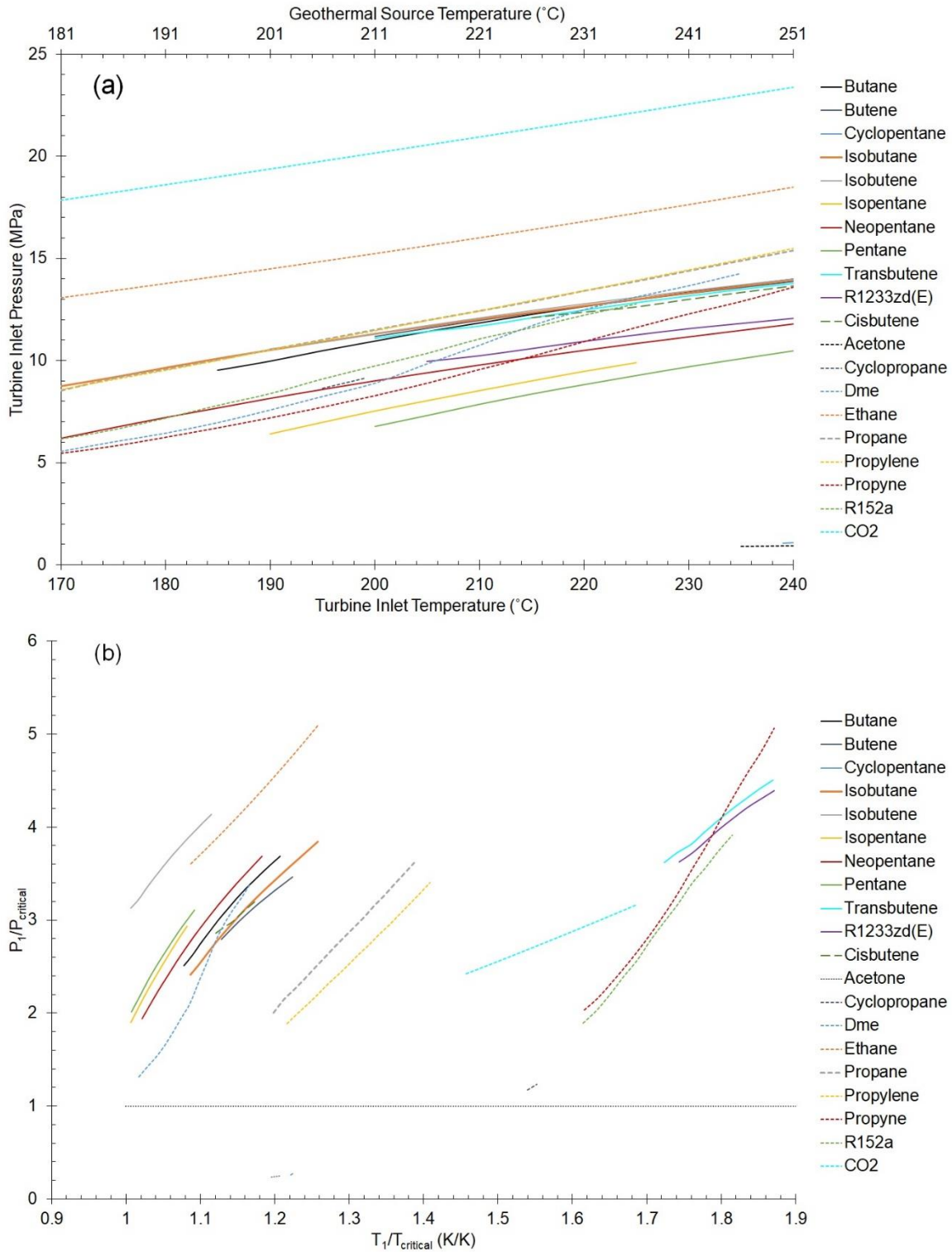
Figure 2-7. Optimized conditions for maximum plant efficiency: (a) turbine inlet conditions; (b) non-dimensionalized turbine inlet conditions in respect to the critical point of the fluid (dry, wet, and isentropic fluids are indicated by solid, dashed, and long dashed lines, respectively)

29

The maximum reversible efficiency for a geothermal resource is best described as a triangle cycle. The optimized second law, or exergy efficiency remained nearly constant for increasing turbine inlet temperature for the tested fluids. This is due to the fact that the slope of the first law efficiency and the plant efficiency were similar in Figure 2-6a and b. In other words, the exergy destruction was nearly constant in the optimized cases for various turbine inlet temperatures. R1233zd(E) had the least exergy destruction while carbon dioxide, acetone, cyclopentane, and ethane had the highest in the analyzed cases. This was mainly due to the turbine inlet conditions being very close to the critical point. For turbine inlet temperatures close to or below the critical point, it can be more advantageous to reduce the cycle upper pressure and operate in a subcritical cycle to improve the plant efficiency.

As the mass flow of each fluid was adjusted to account for the same pinch point in the PHE and geothermal source conditions, the net power of each fluid was compared as opposed to the specific net work. As expected, higher turbine inlet temperatures yielded a higher work output. Carbon dioxide has a high critical pressure of 7.38 MPa as well as a low critical temperature in comparison to the other tested fluids. The optimum pressure for carbon dioxide ranged from 18 to 23 MPa which required high pump work. Therefore, the net power produced by carbon dioxide was significantly less than the other tested fluids.

The optimum cycle high pressure was compared to the critical point. Pressures below the critical point correspond to a subcritical cycle, as indicated by the dotted line in Figure 2-7b. The trends were nearly linear. Acetone and cyclopentane were the only fluids that were optimal in subcritical cases. To optimize the plant efficiency, a supercritical cycle was more efficient than subcritical cycles for the tested parameters for the rest of the tested fluids. The fluids with a solid line in the figures are dry fluids while the rest are wet (dashed line) except cisbutene which is an

30

isentropic fluid. As evident in Figure 2-6b and d, wet fluids generally had lower plant efficiencies and net work than the dry fluids. The benefit of dry and isentropic fluids is that the expansion is always guaranteed to occur in the vapor phase, which was one of the constraints. As explained by Chen et al., isentropic fluids (cisbutene) perform well at supercritical cycles. For dry fluids, superheating generally reduces the cycle efficiency [80]. Therefore, no dry fluids performed well in cycle efficiency and why not just one dry fluid performed the best in plant efficiency and net work across the range of temperatures.

2.4.3 Expander Considerations

The volumetric expansion ratio (V_{ratio}) is shown in the equation below, where v is the specific volume (kg/m^3). Typical ORC expanders can work in single stage or multi-stage for a total volumetric expansion ratio up to 20 [81].

$$V_{ratio} = v_5/v_4 \qquad (20)$$

As shown in Figure 2-8a, the optimal operating conditions for some fluids to maximize the plant efficiency, exceeded 20. Isopentane and pentane had expansion ratios over 150. Figure 2-8b shows the fluids with expansion ratio only below 20. Only CO_2, cyclopropane, DME, ethane, propane, propylene, propyne, and R152a met the desired expansion ratio constraint. While CO_2 and ethane had the lowest expansion ratios, they also had the lowest plant efficiencies of these fluids. It is recommended that propylene, propane, propyne, R152a, and DME be utilized in geothermal plants.

2.5 Exergy Analysis

For the exergy comparison, a geothermal reservoir temperature of 251°C was selected. These conditions corresponded to a turbine inlet temperature in the supercritical ORC of 240°C where R1233zd(E) had the highest plant and second law efficiencies of 16.2% and 52.3%,

31
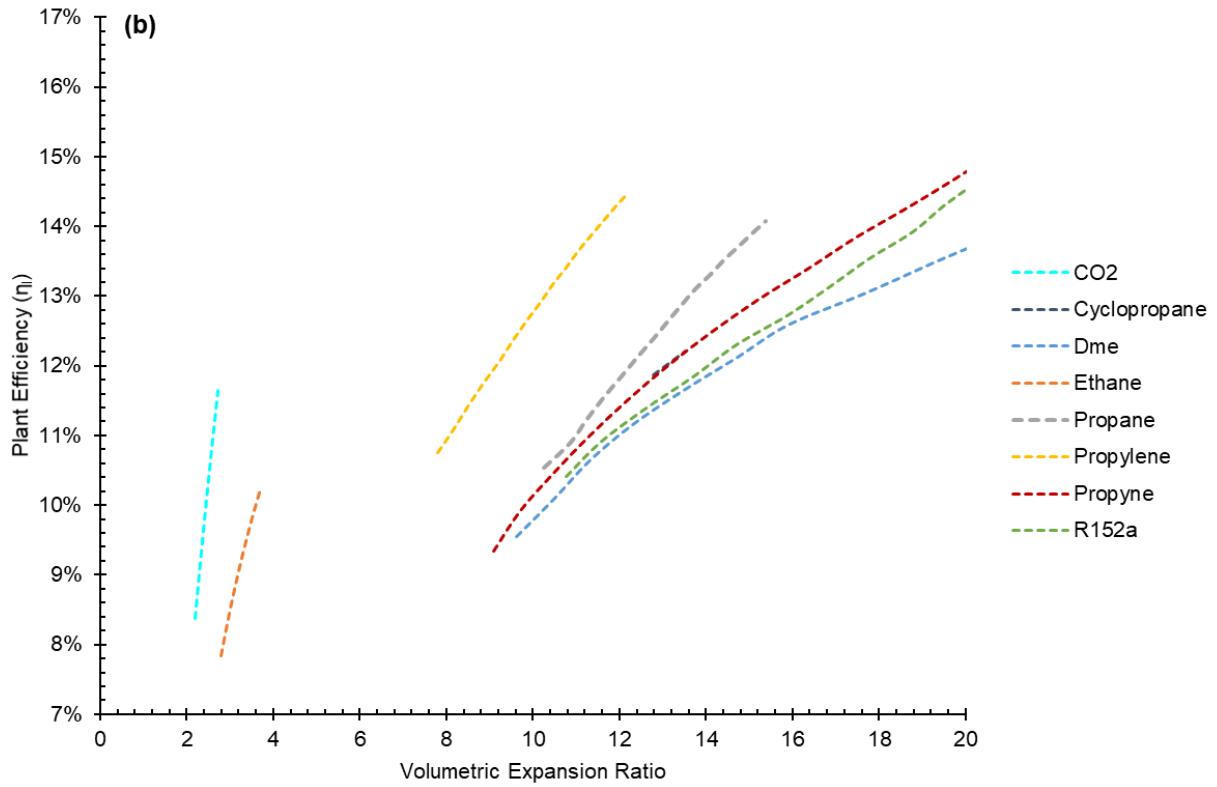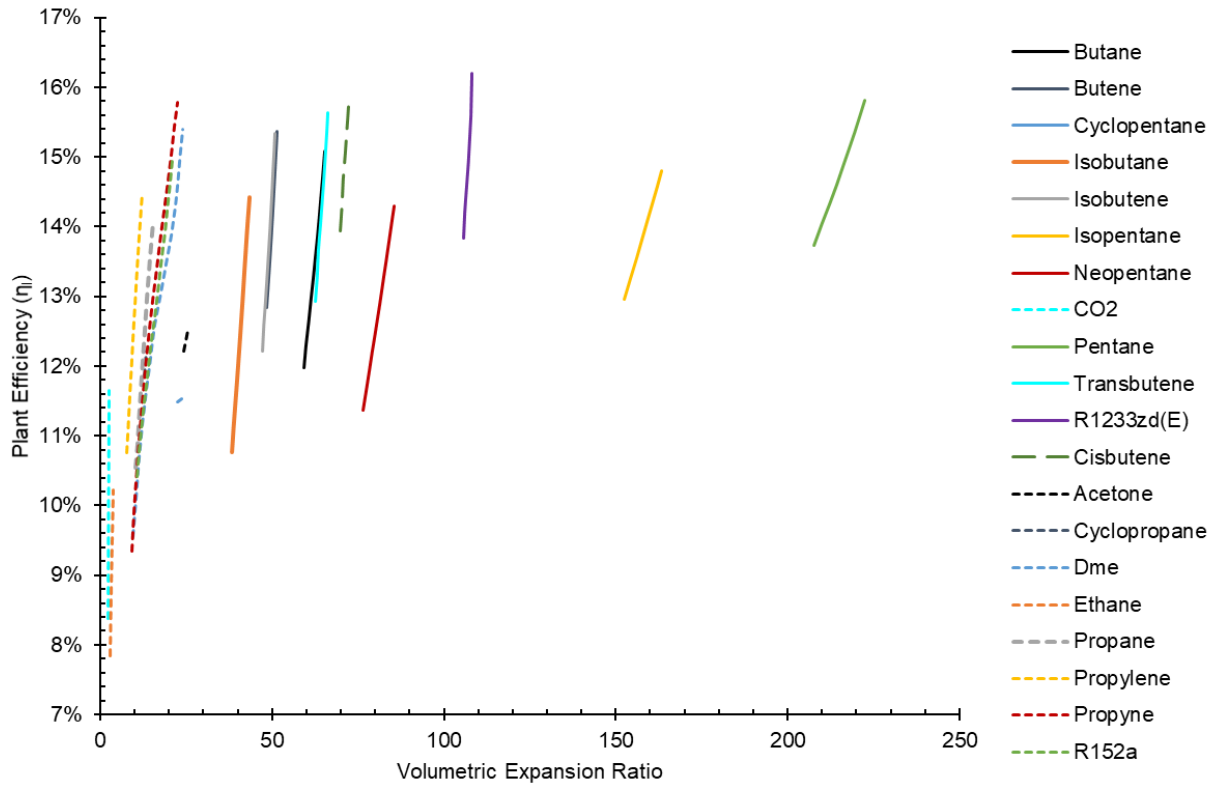
Figure 2-8. Expansion ratio versus plant efficiency for (a) all fluids; (b); fluids with an expansion ratio below 20

The turbine inlet pressure was selected as 12.1 MPa to maximize the plant efficiency for R1233zd(E) in the binary plant. The temperature of the geofluid leaving the primary heat exchanger was 68°C. The single flash plant was modeled at the same conditions as the binary plant. The condensing temperature of the single flash plant was matched to the geofluid reinjection temperature for the binary cycle (68°C). The optimum flashing pressure was iterated to maximize the produced work. The corresponding turbine exit vapor quality was 0.89 in this case. It is assumed that vapor droplets have a negligible impact on the turbine performance.

Table 2-3 contains the results from the exergy analysis for both systems with a water-cooled condenser. As the inlet geothermal conditions were identical, the exergy input was the same. The net work of the single flash is almost a third of that of the binary system. One of the reasons is that much of the exergy is wasted before the steam is introduced to the turbine. Only a fraction of the geofluid is directed to the turbine after flashing. This introduces much less exergy to the turbine in the single flash plant. This is also evident in the exergy reinjection losses. For the binary system, the geofluid exits the primary heat exchanger at 68°C. For the single flash plant, the geofluid is flashed to 159°C into two streams. At a flashing quality of 0.20, 20% of the geofluid, or 0.20 kg/s, exits as a saturated vapor which reaches a temperature of 68°C after passing through the turbine. The remaining 0.80 kg/s is at 159°C, wasting a significant amount of exergy. To extract more power, this stream can be flashed again and sent to a lower pressure steam turbine before reinjection. A double flash power can produce more power than a single flash but less than double the amount. So, in terms of work output, a double flash plant would still not be competitive to the supercritical ORC with R1233zd(E). The largest exergy destruction of the binary cycle lies in the turbine. The ratio of the net work to the exergy input is also a form of exergy efficiency [23]. The binary ORC with R1223zd(E) had a ratio of 0.58 accounting for mechanical efficiencies, close to

its second law efficiency of 0.52. Since most of the exergy input is rejected during flashing, the

single flash plant had a net work to exergy input ratio of 0.27. This can be improved if it is upgraded

to a double flash or a bottoming binary cycle is used to extract the unused heat.

Table 2-3. Exergy analysis comparison between binary ORC with R1233zd(E) and a single flash
plant for a geothermal source of 251°C

	Binary ORC	Single Flash
Exergy Input [kW]	272.04	272.04
Turbine Exergy Destruction [kW]	33.85	29.92
Condenser Exergy Destruction [kW]	8.56	12.47
Pump Exergy Destruction [kW]	4.88	–
Primary Heat Exchanger Exergy Destruction [kW]	15.85	–
Internal Heat Exchanger Exergy Destruction [kW]	2.62	–
Flashing Exergy Destruction [kW]	–	30.59
Reinjection Exergy Loss [kW]	19.10	86.94
Condenser Exergy Loss [kW]	2.47	29.80
Net Work (without mechanical losses) [kW]	184.71	72.32
Net Work (with mechanical losses) [kW]	159.13	74.09
Net Work/Exergy Input (without mechanical losses)	0.68	0.30
Net Work/Exergy Input (with mechanical losses)	0.58	0.27

2.6 Conclusion and Recommendations

This section analyzed the effect of pressure in order to optimize the first law efficiency,

plant efficiency, second law efficiency, and net power of a supercritical ORC with turbine inlet

temperatures between 170 and 240°C, suitable for medium temperature geothermal reservoirs. It

was found that carbon dioxide and ethane performed the worst. R1233zd(E), butane, isopentane,

pentane, cisbutene, and neopentane performed the best in plant efficiency under the tested

parameters but resulted in very high and unrealistic turbine efficiencies. Therefore, the

34

recommended environmental working fluids include propylene, propane, propyne, R152a, and DME which resulted in high efficiencies but met the expansion ratio constraint. To optimize the system, higher turbine inlet temperatures require higher pressures, but in turn, operate at higher efficiencies. However, this analysis was performed regarding the available geothermal resource. For the analysis, a heat source temperature of 11°C greater than the turbine inlet temperature was used. This analysis provides the type of system performance that can be expected in a supercritical ORC for medium temperature geothermal reservoirs. An exergy analysis was performed of the fluid that yielded the highest efficiency, R1233zd(E), with a turbine inlet temperature of 240°C to a single flash plant with the same geothermal reservoir and plant conditions. The binary plant performed significantly better than the single flash plant. It is recommended in future analyses to add auxiliary power and to optimize the pinch points in the heat addition and rejection heat exchangers.

CHAPTER 3: DESIGN OF A COMBINED CYCLE
WITH A SUPERCRITICAL ORGANIC RANKINE CYCLE

3.1 Introduction

Combined cycles take the advantage of a high temperature heat source while utilizing the waste heat of the cycle for additional power generation through a lower efficiency cycle. Before a combined cycle can be implemented in a solar thermal-geothermal hybrid system, various combined cycle configurations need to be analyzed and optimized.

3.1.1 Topping Cycle Background

There are many power cycles and combined cycles depending on the heat source and the temperature. Yu et al. reviewed cycles for high temperatures above 700K (427°C) [11]. The steam Rankine cycle is commonly used for solar and waste heat applications. Subcritical steam Rankine can achieve efficiencies around 40% [11]. Better heat transfer fluids can allow the steam to reach higher temperatures. With molten salt as the heat transfer fluid in a solar power tower (SPT) plant, the steam can reach temperatures up to 540°C [82]. However, Rankine cycles are limited to temperatures below 600°C due to very high pressures. Nickel alloys are suitable for high temperature steam but are very costly [83]. Supercritical steam cycles have been analyzed in the literature [9]. Singer et al. studied an ultrasupercritical steam cycle for SPT [84]. A supercritical Rankine cycle with a turbine inlet temperature over 720°C and a pressure of 35 MPa was found to have an efficiency of up to 53% [84]. The problem is the cost of the high pumping requirement and the cost of the nickel alloy piping [83]. The Kalina cycle uses a mixture of ammonia and water and can produce almost 1.5 times the power and efficiency of a single pressure steam cycle. With

36

the high condensing pressure, the Kalina cycle has not been used in a plant with temperatures above 427°C [11]. Another efficient cycle is the Stirling cycle. While it can achieve efficiencies close to the Carnot efficiencies, it has only had success in small configurations [11].

A sCO$_2$ Brayton cycle is attractive due to its ability to achieve high temperatures and its high efficiencies from low compressor work and effective recuperation [85]. There are many configurations of sCO$_2$ Brayton cycles. A recompression cycle splits the flow into two streams, one which is further cooled, to be compressed separately. This reduces the compressor work compared to a simple cycle and is capable of much higher efficiencies [12,86]. The partial cooling cycle contains an extra compressor and cooler in comparison to the recompression cycle. This cycle can achieve slightly higher stand-alone efficiencies than the recompression cycle [12]. Al-Sulaiman et al. compared five configurations: simple, regenerative, recompression, pre-compression, and split expansion. It was found that the recompression Brayton cycle performed the best with 52% cycle efficiency at a turbine inlet temperature around 1100K (827°C) [87]. Neises et al. looked at various configurations, focusing on the recuperator conductance [88]. Supercritical CO$_2$ Brayton cycles are very reliant on a recuperator to improve their performance. At very low recuperator conductance, partial cooling performs better than a recompression cycle. Otherwise, recompression and partial cooling cycles are comparable [88]. Another study focused on recompression sCO$_2$ cycles with and without reheat [89]. The cycle with reheat did 1% better than the cycle without reheat in exergy and thermal efficiency; therefore the reheat portion did not significantly improve the cycle [89]. Iverson et al. studied a split-flow recompression sCO$_2$ Brayton cycle for solar energy experimentally and numerically and found that the cycle is resistant to transients for short periods of time, such as cloud cover, due to the thermal mass of the CO$_2$ and the thermal capacitance of the piping [90]. There has been some focus on helium Brayton cycles.

37

Theoretically, these cycles achieve turbine inlet temperatures of 670-820°C [91]. However, these cycles require very high flow rates compared to sCO_2 cycles, making them less attractive [83,91].

3.1.2 Combined Cycle Efficiency Review

Combined cycles are typically two cycles in series, where the waste heat from the high temperature cycle is utilized in the bottoming cycle. Steam and organic Rankine cycles (ORC) are more commonly used than Kalina and Stirling cycles due to cost and feasibility [11]. Steam is typically used with a gas-turbine due to the high temperatures. At lower temperatures, ORCs are more efficient.

There has been an effort to apply combined cycles to solar energy to achieve higher efficiencies and introduce flexibility. Mabrouk et al. combined parabolic trough collectors (PTC) with a gas fired combined cycle [92]. Various temperatures from solar source are integrated throughout the system. As the availability of solar energy increases, it extracts more heat from the solar field through the addition of low temperature heat exchangers. The system was found to adapt well to transients [92]. A solar hybrid gas-turbine system was investigated by Buck et al. [93]. Solar power tower was used to preheat the air before a gas combustor with a steam Rankine bottoming cycle. The incremental solar thermal to electricity efficiency, the additional work added in comparison to the thermal heat added by solar, was 32.3% [93]. A similar configuration was studied where the solar energy was capable of fully heating the air without a gas combustor at design conditions [94]. This study was more cost effective than the SPT configurations in operation at the time [94]. The work of Besarati et al. looked at various configurations of a supercritical carbon dioxide (sCO_2) Brayton cycles with a bottoming subcritical for solar applications [12]. Besarati found that the recompression sCO_2 performed better than partial cooling cycle in a

38

combined cycle with a subcritical ORC. A recompression cycle can operate at higher efficiencies and lower pressure ratios than the partial cooling cycle.

3.1.3 Objective

The sCO_2 Brayton cycle has been shown to have the potential to work well with solar power tower. Its high recuperation and low temperature waste heat in comparison to gas turbine systems makes it suitable to use an ORC as a bottoming cycle as opposed to a Rankine cycle. The prior chapter analyzed various environmental fluids for geothermal applications and found that a supercritical cycle was more advantageous to improve the system efficiency in most cases. The performance of a sCO_2 Brayton cycle could be improved by implementing a supercritical ORC and optimizing the approach pinch point in the heat recovery heat exchanger (the temperature difference between hot fluid in and the cold fluid out). This chapter will optimize the pressure ratio in both the topping and bottoming cycle as well as the approach pinch point to see if a supercritical ORC is in fact more efficient than a subcritical ORC for combined cycle applications.

3.2 Methodology

MATLAB$^{®}$ was used to model the combined cycle [95]. NIST REFPROP was utilized to calculate the fluid properties [96].

3.2.1 Topping Cycle

Two topping cycles were chosen based on the literature review above: the simple and recompression recuperative sCO_2 Brayton cycles, as shown in Figure 3-1. The main difference between the two cycles is that the recompression cycle splits the flow to two different compressors the main compressor (MC) and the recompressor (RC). This reduces the cooling and compression loads. This configuration is also better suited for two recuperators, a low-temperature and a high-temperature, where the simple cycle only has one recuperator. The mechanical efficiency is

39

considered for both the turbine and the recuperator, as was done for the ORC (Chapter 2). For the recompression cycle, the heat balance through the high temperature recuperator (HTR) is calculated in Equation (3-1. The heat balance of the low temperature recuperator (LTR) in the recompression cycle is shown in Equation (3-2. The effectiveness of the hot temperature recuperator can be defined in many ways; the definition used here is based on the temperatures as used by Sarkar (Equation (3-3). The effectiveness of the hot stream recuperator is defined as the ratio of the actual heat recuperated compared to the heat that could transferred if the final recuperator hot stream outlet was cooled to the compressor outlet temperature (Equation (3-4) [12].
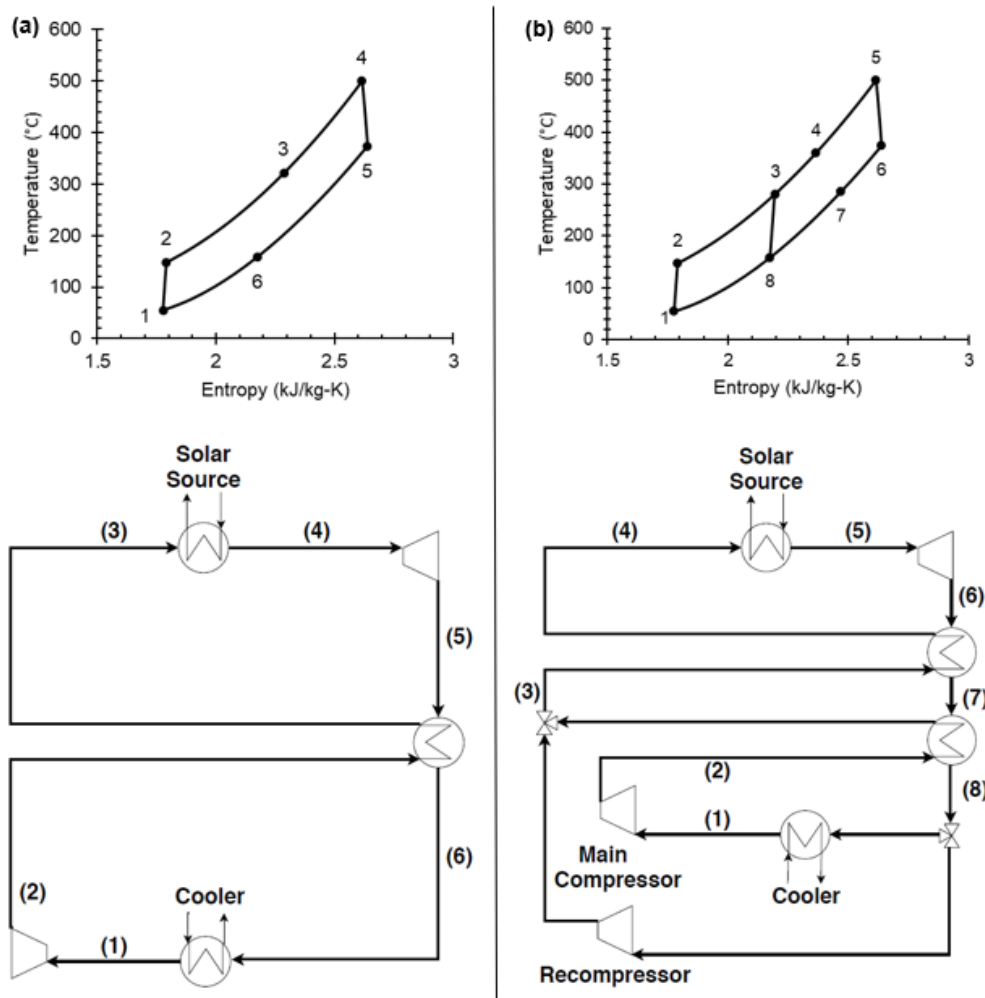

Figure 3-1. sCO$_2$ Brayton configurations: (a) simple and (b) recompression

40

The main compressor work, recompressor work, and total compressor work for the recompressive cycle are shown in Equations (3-5 to (3-7.

The recompressive cycle turbine work is calculated in Equation (3-8. For the simple cycle, the recuperator heat balance is shown in Equation (3-10. The work for the turbine and compressor is calculated in Equations (3-12 and (3-13. The hot stream effectiveness was adapted from the definition used for the recompressive cycle (Equation (3-11). The net work is the difference between the total turbine and compressor work ((3-15). The first law efficiency, also known as the thermal efficiency, is the ratio of the useful power to the total heat input to the cycle ((3-16). The combined cycle efficiency is then the total work from both the CO_2 cycle and the bottoming ORC divided by the total heat input into the system, or the heat input into the CO_2 cycle ((3-9 and (3-14).

The equations for the recompression sCO_2 Brayton cycle:

$$h_6 - h_7 = h_4 - h_3 \tag{3-1}$$

$$h_7 - h_8 = \left(1 - x_{fr}\right)(h_3 - h_2) \tag{3-2}$$

$$\varepsilon_{HTR} = \frac{T_6 - T_7}{T_6 - T_3} \tag{3-3}$$

$$\varepsilon_{hot\ stream} = \frac{h_6 - h_8}{h_6 - h_8(T_2, P_8)} \tag{3-4}$$

$$\dot{W}_{mc} = \dot{m}_{CO2}(1 - x_{fr})\frac{h_2 - h_1}{\eta_{p,m}} = \dot{m}_{CO2}(1 - x_{fr})\frac{h_{2s} - h_1}{\eta_{p,m}\eta_{p,s}} \tag{3-5}$$

$$\dot{W}_{rc} = \dot{m}_{CO2}\,x_{fr}\frac{h_3 - h_8}{\eta_{p,m}} = \dot{m}_{CO2}\,x_{fr}\frac{h_{3s} - h_8}{\eta_{p,m}} \tag{3-6}$$

$$\dot{W}_c = \dot{W}_{mc} + \dot{W}_{rc} \tag{3-7}$$

$$\dot{W}_t = \dot{m}_{CO2}\eta_{t,m}(h_5 - h_6) = \dot{m}_{CO2}\eta_{t,m}\eta_{t,s}(h_5 - h_{6s}) \tag{3-8}$$

$$\dot{Q}_{in} = \dot{m}_{CO2}(h_5 - h_4) \tag{3-9}$$

41

The equations for the simple sCO_2 Brayton cycle are:

$$h_5 - h_6 = h_3 - h_2 \tag{3-10}$$

$$\varepsilon_{hot\ stream} = \frac{h_5 - h_6}{h_5 - h_6(T_2, P_6)} \tag{3-11}$$

$$\dot{W}_t = \dot{m}_{CO2}\eta_{t,m}(h_4 - h_5) = \dot{m}_{CO2}\eta_{t,m}\eta_{t,s}(h_4 - h_{5s}) \tag{3-12}$$

$$\dot{W}_c = \dot{m}_{CO2}\frac{h_2 - h_1}{\eta_{p,m}} = \dot{m}_{CO2}\frac{h_{2s} - h_1}{\eta_{p,m}\eta_{p,s}} \tag{3-13}$$

$$\dot{Q}_{in} = \dot{m}_{CO2}(h_4 - h_3) \tag{3-14}$$

The equations for both cycles are:

$$\dot{W}_{net} = \dot{W}_t - \dot{W}_c \tag{3-15}$$

$$\eta_I = \frac{\dot{W}_{net}}{\dot{Q}_{in}} \tag{3-16}$$

$$\eta_{CC} = \frac{\dot{W}_{net,CO2} + \dot{W}_{net,ORC}}{\dot{Q}_{in}} \tag{3-17}$$

3.2.2 Bottoming Cycle

For the bottoming cycle, an organic Rankine cycle (ORC) was used. An ORC with a recuperator is shown in Figure 3-2. The cycle is modeled in accordance with the equations presented in Chapter 2. The efficiency used in this section is the thermal efficiency, not the plant efficiency, as this chapter only considers the cycle performance without the consideration of heat sources. The pinch point analysis was used to determine the mass flow of the ORC and outlet temperature of the CO_2 through the heat recovery. The outlet temperature of the ORC was determined through the optimization of the approach pinch point in the heat exchanger. The pinch point and approach pinch point are shown in Figure 3-3. The approach pinch point is the difference between the hot fluid inlet and the cold fluid outlet through the primary heat exchanger (PHE) of

42
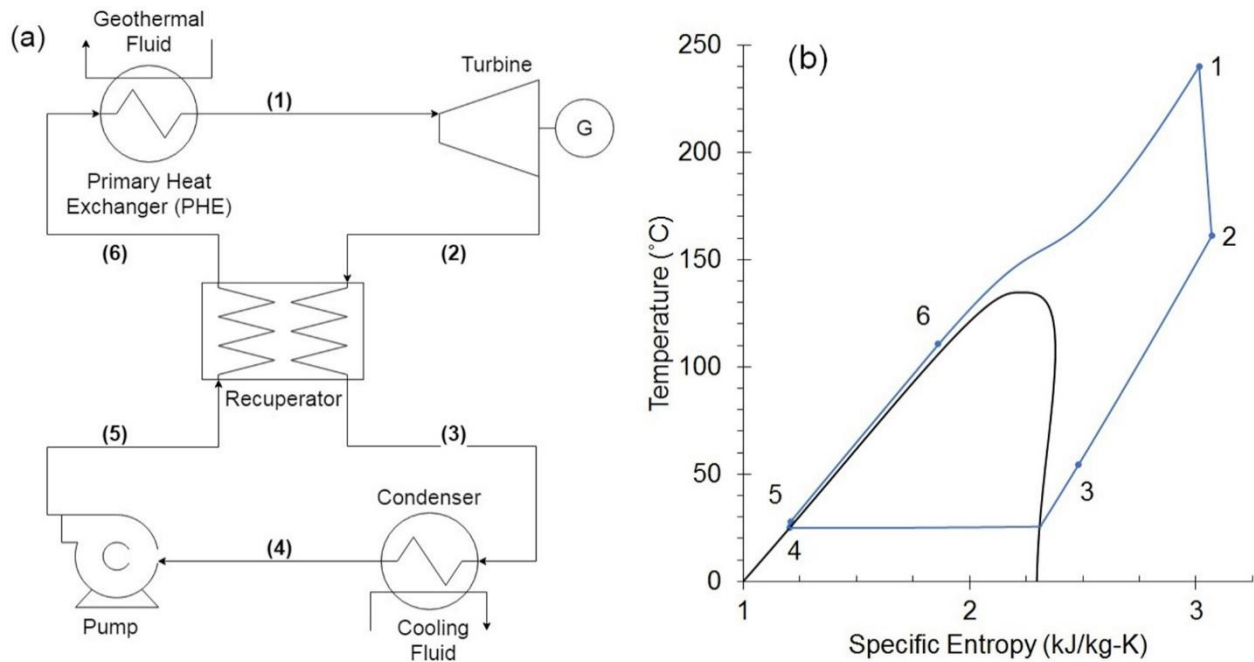
Figure 3-2. ORC layout and T-s diagram

the ORC. The pinch point is the minimum temperature difference at any point across the heat

exchanger. First an approach pinch point was selected. The low temperature of the ORC and CO_2

cycles were set. Now the inlet and outlet temperatures of the ORC can be determined. The CO_2

inlet temperature is determined from the above equations (assuming the CO_2 optimum pressure

ratio is known, or a guess is used for the calculation and then iterated during the optimization).

The specific heat is discretized across the ORC stream, and the temperature is calculated. The

pressure is assumed constant through the heat exchanger. In this case, the CO_2 mass flow is set at

1 kg/s. The ORC mass flow is guessed, and the temperature across the CO_2 stream can be

calculated. The temperature difference is calculated across the heat recovery process. If the

minimum pinch point is not met, the ORC mass flow is adjusted and iterated until the pinch point

meets the design condition within 10^{-6}. The minimization was performed with the "fmincon" tool

in MATLAB within the optimization toolbox [95]. The "fmincon" function works on objective

43

functions and constraints that are continuous and that have continuous first derivatives. Using gradients, the function locates the local minimum.

3.2.3 Validation

The recompression and simple cycle were first validated to the literature and matched within one percent [10,97]. The organic Rankine cycle was validated to the work of Le et al. [66]. Besarati et al. modeled a sCO_2 cycle with a bottoming ORC with a saturated vapor turbine inlet condition [12]. The corresponding combined cycle model of this study was compared with the Besarati, et.al. study; the validation is shown in Figure 3-4. For R236ea, using the listed value of 2.99MPa in Besarati et al. over the saturated pressure matched much better [12]. The mass flow in the recompression cycle was calculated higher than Besarati's values for butene and isobutane by 8 and 19%, respectively. In these instances, there was either a typo or the parameters of the genetic algorithm converged on a slightly different result and a higher resulting efficiency. The rest of the values matched within ±5%. Along with the validation of the individual cycles this was determined sufficient to continue.
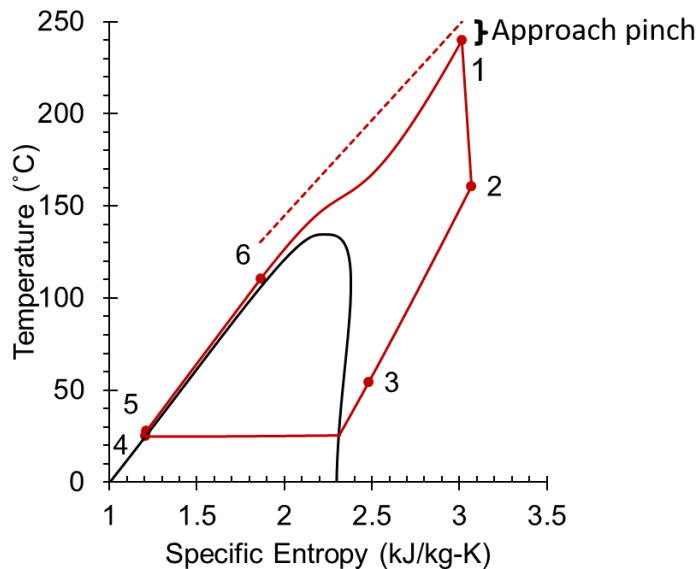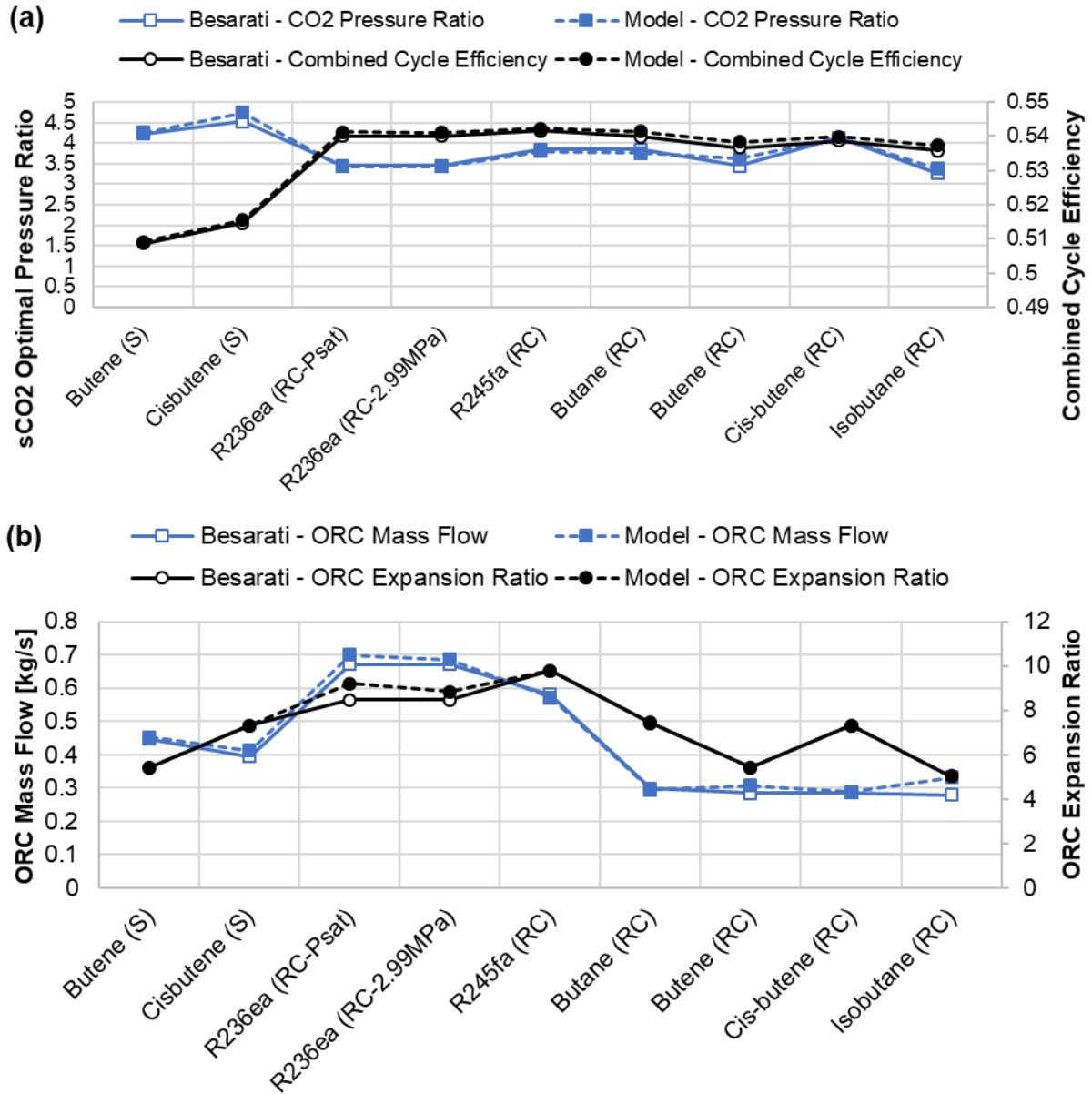

Figure 3-3. Approach pinch (ap) [108]

44

Figure 3-4. Validation of combined cycle to Besarati et al. [12]

3.2.4 Optimization

The following parameters are optimized in this chapter:

1.   The pressure ratio of the supercritical carbon dioxide cycle

2.   The upper pressure of the ORC, including supercritical conditions

3. The approach pinch in the heat recovery between the CO2 inlet temperature and the ORC working fluid outlet temperature (Figure 3-3)

4. The optimal organic fluid for the bottoming cycle

The analysis is performed for both a simple and recuperative sCO_2 Brayton topping cycle.

3.2.4.1 Genetic Algorithm

There are a variety of gradient-based optimization techniques to find the minima of a problem. However, for non-linear problems, these techniques fall short. For this multi-parameter, single-objective optimization, the genetic algorithm was chosen. Although the simulations can be time consuming, the genetic algorithm can be beneficial to find the global minimum (or maximum). Depending on the shape of the problem and the parameters of genetic algorithm, local minima (or maxima) can be located instead. It is crucial to define the parameters of the problem in such a way that there is a higher chance the global minimum is found. The genetic algorithm works by initially guessing numerous points within the range. The point with the best objective continues through to the next iteration. Within the original population, certain parameters are swapped, resulting in children points, and other points are mutated. The new generation is then tested, and the best objective value is evaluated against the prior population. This process is repeated until a certain criterion is met. This could be the maximum number of generations or, as in this case, the function tolerance that is the change in the objective value across a maximum number of specified generations (stall generations). For example, if the maximum number of stall generation is 100, and the function tolerance is 1e-6, 100 stall generations must pass without the objective value changing more than 1e-6 to terminate the genetic algorithm.

To ensure the genetic algorithm was locating the global minimum, it was combined with another optimization function, called a hybrid function in MATLAB. The "patternsearch" function

46

was used as it does not require a linear or continuous function. The "patternsearch" tries different solutions starting from an initial value, in this case the solution from the genetic algorithm. The function searches in various directions to minimize the objective function.

The combined cycle efficiency was the objective value to be maximized. To turn this into a minimization problem for the purposes of the algorithm, the efficiency was subtracted from one during the optimization.

3.2.5 Design Constraints

All fluids from Chapter 2 were analyzed in the combined cycle configurations apart from ethane and carbon dioxide as these fluids critical temperatures were below the lower temperature limit. These fluids are environmentally friendly, with global warming potential (GWP) below 150 and ozone depleting potential (ODP) less than 1 as per restrictive guidelines and regulations by directives such as by the European Union [72].

The values used in the analysis are shown in Table 3-1. Then the mechanical efficiency was added, and the ORC parameters were changed to match those of Chapter 2. The upper pressure of the sCO$_2$ Brayton cycle is selected as 25 MPa based on piping that is both available and cost-effective [10]. The lower temperature of the combined cycle system was determined based on the ambient temperature of a suitable location. Wagner et al. found that a temperature difference between the cooling source at ambient temperature and the cooler inlet is 15.5 K [98]. As a reference, the 99.6[th] percentile annual dry bulb temperature is used from ASHRAE climate design data [10,47,98]. Stillwater, Nevada is home to the world's first operating solar-geothermal hybrid power plant. Therefore, this location was used. The 99.6[th] percentile annual dry bulb temperature for a summer design day is 37.4°C. The corresponding minimum cycle temperature is 52.9°C. However, 55°C was selected cooling temperature as it was in the suitable range and was the base

47

temperature used in combined cycle analyses in the literature for Daggett, CA, allowing for suitable comparison to the literature [10,12,99]. All the fluids from Chapter 2 were analyzed in this section for the bottoming ORC apart from ethane and CO_2 which have a critical point below the minimum cycle temperature.

The expansion ratio was limited to 20 across the ORC turbine due to the limitations of expanders for ORC applications. Branchini et al. reviewed expanders that were tested in the literature or being produced by manufacturers (Figure 3-5) [100]. Volumetric expanders are generally limited to a volume expansion ratio (VER) of 10 or less, with radial turbines expanding up to around 50. The majority of the ORC expanders are below 20; this value was selected as a limit during the optimization. Additionally, any expansion through the dome was limited to a quality greater than 0.9. It was proven experimentally that as long as the exit of the turbine is not a mixture, then there is not enough residence time in the turbine for the phase change to occur and for droplets to damage the turbine or expander [78]. A quality limit was put in place in this section to ensure any supercritical condition was expanding to the right of the dome and not cutting across
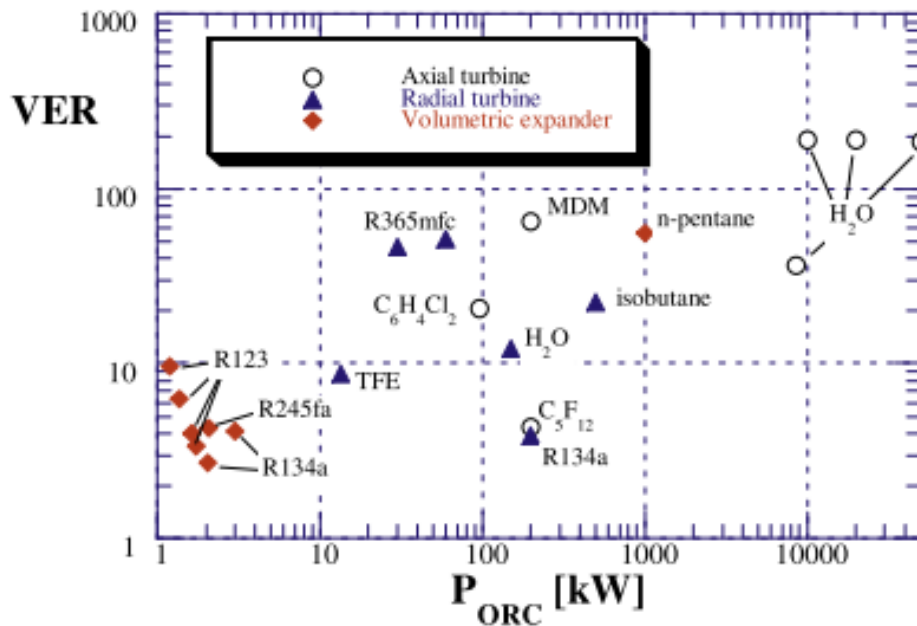

Figure 3-5. Volume expansion ratios (VER) for ORC expanders [100]

48

from the left side of the dome. Reaching a quality of 0.9 has been shown to not have an effect on the efficiency [12].

The following assumptions were taken in the analysis:

- No heat losses or pressure drop in heat exchangers or piping

- Expansion and compression processes are adiabatic

- Auxiliary power consumption is negligible

- Each process has reached steady state operation

Table 3-1. Combined cycle operating conditions

Parameter	Values for full optimization
CO_2 Cycle Parameters:	
CO2 mass flow	1 kg/s
Maximum cycle temperature	500°C and 800°C
Minimum cycle temperature	55°C
Maximum cycle pressure	25 MPa
Turbine isentropic efficiency	90%
Compressor isentropic efficiency	89%
Turbine mechanical efficiency	98%
Compressor mechanical efficiency	95%
Hot stream effectiveness	0.95
Recuperator pinch point	5°C
ORC Cycle Parameters:	
Minimum cycle temperature	55°C
Expander isentropic efficiency	87%
Compressor isentropic efficiency	85%
Turbine mechanical efficiency	90%
Compressor mechanical efficiency	90%
Internal heat exchanger (IHE) effectiveness	0.8
Pinch Point	10°C
Maximum expansion ratio	20

49

3.3 Results and Discussion

Initially the combined cycle was optimized to the work of Besarati et al. for comparison [12]. As a simple ORC was used as the bottoming cycle without a recuperator, the recuperator was removed. In addition, the mechanical efficiency was not considered in either cycle. The values are shown for cisbutene in Figure 3-6. For each discrete approach pinch, the optimal lower CO_2
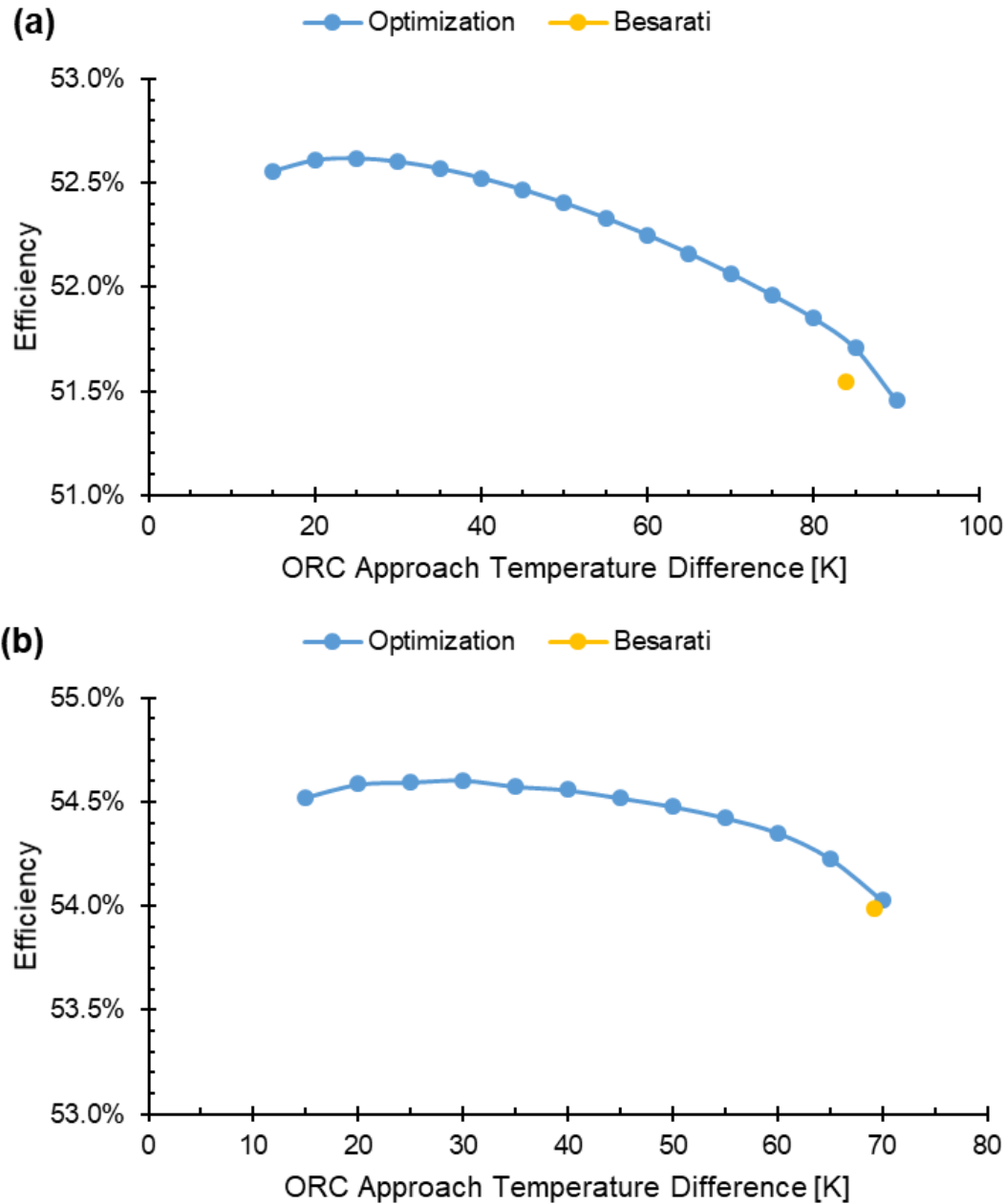

Figure 3-6. Cycle optimization and comparison to Besarati [7] for: (a) simple sCO_2 cycle; (b) recompression sCO_2 cycle

50

operating pressure and ORC upper pressure were found to maximize the combined cycle efficiency. It is clear that for both cases, using a subcritical ORC with no recuperation and with a saturated vapor turbine inlet, does not achieve the maximum possible efficiency. Higher ORC pressures in the supercritical region allow the heat addition to occur more linearly across the heat exchanger (Figure 3-3), reducing the approach pinch point, but allowing the working fluid to reach higher temperatures and extracting as much heat from the topping cycle as possible. The ORC is then able to achieve a higher efficiency.

3.3.1 Approach Pinch Optimization

For each fluid, the combined cycle was optimized for the cycle operating pressures for the topping and bottoming cycles and the approach pinch point between the two cycles. Initially, the cycle was optimized for discrete values of the approach pinch point to sufficiently select the optimal point. Most of the fluids met the optimum efficiency with an approach pinch of 35K. For fluids that met the maximum elsewhere, the difference in the efficiency was less than 0.1. The resulting optimization across various approach pinch points for butane is shown in Figure 3-7. The resulting optimization for butane with an approach pinch of 35K is the maximum of a complex surface depending on the topping cycle and the ORC operating conditions for a particular pressure ratio in the sCO_2 cycle (Figure 3-8 - Figure 3-11). The bounds were affected by the constraints previously described in Section 3.2.5. Other conditions that affected the bounds were unrealistic expander inlet conditions in the ORC such as the following:

1. A supercritical pressure where the turbine inlet temperature did not exceed the critical temperature

2. A subcritical case where the turbine inlet temperature did not exceed the saturation temperature

51
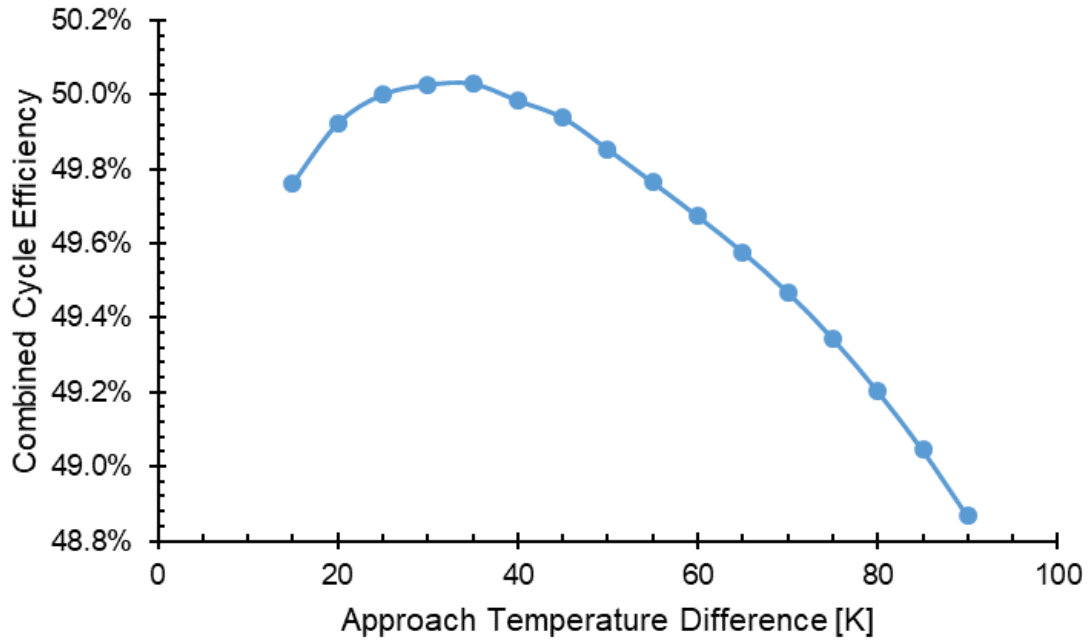
Figure 3-7. Optimized cycle configuration across various approach temperature differences
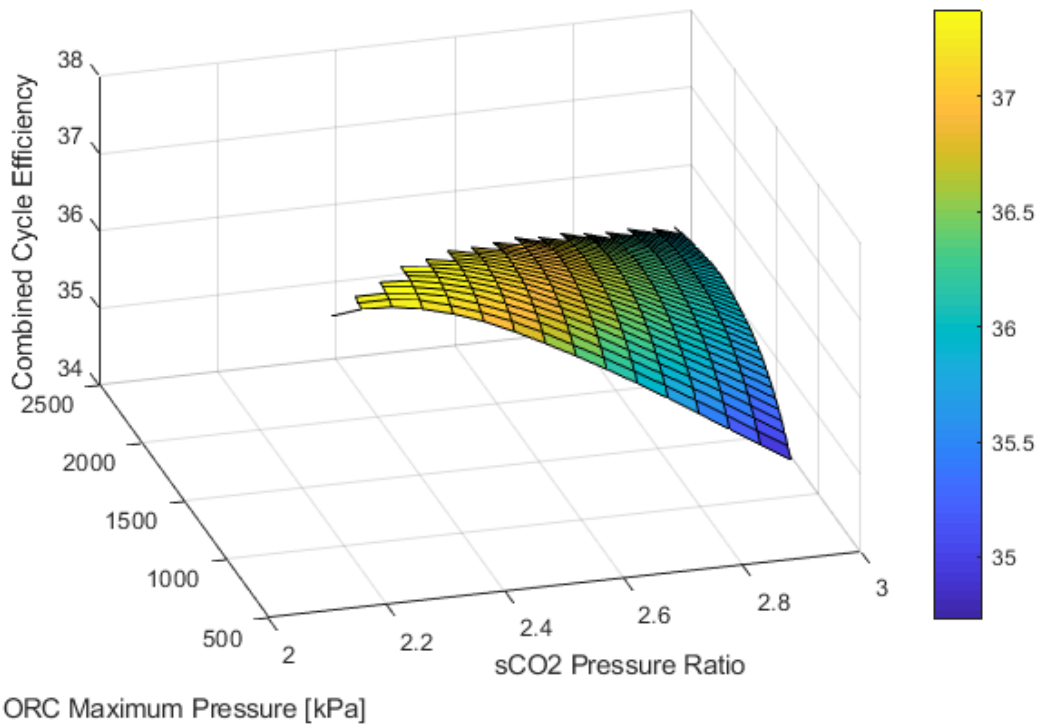

Figure 3-8. Butane combined cycle optimization with an approach pinch of 35K with sCO$_2$ recompression cycle (500°C)
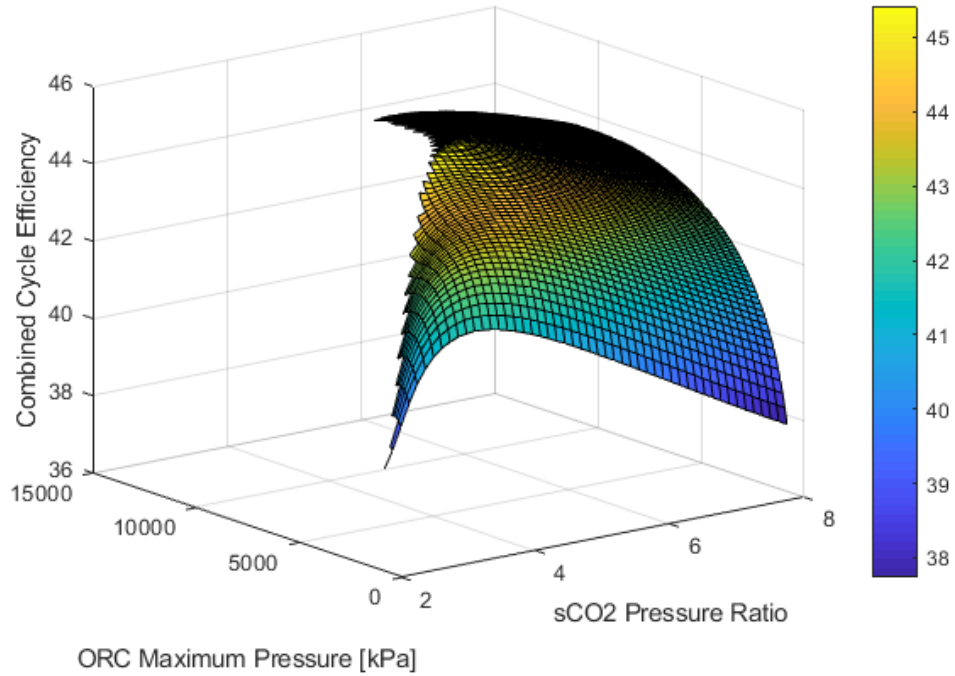
52

Figure 3-9. Butane combined cycle optimization with an approach pinch of 35K with sCO_2 recompression cycle (800°C)
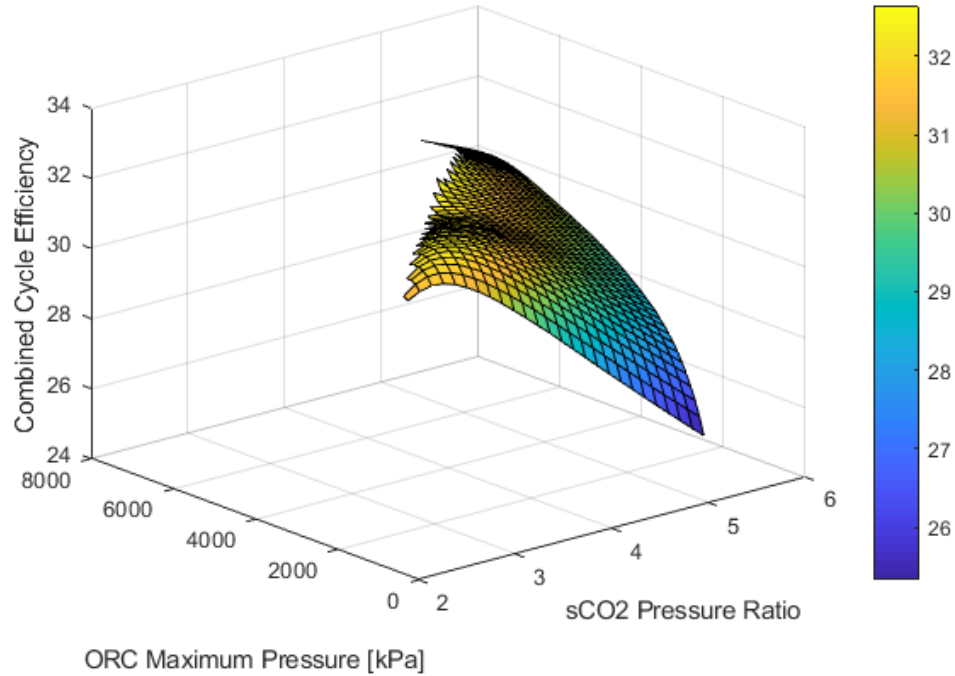

Figure 3-10. Butane combined cycle optimization with an approach pinch of 35K with sCO_2 simple cycle (500°C)

53
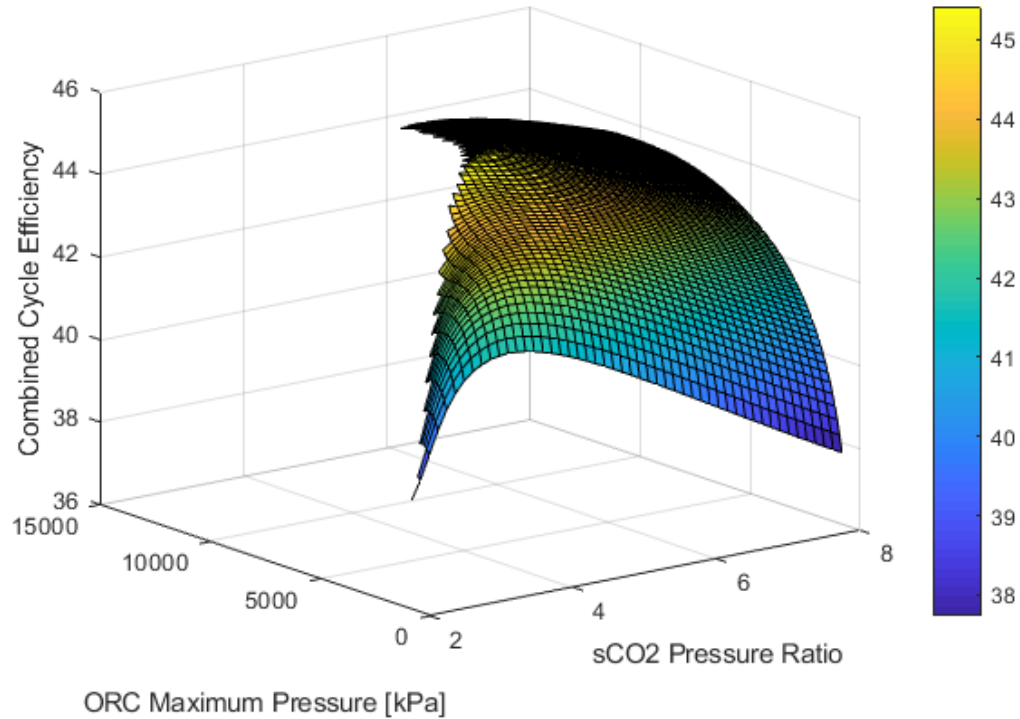
Figure 3-11. Butane combined cycle optimization with an approach pinch of 35K with sCO$_2$ recompression cycle (800°C)

Depending on the nature of the problem and the fluid properties, it appears each case has a different shape. Upon closer inspection it appears that every case has a similar shape to a degree with varying bounds. Evident in Figure 3-10 is the presence of two maxima. The critical point of butane is 3.8 MPa. One of those maxima occurs in the supercritical range, the other in the subcritical range. This phenomenon is due to the pinch point criteria and the corresponding mass flow of the working fluid for the ORC.

All of the selected working fluids were optimized in the combined cycle at an approach pinch of 35K. The results for the recompression topping cycle are show in Figure 3-13 and Figure 3-14 with a maximum temperature in the topping cycle of 500°C and 800°C, respectively. The results for the simple topping cycle are show in Figure 3-15 and Figure 3-16 with a maximum sCO$_2$ temperature 500°C and 800°C, respectively. The results are displayed with increasing combined cycle efficiency for each cycle configuration. The combined cycle performed the best

54

with the recompression topping cycle. However, the ORC performed at higher efficiencies in the simple sCO_2 Brayton cycle configurations. The ORC was able to extract more heat from the simple sCO_2 cycle. The flow splits in the recompression cycle, so less heat is available for heat recovery than in the simple cycle configuration. The resulting mass flow ratio between the bottoming and topping cycle is higher in the simple cycle cases than with the recompression cycle, as shown in Figure 3-17. This is more clearly seen for the configurations with a maximum sCO_2 of 500°C. In the 800°C cases, the mass flow of the ORC working fluid per unit mass flow of CO_2 is only marginally higher. A higher pressure ratio in the sCO_2 results in a higher temperature entering the heat recovery exchanger (Figure 3-18). Introducing a higher temperature to the ORC and increasing the maximum ORC pressure to above critical, increases the maximum temperature in the ORC cycle and therefore the efficiency. For both maximum temperatures of the sCO_2 cycle (500 and 800°C), the optimal simple configurations operated at higher temperatures and pressures in the ORC (Figure 3-19 and Figure 3-20).
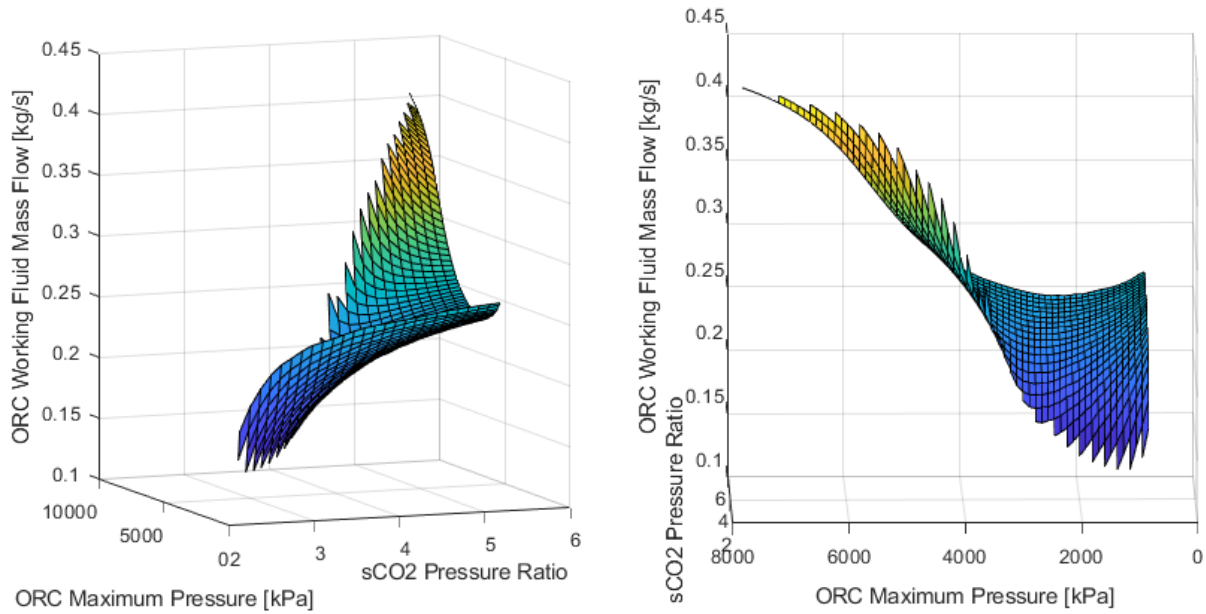
Figure 3-12. Mass flow of butane for combined cycle optimization with an approach pinch of 35K with sCO2 recompression cycle (500°C)

55
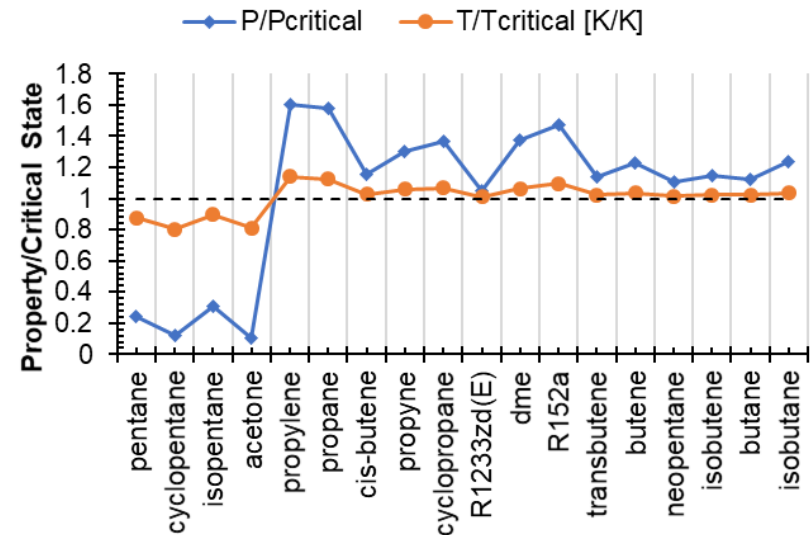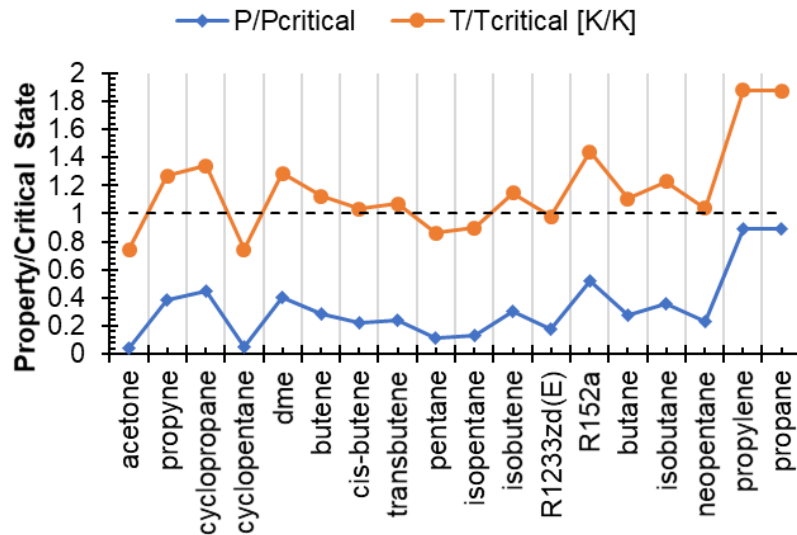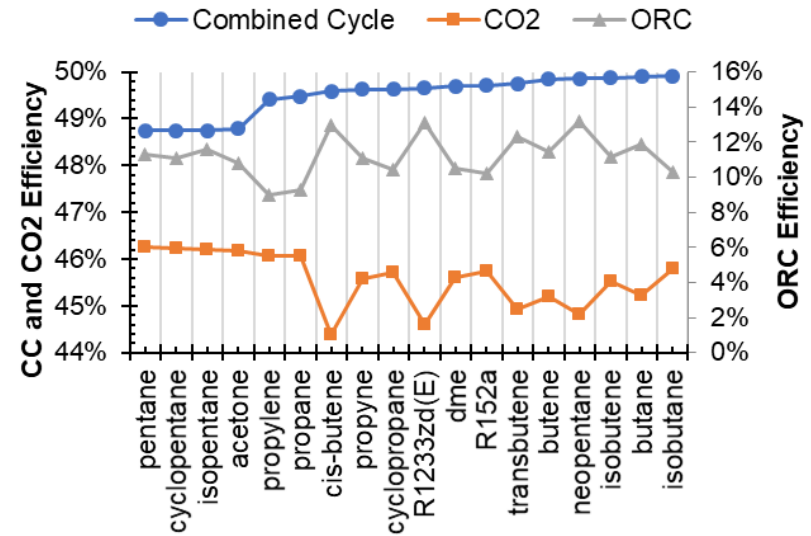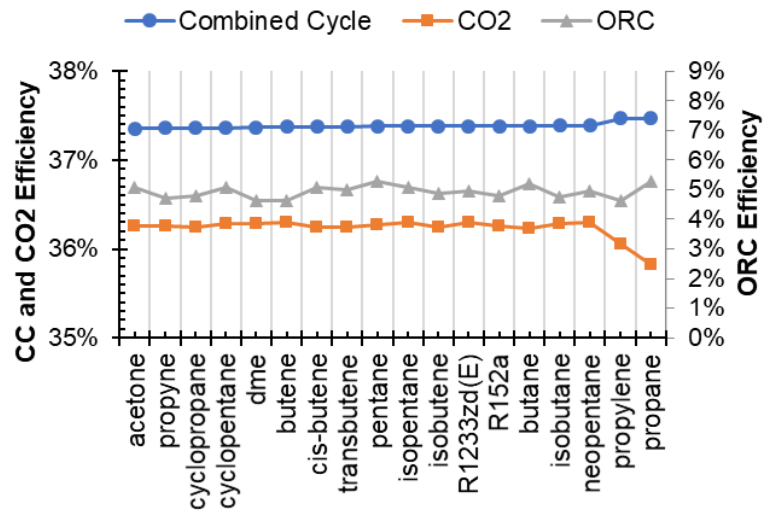
Figure 3-13. Combined cycle optimization for multiple ORC working fluids with topping sCO₂ recompression cycle (500°C)

Figure 3-14. Combined cycle optimization for multiple ORC working fluids with topping sCO₂ recompression cycle (800°C)
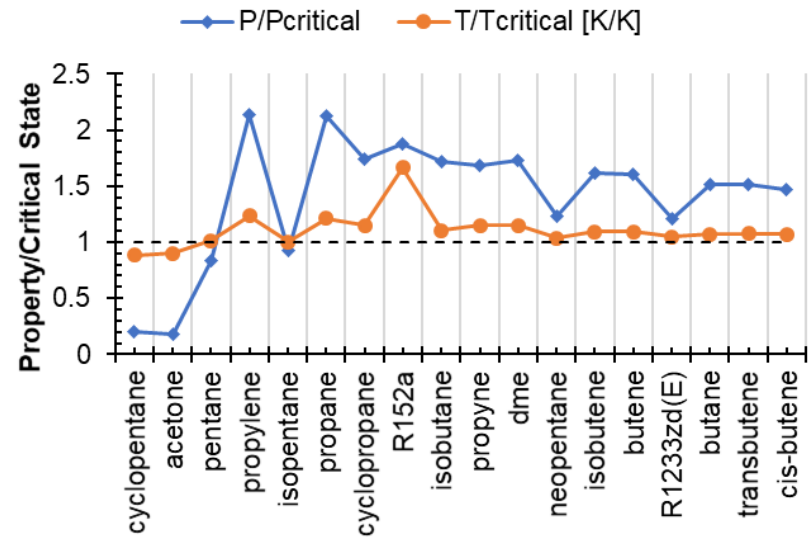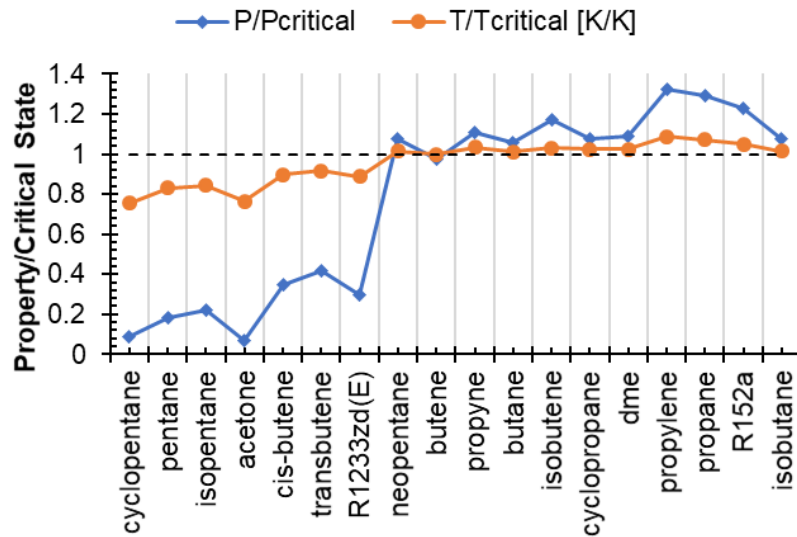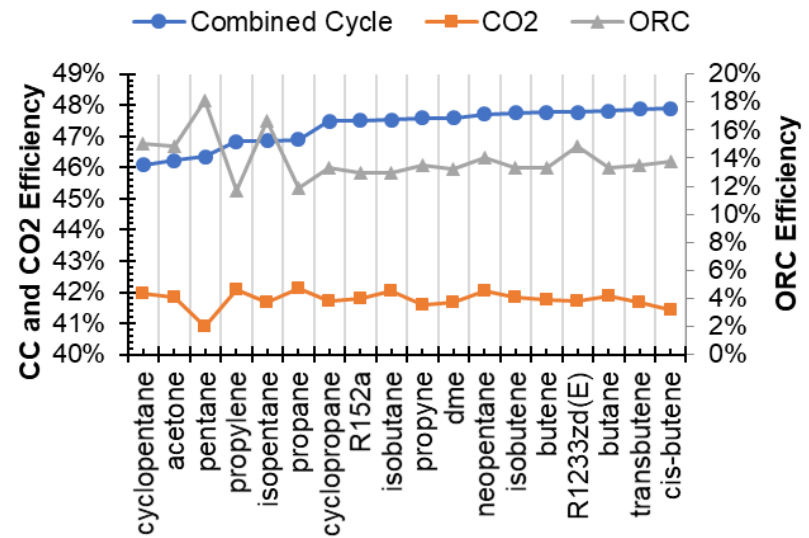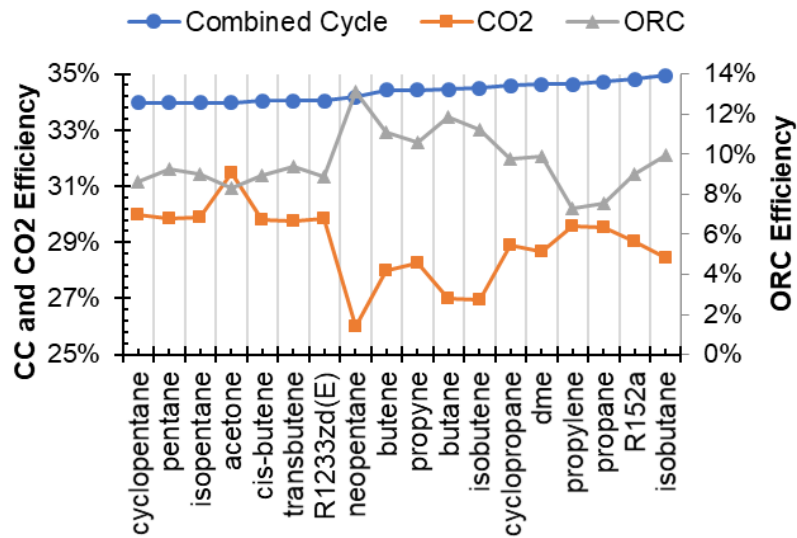
Figure 3-15. Combined cycle optimization for multiple ORC working fluids with topping sCO$_2$ simple cycle (500°C)

Figure 3-16. Combined cycle optimization for multiple ORC working fluids with topping sCO$_2$ simple cycle (800°C)

57
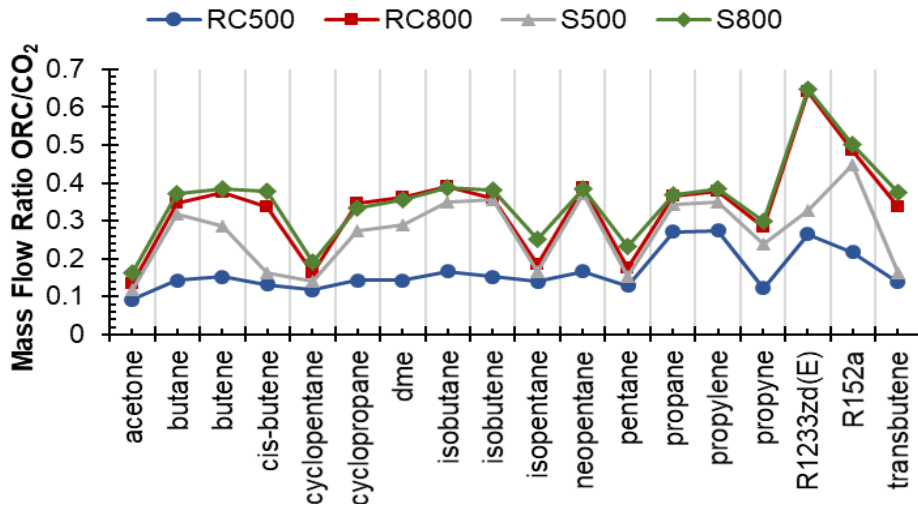
Figure 3-17. Optimal mass flow in the heat recovery heat exchanger
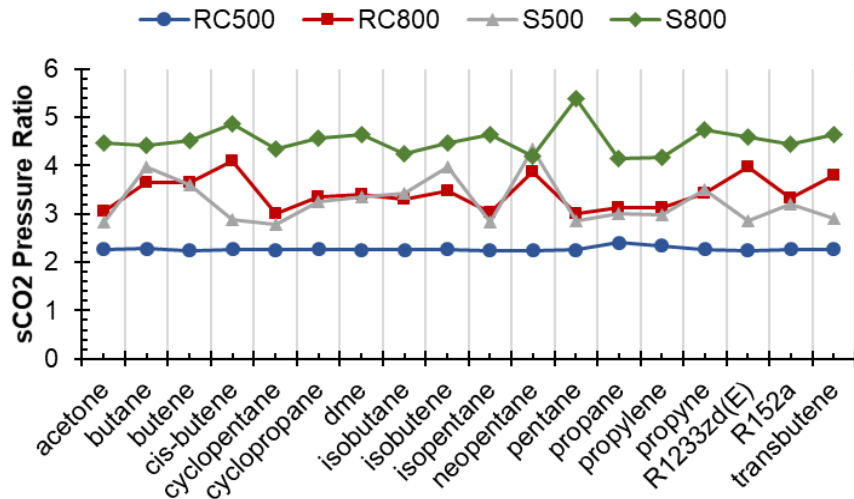
Figure 3-18. Optimal pressure ratio in sCO$_2$ cycle
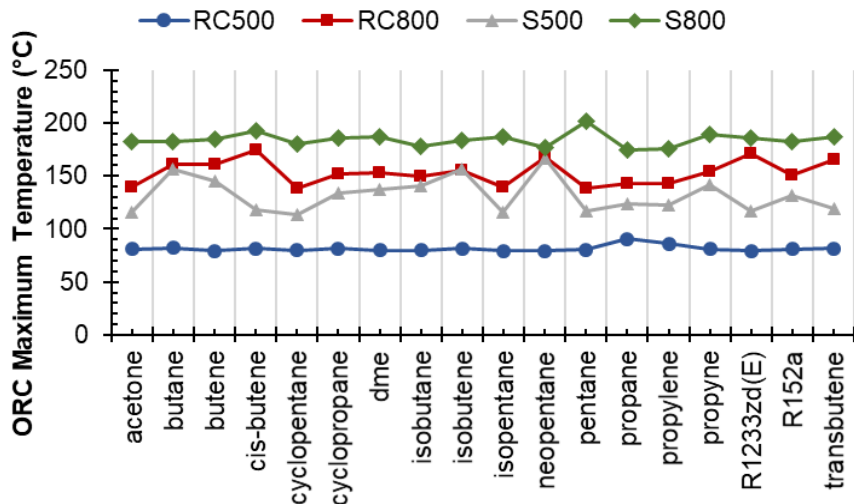
Figure 3-19. Optimal maximum ORC temperature

58
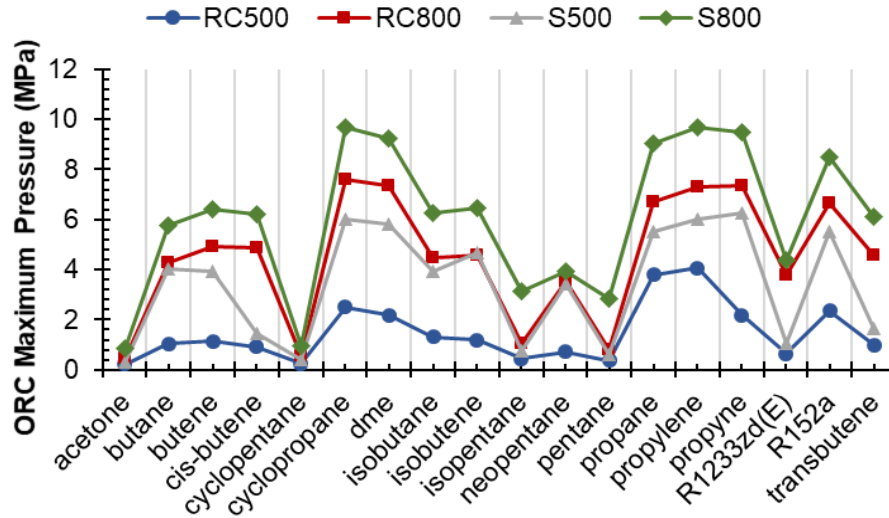
Figure 3-20. Optimal maximum ORC pressure

No one fluid performed the best in each cycle configuration. However, the difference in combined cycle efficiency between the best and worst performing fluids in the 500°C cases was 0.11% for the recompression cycles and about 1% across the simple cycles. There was larger deviation across the combined cycle at higher sCO$_2$ temperatures. Acetone, pentane, cyclopentane, and isopentane consistently did the worst in all configurations. These fluids did not perform the best in the ORC optimization in a geothermal system in the prior chapter, either. They also resulted in the lowest expansion ratios for any combined cycle configuration tested. A low expansion ratio results in less power. The combined cycle at 500°C with recompression achieved an efficiency of 37% while the simple configuration achieved 33%. For a maximum temperature of 800°C, the recompression cycle configuration outperformed the simple with a maximum efficiency of 50% compared to 46%.

3.4 Conclusion

A combined cycle of a sCO$_2$ Brayton cycle with a bottoming ORC was optimized. The approach pinch is a crucial parameter that should not be ignored. For the selected design parameters, the optimal pinch point was selected as 35K. The mechanical efficiency was also taken

59

into account to provide more of a realistic expectation for the system performance. The recompression cycle configurations out-performed the combined cycle with a topping simple cycle, as reported in the literature. However, for integration with geothermal, the bottoming cycle operating on geothermal must not be under designed. The efficiency of the ORC was much higher in the combined cycles with a simple sCO_2 cycle. Therefore, the simple configuration cannot be ignored. On the other hand, higher pressure ratios are required in the simple sCO_2 cycle, increasing the cost of the system.

CHAPTER 4: PERFORMANCE ANALYSIS OF
SOLAR THERMAL GEOTHERMAL HYBRID SYSTEMS

4.1 Introduction

Three configurations were analyzed for implementation of geothermal into a combined cycle operating on solar power tower (SPT). The base configuration is the combined cycle that was studied and optimized in the Chapter 3. The main cycle is composed of a supercritical carbon dioxide (sCO_2) Brayton cycle with a bottoming organic Rankine cycle (ORC). At its most basic operation, solar energy could power the combined cycle during the day time and geothermal could power the bottoming cycle during night or during periods of intermittency. There was only one solar-geothermal hybrid system containing SPT. Hot dry rock heated carbon dioxide that was superheated by solar energy. As reviewed in Chapter 1, most of the solar-geothermal power systems used solar energy to add extra heat to either the working fluid or the geothermal brine. This chapter analyzes the potential for geothermal to add additional heat into a combined cycle for additional power and to further utilize geothermal energy during the conversion of solar energy.

4.2 Methodology

MATLAB® was used to model the combined cycle [95]. NIST REFPROP was utilized to calculate the fluid properties [96].

4.3 Hybrid Configurations

There are three opportunities to introduce a low temperature grade source into the combined cycle where the topping cycle achieves temperatures above 500°C. The first is for the geothermal energy to preheat the carbon dioxide after compression. Figure 4-1 displays this

61
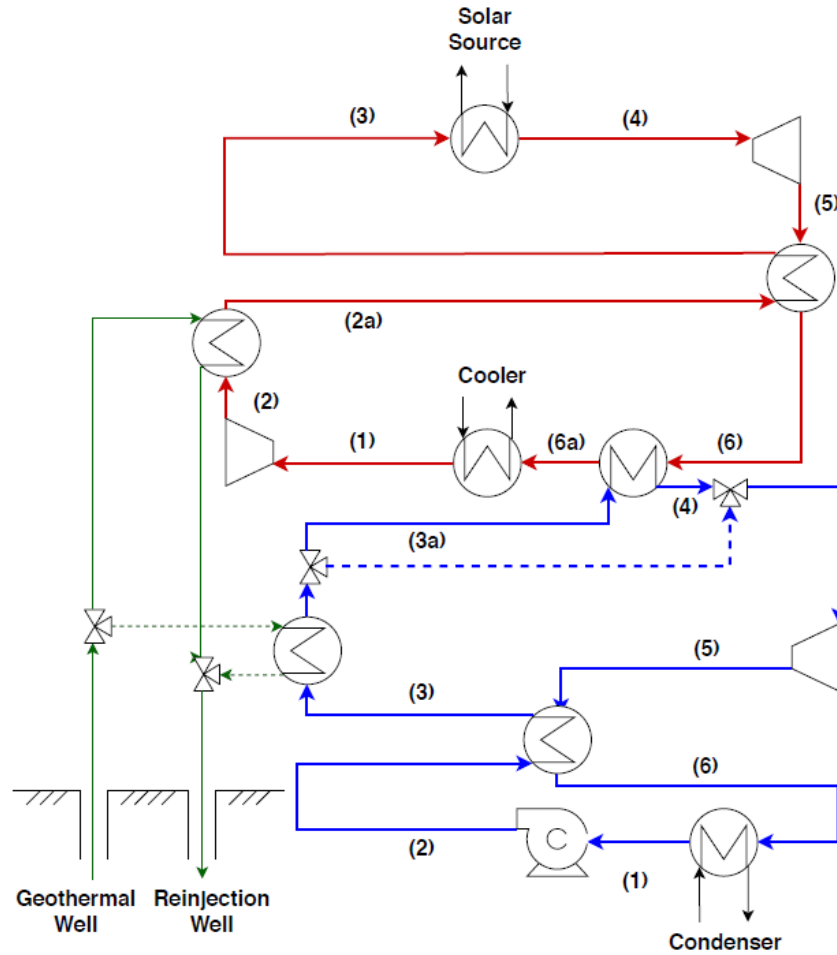
Figure 4-1. Solar geothermal hybrid preheat configuration

configuration with a topping simple sCO_2 cycle. The dotted lines indicate geothermal only operation. Limitations of this configuration are the temperature of geothermal source and the recuperation of the Brayton cycle. Recuperation is crucial to the efficiency and operation of the system. However, the addition of heat before the recuperator shifts the low temperatures of the low temperature recuperator up, increasing the heat available to the bottoming cycle. Essentially, this system introduces low temperature heat to be used at a higher quality and temperature later in the cycle. This configuration will be referred to as the "preheat system".

The second configuration is the "reheat system" (Figure 4-2). The low-pressure CO_2 leaving the recuperator will be heated by geothermal before being sent to the heat recovery. The

62
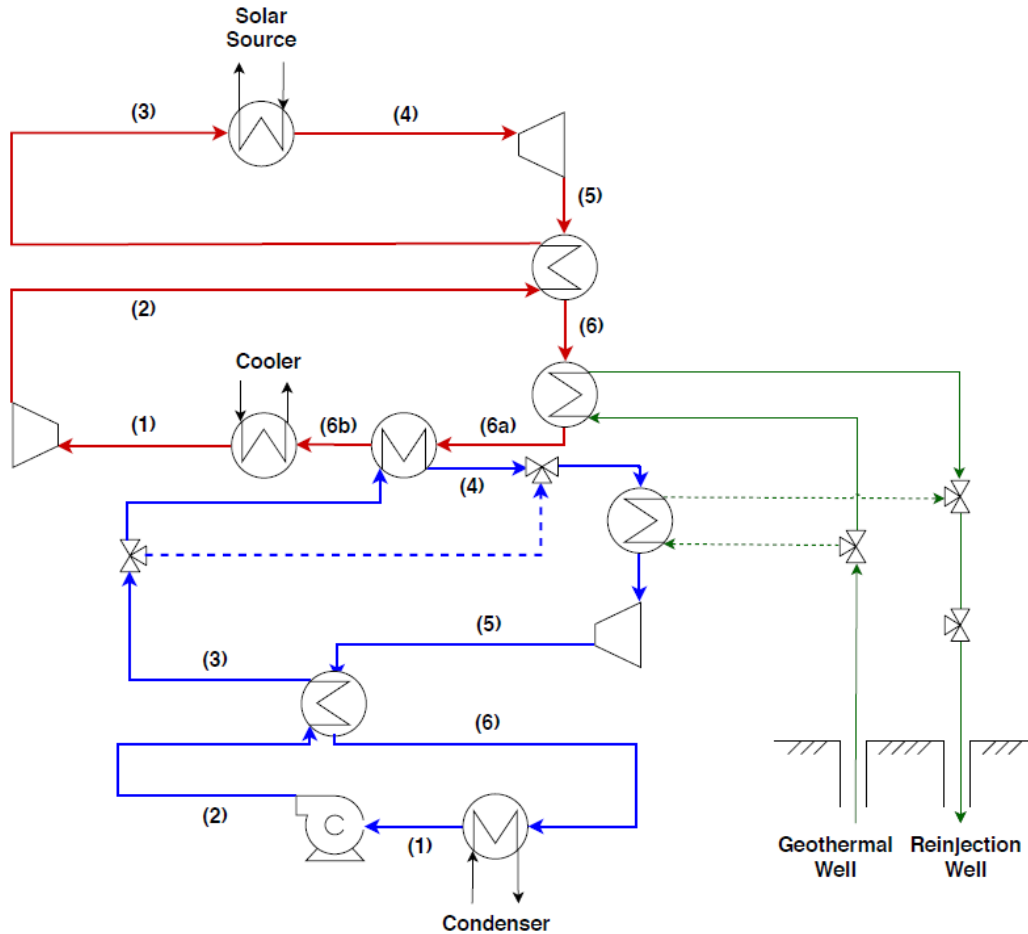
Figure 4-2. Solar geothermal hybrid reheat configuration

final system uses geothermal to superheat the ORC working fluid after leaving the heat recovery

unit (Figure 4-3). This is akin to using SPT to superheat the ORC working fluid of a binary system.

A key performance factor to describe hybrid systems is the efficiency of the additional

component [23,32,38,101]. In all of these cases, solar energy was used to supplement geothermal

and the additional work produced in comparison to solar energy added to the system was

compared. In these cases, this term was called the incremental or additional efficiency. This can

be misleading as it does not represent the whole system nor is it a difference between the hybrid

and original stand-alone systems. This factor will be called the incremental effectiveness in this

study. This effectiveness shows ratio of incremental work that was converted from the incremental

63

amount of heat added to the system from the stand-alone combined cycle operating only on solar energy or a high temperature source in comparison to the hybrid system with geothermal heat added. In the preheat case, the amount of solar energy is reduced with the addition geothermal energy, therefore the incremental heat added to the system is less than the amount of geothermal heat. For the reheat and superheat cases, the incremental heat is the amount of geothermal energy added to the system.

$$\varepsilon_{\text{inc}} = \frac{\dot{W}_{\text{net,hybrid}} - \dot{W}_{\text{net,CC}}}{\dot{Q}_{in,\text{hybrid}} - \dot{Q}_{in,\text{CC}}} \tag{4-1}$$

The reinjection temperature for a geothermal well is dependent on the dissolved solids. This varies from location to location but has been restricted to 70°C in the literature. To keep the
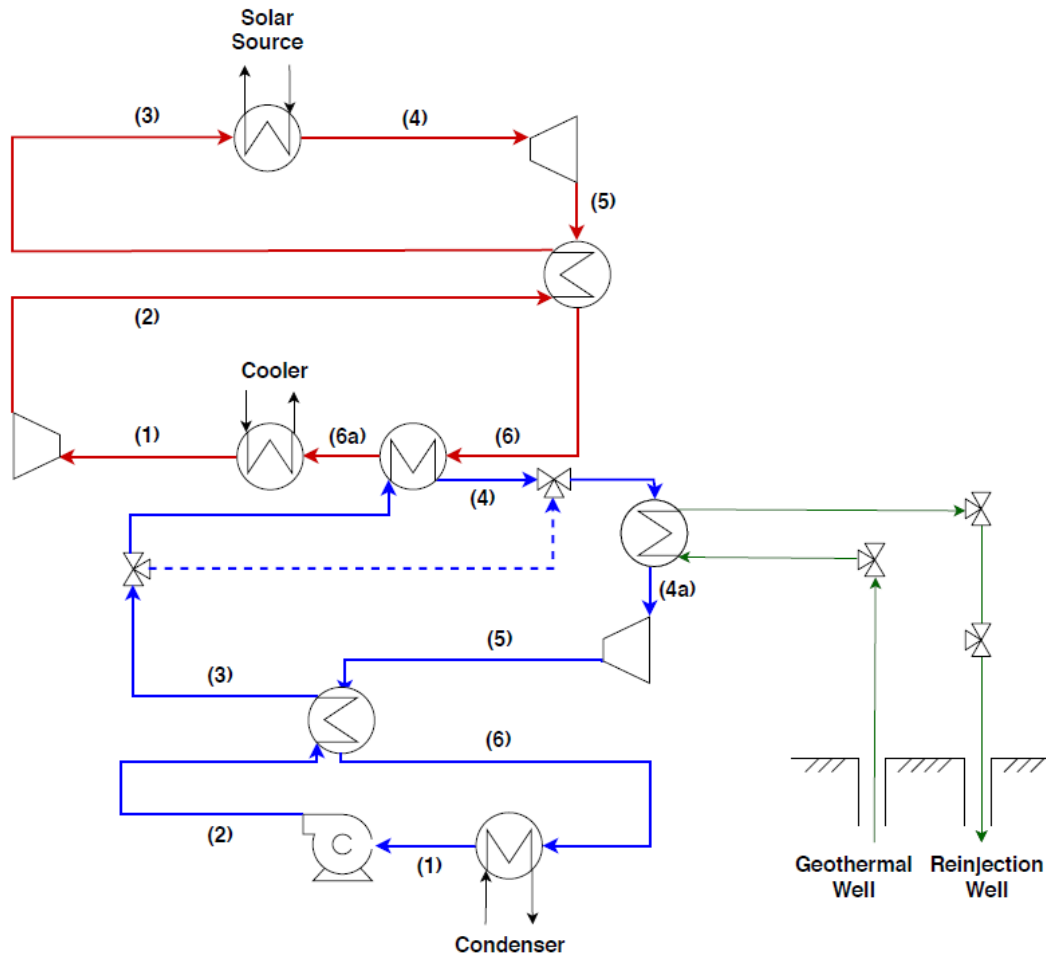
Figure 4-3. Solar geothermal hybrid superheat configuration

64

analysis consistent between systems, the minimum geothermal temperature was limited to 70°C. In chapter 2, the minimum ORC cycle temperature for a geothermal system was set to 25°C, allowing the geothermal source to cool below 70°C. The lowest cycle temperature was set to 55°C in this chapter, consistent with Chapter 3. This temperature represents the 99.6[th] percentile temperature that can be accommodated by ambient cooling air or water in the condensers and cooler for Stillwater, NV. This temperature limit impacts how effectively geothermal can benefit the combined cycle. The geothermal source temperature was selected as 200°C, representative of medium-temperature geothermal sources. In some instances, the geothermal temperature was not hot enough to add additional heat to the system at its point of interaction; these cases were removed from the analysis.

The optimized approach pinch value for the stand-alone combined cycle system was found to be 35K in the prior chapter and the same value was used in this analysis. Regardless of configuration, the approach pinch was set as the difference between the temperature of the CO_2 fluid entering the heat recovery heat exchanger, and the temperature of organic working fluid leaving the heat recovery unit.

The simulation was performed at the optimized conditions found for the combined cycle in the prior chapter to determine how the addition of geothermal energy directly into the combined cycle would affect the system. The operating parameters are found in Table 3-1.

The following assumptions were used in the analysis:

- No heat losses or pressure drop in heat exchangers or piping
- Expansion and compression processes are adiabatic
- Auxiliary power consumption is negligible
- Each process has reached steady state operation

65

4.4 Results and Discussion

The incremental effectiveness and combined cycle efficiency results are shown in Figure 4-4 through Figure 4-11. Except for propane in the preheat cycle, the geothermal source was not hot enough for the preheat and reheat configurations including a combined cycle with a topping simple cycle and a high temperature of 800°C. Initially, it appears reheat and superheat should be sufficient for all configurations. However, in the case of the reheat system, the geothermal source must be a higher temperature than the low-pressure CO_2 exiting the recuperator. The organic Rankine cycle included a recuperator. This is beneficial for supercritical conditions where the temperature gradients in the high and low-pressure sides are parallel, unlike a subcritical ORC. Achieving a higher temperature in the cycle, increases the amount of heat that is recuperated, reducing the amount of heat that can be extracted for the topping cycle. For some cases for the reheat and superheat systems, the recuperator prevented the ORC from reaching the final design temperature in the cycle; the high-pressure working fluid exiting the recuperator would be higher than the temperature of the heat source. These instances were removed from the analysis.

The superheat systems had the highest incremental effectiveness and highest combined cycle efficiency for most points as evident in Figure 4-4 through Figure 4-7. However, the superheat systems did not result in the highest combined cycle efficiencies. While the superheat system was the best for the recompression sCO_2 cycle with a maximum temperature of 500°C, the preheat and reheat systems were fairly comparable in terms of combined cycle efficiency for the rest of the analyzed cases. The hybrid systems with a simple topping cycle at 500°C outperformed the ones with recompression at 500°C with almost double the incremental effectiveness. The simple cycle contains less components and heat exchangers and can be more cost-effective than the recompression sCO2 cycle. Introducing geothermal into a combined cycle with a simple

66

Figure 4-4. Incremental effectiveness for sCO$_2$ recompression 500°C
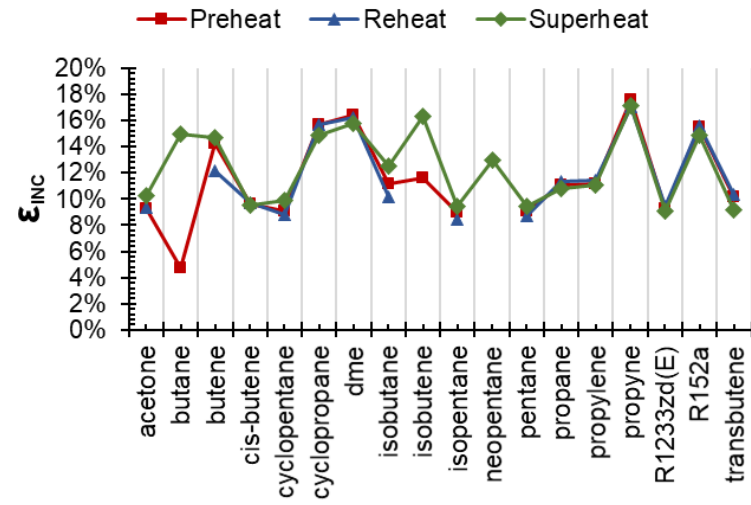
Figure 4-5. Incremental effectiveness for simple sCO$_2$ 500°C
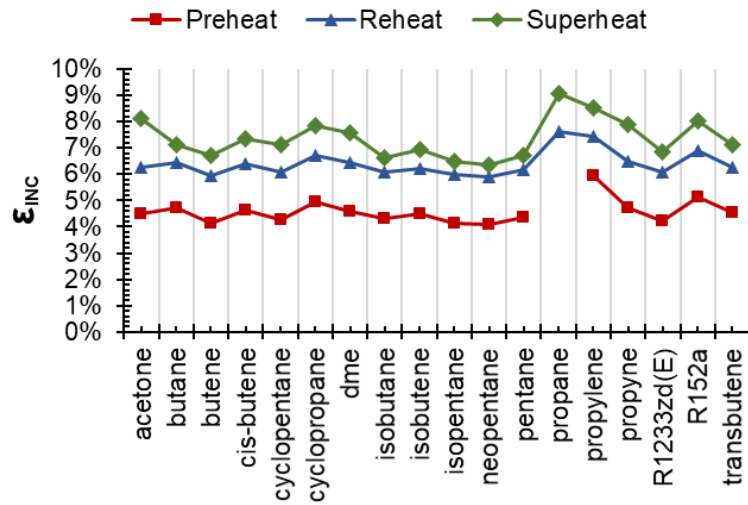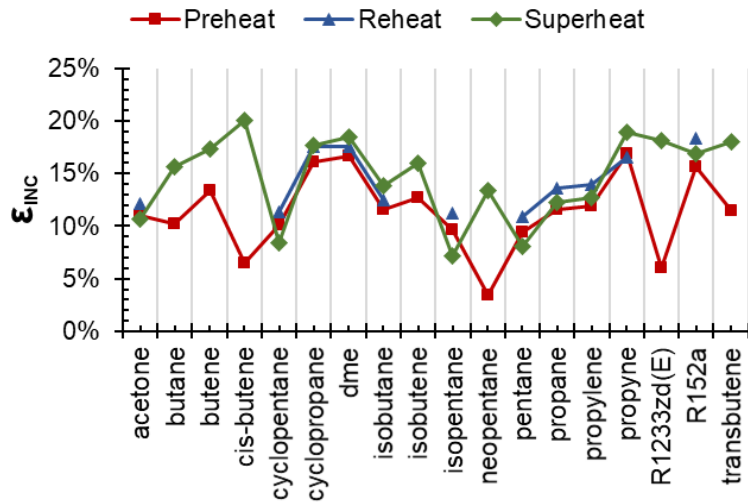

Figure 4-6. Incremental effectiveness for recompression sCO$_2$ 800°C
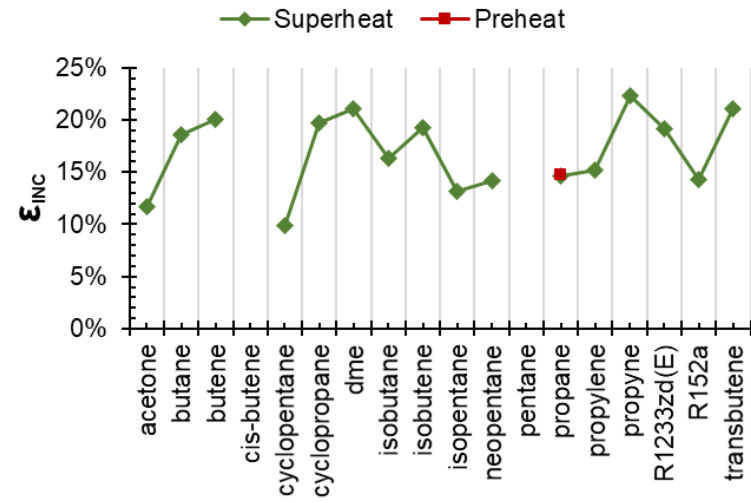
Figure 4-7. Incremental effectiveness for simple sCO$_2$ 800°C

67
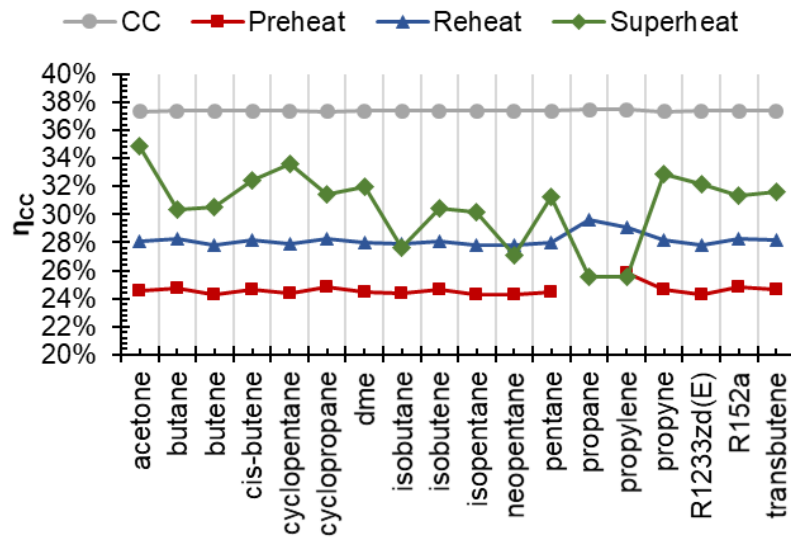
Figure 4-8. Combined cycle efficiency for recompression 500°C
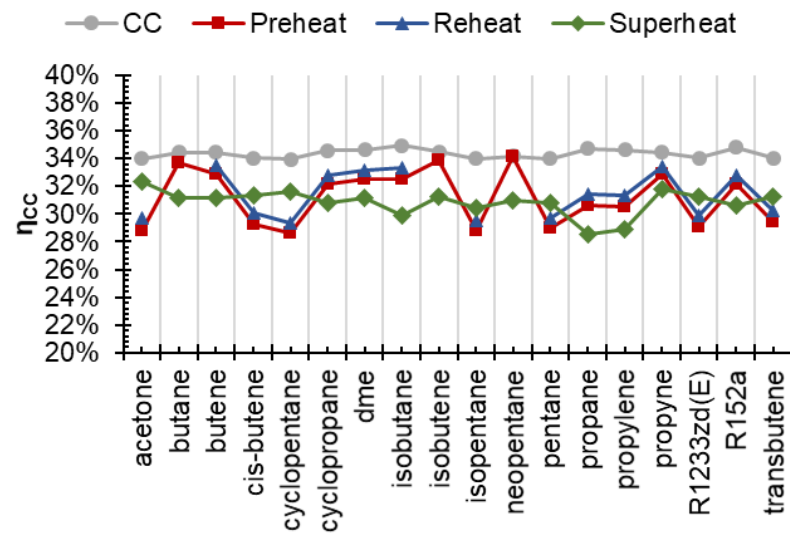
Figure 4-9. Combined cycle efficiency for recompression 500°C
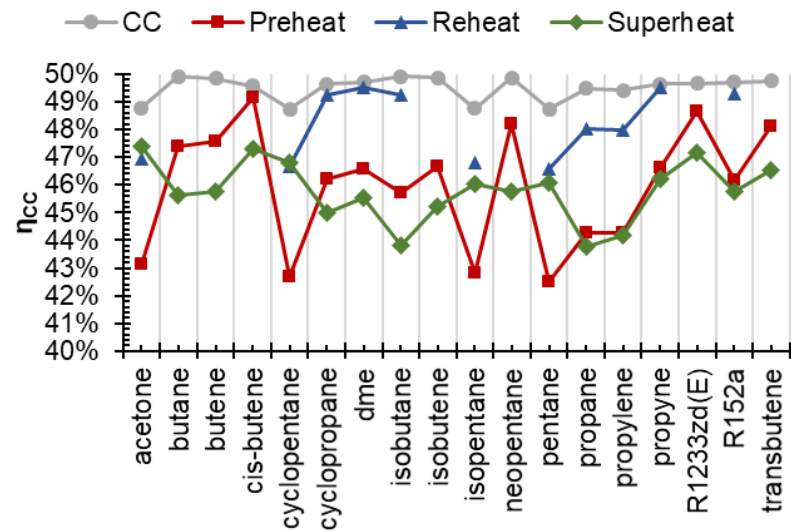
Figure 4-10. Combined efficiency for recompression 800°C
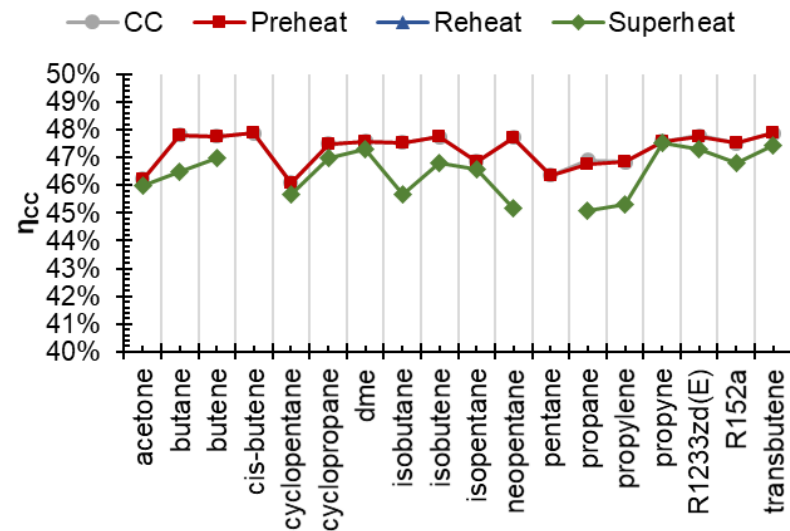
Figure 4-11. Combined efficiency for recompression 800°C

68

topping Brayton cycle would be very beneficial to the system. Cyclopropane, propylene, and dme were the ORC working fluids that converted the extra heat from geothermal the most effectively compared to the non-hybrid combined cycle.

The incremental effectiveness for the systems with a simple sCO_2 cycle was much higher than for the recompression cases. While the stand-alone combined cycle or a combined cycle operating only with solar energy is far more efficient with a recompression as opposed to a simple sCO_2 cycle, the hybrid configuration makes the simple system much more competitive. Closer combined cycle efficiencies are achieved between the two setups, yet the best recompression cases still outperform the best simple cases. The incremental effectiveness cannot be taken in alone. There is a trade-off with the incremental effectiveness and how much geothermal heat was added to the system. The system needs to be able to convert the heat input from both solar and geothermal effectively. At a sCO_2 upper temperature of 500°C, the superheat recompression case with acetone in the ORC performed the best in combined cycle efficiency (34.8%). This was about 1% higher than the best simple configuration at 500°C for isobutene in the preheat hybrid system. At 800°C, dme in the reheat configuration with a recompression sCO_2 achieved the best combined cycle efficiency (49.5%). These cases did not have the best incremental effectiveness but were in the top 30% for incremental effectiveness for their respective categories.

As the pressures for both cycles were optimized for the stand-alone cycle, the ORC upper pressure was held constant for each hybrid configuration. The ORC expander inlet temperature in respect to the critical point is shown in Figure 4-12 for the four combined cycles analyzed as well as for the optimized condition for the stand-alone geothermal operation. The geothermal cycle was optimized for the plant efficiency (Chapter 2) but with the operating conditions for the ORC of this chapter. The condensing temperature was increased from 25 to 55°C and the expansion ratio

69

was limited to 20. The optimized ORC pressure for the simple combined cycle at 800°C was the closest to the resulting geothermal optimization. In the superheat hybrid configuration with simple sCO$_2$ at 800°C, all ORC fluids achieved a maximum temperature of 190°C, the same as in the geothermal case. This was limited by the selected pinch point of 10°C. Therefore, the combined cycle with a simple sCO$_2$ Brayton cycle with a maximum temperature of 800°C is the best configuration to operate the ORC efficiently in the hybrid system or with only geothermal heat.
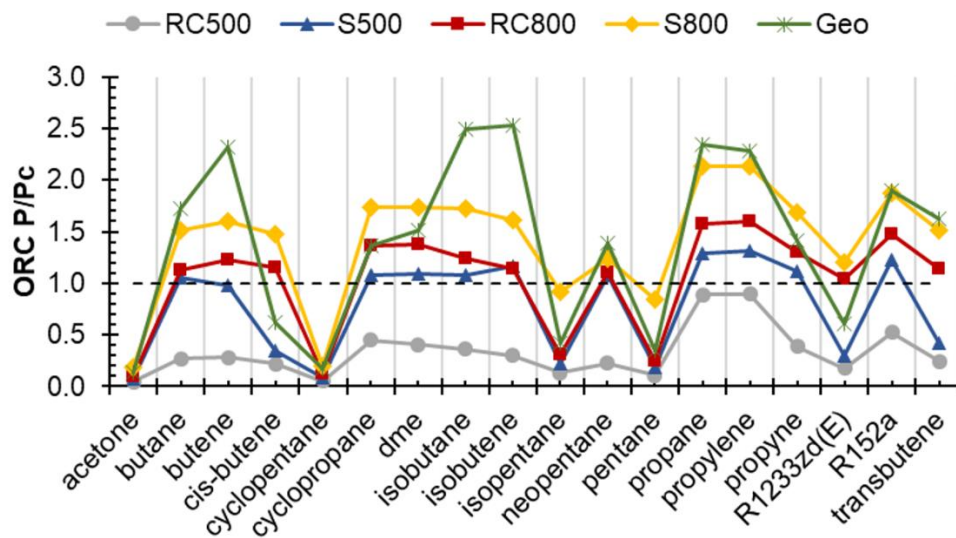
Figure 4-12. Optimized ORC upper pressure for recompression (RC) and simple (S) combined cycles as well as stand-alone geothermal

4.5 Conclusion

In the analysis, the approach pinch in the heat recovery unit was held constant. There is an opportunity to optimize this to further improve the system. The superheat and reheat configurations would benefit from optimizing this value the most to ensure the most heat is being recovered from topping cycle as possible, despite the recuperation in the ORC. For further improvement, the upper pressure of the ORC can be optimized especially for the superheat hybrid system as it is the most capable of achieving the highest temperatures in the ORC. Higher turbine inlet temperatures result

in higher optimized pressures. Cyclopropane, propylene, and dme were the fluids that performed the best with the additional heat. However, acetone (subcritical ORC) and dme (supercritical ORC) achieved the best hybrid configurations with a recompression topping cycle for maximum temperatures of 500 and 800°C, respectively. The superheating hybrid system with a simple topping cycle with a maximum temperature of 800°C was found as the optimal configuration for hybrid and geothermal only operation.

71

CHAPTER 5: TRANSIENT ANALYSIS OF A
SOLAR THERMAL GEOTHERMAL HYBRID SYSTEM

5.1 Introduction

The prior analyses were steady state simulations where operation and parameters were constant. In actual operation, there are transients, especially with solar energy. When studying an innovative system, it is important to determine the performance in more realistic conditions. In the literature, many state-of-the-art renewable energy systems have been simulated in transient conditions. There is an opportunity to apply thermal storage to the hybrid system to extend the availability of the high temperature source through the night. This chapter analyzes the performance throughout the year of the system.

5.2 Methodology

EBSILON® Professional was used for the transient analysis. EBSILON® Professional is a component-based software that solves for steady state or transient operation using energy and mass balance around each component. NIST REFPROP was utilized to calculate the working fluid properties in the ORC [1].

First the system was validated against the work from Chapter 4. The operating conditions matched within 2%. Once modeled and validated in steady state operation, the off-design operating conditions were selected.

5.2.1 Design Conditions

The solar field was modeled after GEMASOLAR, the first commercial solar tower plant with molten salt storage located in Spain [102]. The system has a 120 MWth solar receiver and a

72

y

3819 m^3 storage tank suitable for about 15 hours of storage with 19.9MWe of turbine power [102]. The power block at GEMASOLAR is a reheat steam Rankine cycle [103]. With these conditions in Stillwater, NV, the solar field was not large enough to fully charge the storage tank. Therefore, the same solar field was used, however, the turbine power of the topping cycle was limited to 10 MWe. Two levels of storage were analyzed: 2,000 and 4,000 tonnes of molten salt. The solar field characteristics were used from the work on GEMASOLAR from the literature [103–105].

The power block was selected from the best operating system from the hybrid combined cycle analysis in Chapter 4. The upper temperature of the topping cycle was chosen to be 500°C to work with molten salt as the heat transfer fluid through the solar field. Solar salt (60% NaNO$_3$ 40% KNO$_3$) is commonly used and cost effective but is only thermally stable up to 585°C [105]. The configuration with the maximum combined cycle efficiency was selected as the power system. The recompression sCO$_2$ topping cycle with a bottoming ORC superheated with geothermal heat achieved a combined cycle efficiency of 34.89% using acetone as the working fluid. This hybrid configuration had a 9.06% incremental effectiveness with geothermal energy in comparison to the stand-alone combined cycle with only solar energy. The selected operating conditions are listed in Table 5-1.

Table 5-1. Transient modeling parameters

Parameter	Value
CO$_2$ Cycle Parameters	
CO2 mass flow	1 kg/s
Minimum cycle temperature	55°C
Maximum cycle pressure	25 MPa
Turbine isentropic efficiency	90%
Compressor isentropic efficiency	89%
Turbine mechanical efficiency	98%
Compressor mechanical efficiency	95%
Hot stream effectiveness	0.95
Recuperator pinch point	5°C

Table 5-1 (Continued)

Parameter	Value
ORC Cycle Parameters	
Minimum cycle temperature	55°C
Expander isentropic efficiency	87%
Compressor isentropic efficiency	85%
Turbine mechanical efficiency	90%
Compressor mechanical efficiency	90%
Internal heat exchanger (IHE) effectiveness	0.8
Pinch Point	10°C
Geothermal Parameters	
Maximum well temperature	200°C
Solar Field Parameters	
Latitude (Stillwater, NV)	
Longitude (Stillwater, NV)	
Number of heliostats	2,650
Total reflective area	306,658 m^2
Tower height	258 m
Receiver coating emittance	0.1
Receiver coating absorptance	0.95
Tracking power per heliostat	0.055 kW_e
Tower height	134 m
Receiver height	16 m
Receiver diameter	8 m
Receiver view	360°
Mirror reflectivity	0.93
Heat transfer fluid pump isentropic efficiency	0.85

5.2.2 Operating States

To operate in transient conditions, controls were put in place to stabilize outputs. There were three operating states that were selected to operate the transient conditions. These states were based on the solar radiation available and the amount of thermal storage available. The main operating state was the "Storage" state. This operating condition was used for charging and discharging the storage. The turbine power output of the topping cycle was controlled to 10 MWe by controlling the mass flow of the working fluid (sCO_2). The mass flow of the heat transfer fluid

74

was adjusted to provide sufficient heat and to control the temperature difference of the heat transfer fluid in the primary heat exchanger of the sCO_2 cycle. The mass flow of the molten salt through the solar receiver was controlled to maintain the maximum temperature of 515°C. Even though this is a closed loop, the mass flow of the heat transfer fluid at the sCO_2 heat exchanger and through the solar field do not have to be equal. If they are equal, the thermal storage is neither being charged nor discharged. A mismatch in the mass flows charges or discharges the hot storage tank (during solar radiation).

During the day, if the hot storage tank was within one kilogram of being filled, the system was set to the "Defocus" state (Figure 5-1). The heat transfer fluid (HTF) flow from the solar field was redirected away from the hot storage tank and directly to the primary heat exchanger of the sCO_2 cycle. The flowrate of the heat transfer fluid was regulated by the needs of the primary heat exchanger to ensure the sCO_2 reached the maximum temperature of 500°C and produced a constant
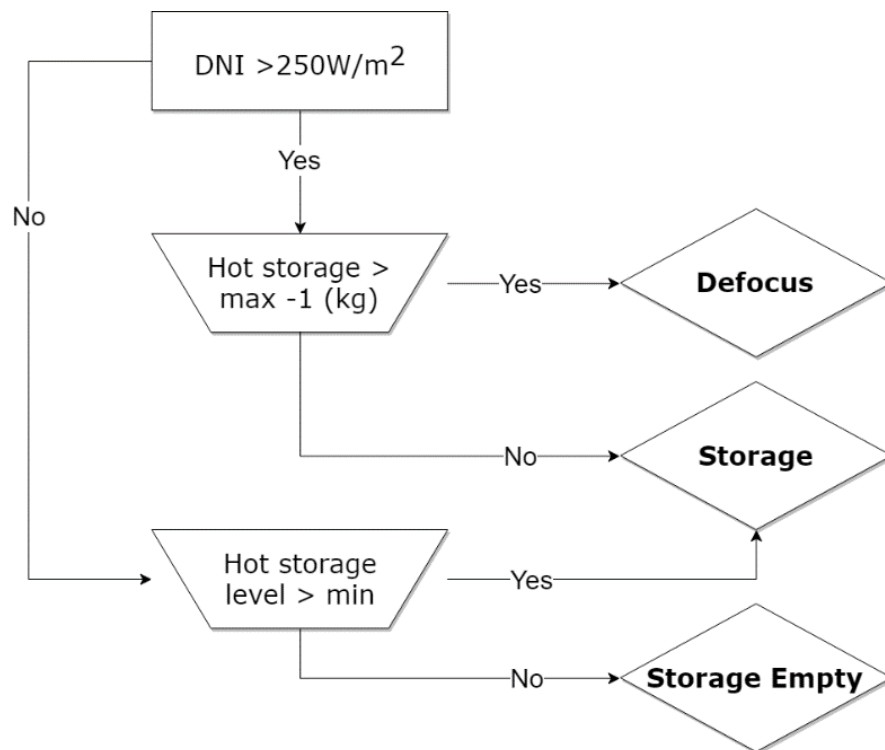
Figure 5-1. Flowchart of off-design states for transient analysis

75

power of 10 MWe. If the maximum flow from the solar field was not sufficient, the thermal storage tank was used to supplement the heat demand.

If the storage tank was empty during the night, the third off-design condition, "Empty Storage" was used. The heat transfer fluid and sCO_2 loops were shut down and the ORC was run only by geothermal energy. The control states are also illustrated in Figure 5-1. This working fluid mass flow of the ORC was operated at the same flowrate as the hybrid operation to limit the effect of off-design conditions.

5.3 Results and Discussion

Two levels of storage were used in the analysis: 2,000 and 4,000 metric tons (tonnes). The minimum storage tank level was assumed as 500 tonnes, reducing the useful storage to 1,500 and 3,500 tonnes. For the low-level storage case (Figure 5-2), the storage size is heavily undersized. The 21st day of each month was modeled. The storage tank was set to empty, and the simulation was started at 5am the day before to give the system a chance to stabilize the storage tank levels
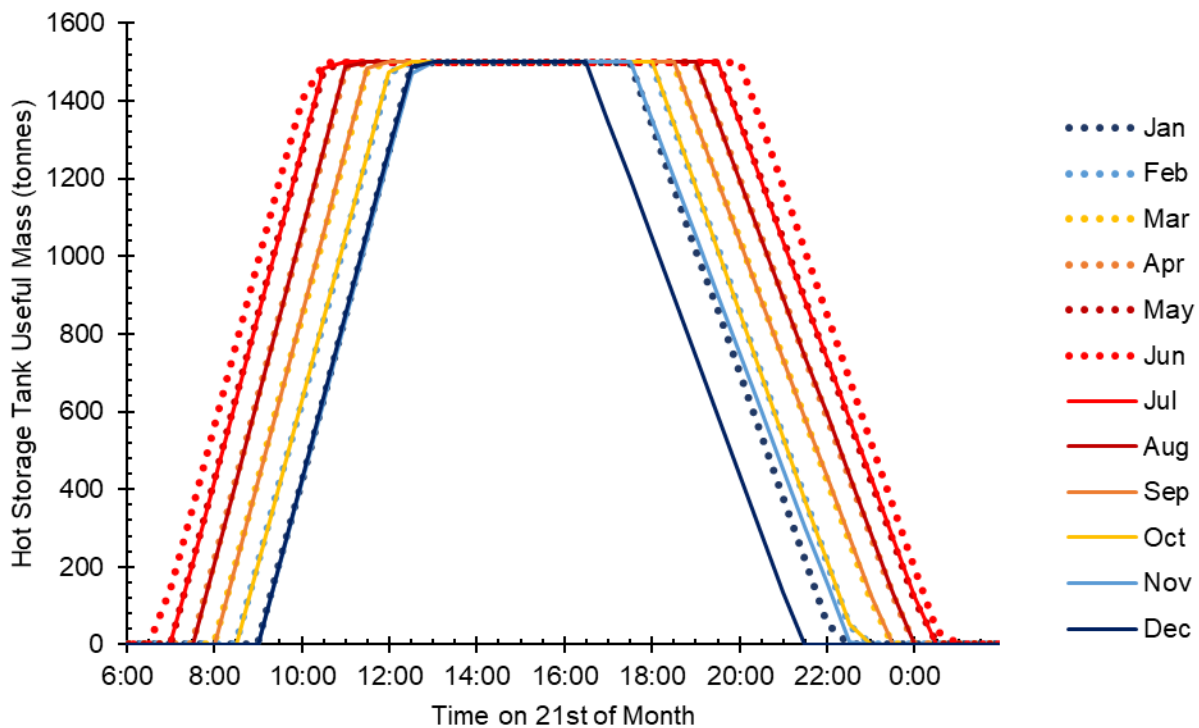
Figure 5-2. Hot storage tank level on 21st of month for low level storage case (2,000 tonnes)

76

during operation. The storage takes about 2 hours to charge and discharge. This is done at a constant rate as solar radiation was available to meet the demands of the power block. When the solar radiation peaks, the extra energy is not redirected into storage or used in the power block. The power block was controlled to operate at constant power (Figure 5-3). Even with a constant rate of charging the thermal storage tank, the solar multiple is clearly large enough to provide more thermal storage. For the worst-case scenario in December, the storage was enough with the radiation to provide high power between 9am and 9pm. For June this extended for 6 am to 2am the following day.

The total storage mass was doubled to 4,000 tonnes, saving 500 tonnes for the minimum level of storage. As shown in Figure 5-4, there was not enough solar radiation to fully charge the storage tank in November, December, and January. May, June and July, however, were fully charged for about 6 hours, requiring running in the Defocus state and wasting the additional solar energy available in the middle of the day. June and July had enough storage to operate at maximum
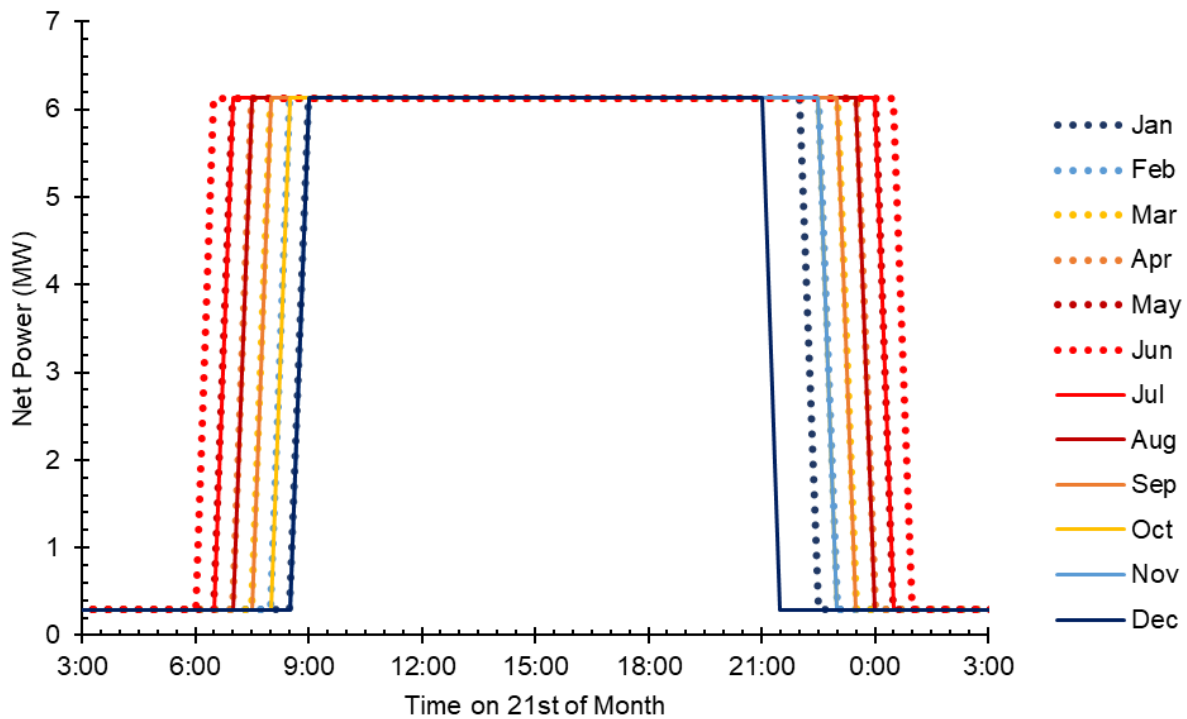
Figure 5-3. Net power for low level storage case on the 21st of each month (2,000 tonnes)

77

power for the whole day. In December, the system operated for 6 hours during the night with only geothermal energy.
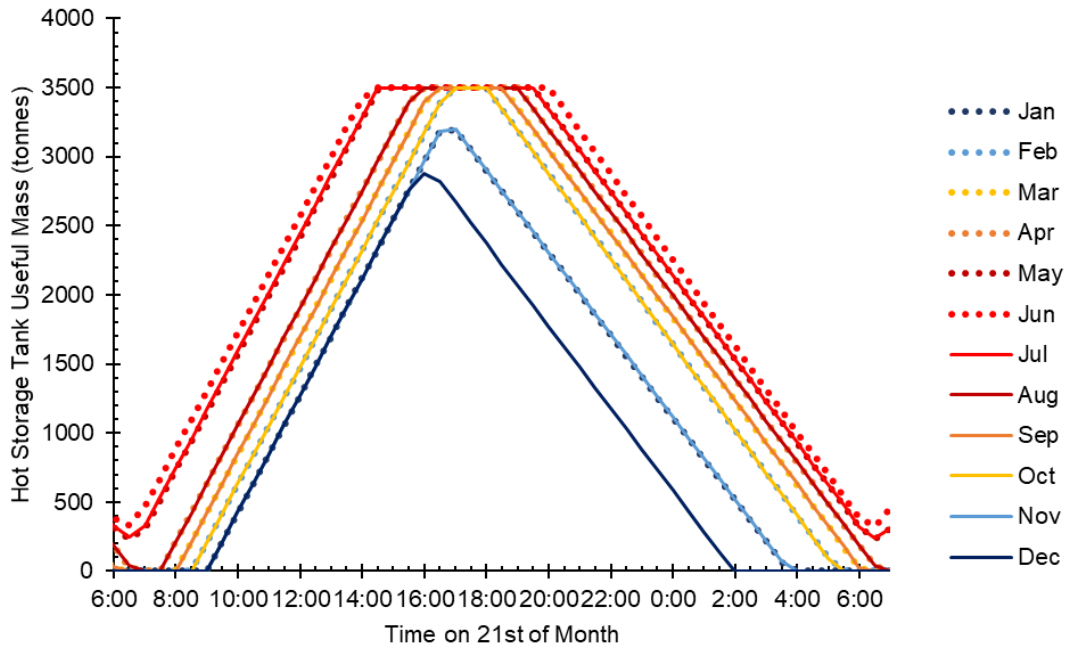
Figure 5-4. Hot storage tank level on 21st of month for high level storage case (4,000 tonnes)
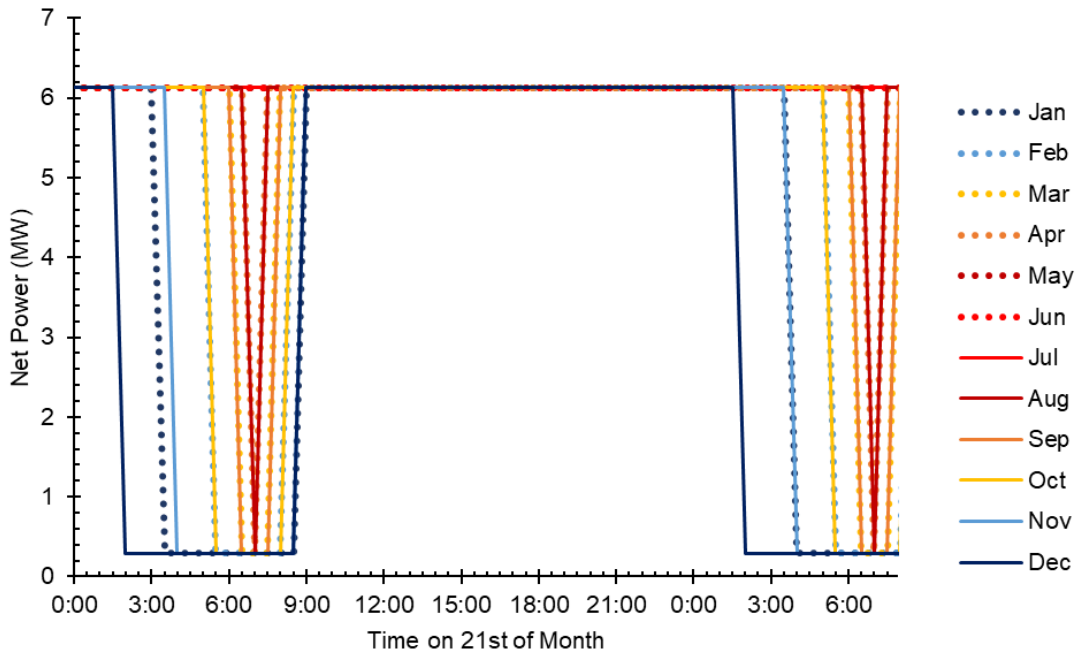
Figure 5-5. Net power for high level storage case on the 21st of each month (4,000 tonnes)

5.4 Conclusion

A hybrid solar-thermal geothermal system was modeled over the course of the year to determine the transient operating conditions. Thermal storage energy can extend the availability of the high temperature source, increasing the time of hybrid operations and limiting the lower efficient geothermal only operation. As the controls were not the focus of this analysis, they were limited to keep the power block at design conditions. There is an opportunity to optimize the charging of the thermal storage by varying the flowrate into the storage tank to take advantage of only the peak of solar radiation instead of using a constant flowrate as soon as solar radiation is available until the storage tank is full. This operating strategy required many hours to operate at the defocus state where some of the incident radiation was being wasted. While 200°C was the selected geothermal well temperature, there are locations that can achieve higher temperatures, which would further increase the power produced in the ORC. Solar thermal energy has the capability to be integrated effectively at high temperatures with geothermal energy at suitable locations.

CHAPTER 6: SUMMARY, CONCLUSIONS, AND RECOMMENDATIONS

6.1 Summary

There is an opportunity to hybridize solar and geothermal energy with thermal energy storage to reduce the intermittency of solar energy and improve the low temperature and low efficiency conversion of geothermal energy. In the southwest United States, suitable areas for solar and geothermal energy overlap. There is one solar geothermal hybrid plant in operation in Stillwater, NV. It contains a photovoltaic (PV) array and uses parabolic trough collectors (PTC) to offset the degradation of an organic Rankine cycle (ORC) run by geothermal energy during the day that is affected by the higher ambient temperatures through the air-cooled condenser. In the literature, there are a few simulations of adding solar energy to geothermal energy in a similar configuration. Typically, PTC at relatively low temperatures for solar energy were used to supplement the enthalpy of the geothermal brine or working fluid to improve the system during the day. As far as cycle configurations, innovative configurations were considered with the addition of cooling or heating applications which are limited to the on-site or very local demand of heating and cooling. One hot dry rock configuration used carbon dioxide as the working fluid in the ground, supplemented by a solar power tower (SPT) in a carbon dioxide Brayton cycle. SPT can provide high temperatures that can be combined with a bottoming ORC. This ORC can be run by only geothermal energy when solar energy and thermal storage are not available. Supercritical ORCs as opposed to typical subcritical cycles receive heat at a high pressure in the supercritical range, avoiding typical vaporization at a constant temperature. This creates a better thermal match between the heat source and the ORC working fluid and the ORC has been shown in the literature

80

to achieve higher efficiencies than subcritical configurations. The main objective of this work was to combine high temperature solar energy through SPT with medium temperature geothermal reservoirs using a supercritical ORC to enhance the system.

First, a recuperative ORC was optimized for medium temperature geothermal sources. Twenty environmental fluids were considered with limited global warming potential (GWP) and ozone depleting potential (ODP). Fluids that are not environmentally friendly and are currently being used but are set to be phased out were not considered. Cyclopentane and acetone were the working fluids considered that operated the best at subcritical conditions for the geothermal system. These fluids did not achieve the highest plant efficiencies. The expansion ratio was not limited in this analysis. The condensing temperature was also chosen at a typical value used in ORC analyses in the literature for better comparison. However, later in Chapter 4, the expansion ratio was limited, and the condensing temperature was increased to a suitable value for the selected location of Stillwater, NV. For the optimization of the stand-alone geothermal ORC, cisbutene, isopentane, pentane, R1233zd(E) were optimized at subcritical conditions along with acetone and cyclopentane. This still left the majority of fluids to be optimized at supercritical conditions.

Next, a combined cycle configuration was selected and optimized. A supercritical carbon dioxide (sCO$_2$) recuperative Brayton cycle was used as a topping cycle with a recuperative bottoming organic Rankine cycle. Four main systems were chosen for the analysis: simple and recompression sCO$_2$ cycles with a maximum temperature in the sCO$_2$ of 500 and 800°C. First, the approach pinch between the waste heat stream of the sCO$_2$ cycle and the ORC working fluid was parametrically analyzed for each fluid and optimized. The pressures of both cycles were optimized to maximize the combined cycle efficiency. As supported by the literature, the recompression configurations outperformed the simple ones. However, the ORC was able to achieve higher

81

temperatures and therefore higher efficiencies with the simple sCO_2 cycle. The simple sCO_2 combined cycles were optimized at higher pressure ratios than the recompression cases which will be a factor to consider in the economics of the system.

The optimized combined cycles with various working fluids in the ORC were then integrated with geothermal energy. Three different configurations were considered. The hybrid operation, the geothermal source could be added to the topping cycle in two locations: after compression (preheat) or after recuperation (reheat). The third configuration superheated the ORC fluid directly after the waste heat recovery. This system used the optimized conditions from Chapter 3. Cyclopropane, propylene, and dme were the fluids that performed the best with the additional heat. However, acetone (subcritical ORC) and dme (supercritical ORC) achieved the best hybrid configurations with a recompression topping cycle for maximum temperatures of 500 and 800°C, respectively.

Finally, the best performing hybrid system with a maximum cycle temperature of 500°C was selected for the transient analysis. Acetone performed the best in a subcritical configuration with superheating from the geothermal cycle. Thermal storage was shown to be significant to extend the maximum power generation of the system. The ratio of the mass flow of acetone to the waste heat stream of the sCO_2 cycle was very low, however. The mass flow in the ORC was held constant through the geothermal only operation. Therefore, the ratio of power during geothermal operation to hybrid operation was very low and can be altered by selecting another fluid.

6.2 Recommendations

Although a hydrothermal source was considered in the analysis, other heat transfer fluids can be considered for hot dry rock (HDR). Similarly, the topping cycle can be supplied by other heat sources than solar (i.e. nuclear, waste heat, gas). The combined cycle operating parameters

82

were only optimized for solar energy operation and applied to the hybrid configurations. However, the approach pinch and upper pressure of the bottoming ORC can be further optimized in the geothermal sources. In most cases, a supercritical ORC was shown as optimal in the combined cycle configurations. This was dependent on fluid properties such as the critical point. Acetone, for instance, had one of the best hybrid configurations that resulted in the highest combined cycle efficiency but with a subcritical ORC with its high critical point. Its critical temperature was below the maximum operating temperature considered. Regardless of configuration, the addition of geothermal heat directly to a combined cycle operating on solar energy resulted in efficiencies comparable to the ORC. Therefore, there is an advantage to operating solar and geothermal energy in a hybrid combined cycle. For the hybrid operation, the cost needs to be calculated and optimized. The combined cycles with a simple topping cycle were not as efficient but a simpler configuration may result in lower costs. On the other hand, higher pressure ratios were required with the simple sCO_2 cycles. In addition, the expected demand profile for the area needs to be determined. This will allow thermal storage to be sized correctly and for the appropriate ORC working fluid to be chosen to control the ratio of hybrid power to geothermal only power while reducing the cost.

REFERENCES

[1]   U.S. EIA, 2019, "Annual Energy Outlook 2019 with Projections to 2050," Annu. Energy Outlook 2019 with Proj. to 2050, **44**(8), pp. 1–64.

[2]   Ellabban, O., Abu-Rub, H., and Blaabjerg, F., 2014, "Renewable Energy Resources: Current Status, Future Prospects and Their Enabling Technology," Renew. Sustain. Energy Rev., **39**, pp. 748–764.

[3]   IEA, 2013, *World Energy Outlook 2013*, Paris, France.

[4]   Dincer, I., and Acar, C., 2015, "A Review on Clean Energy Solutions for Better Sustainability," Int. J. Energy Res., **39**(5), pp. 585–606.

[5]   California Independent System Operator, 2016, *California ISO Fast Facts*.

[6]   Dubey, S., Sarvaiya, J. N., and Seshadri, B., 2013, "Temperature Dependent Photovoltaic (PV) Efficiency and Its Effect on PV Production in the World - A Review," Energy Procedia, **33**, pp. 311–321.

[7]   Islam, M. T., Huda, N., Abdullah, A. B., and Saidur, R., 2018, "A Comprehensive Review of State-of-the-Art Concentrating Solar Power (CSP) Technologies: Current Status and Research Trends," Renew. Sustain. Energy Rev., **91**(November 2017), pp. 987–1018.

[8]   Vignarooban, K., Xu, X., Arvay, A., Hsu, K., and Kannan, A. M., 2015, "Heat Transfer Fluids for Concentrating Solar Power Systems - A Review," Appl. Energy, **146**, pp. 383–396.

[9]   Stein, W. H., and Buck, R., 2017, "Advanced Power Cycles for Concentrated Solar Power," Sol. Energy, **152**, pp. 91–105.

[10]   Turchi, C. S., Ma, Z., Neises, T. W., and Wagner, M. J., 2013, "Thermodynamic Study of Advanced Supercritical Carbon Dioxide Power Cycles for Concentrating Solar Power Systems," J. Sol. Energy Eng., **135**(4), p. 041007.

[11]   Yu, S.-C., Chen, L., Zhao, Y., Li, H.-X., and Zhang, X.-R., 2015, "A Brief Review Study of Various Thermodynamic Cycles for High Temperature Power Generation Systems," Energy Convers. Manag., **94**, pp. 68–83.

[12]   Besarati, S. M., and Yogi Goswami, D., 2013, "Analysis of Advanced Supercritical Carbon Dioxide Power Cycles With a Bottoming Cycle for Concentrating Solar Power Applications," J. Sol. Energy Eng., **136**(1), p. 011020.

[13] Smith, M. C., 1983, "A History of Hot Dry Rock Geothermal Energy Systems," J. Volcanol. Geoth. Res., **15**, pp. 1–20.

[14] Hettiarachchi, H. D. M., Golubovic, M., Worek, W. M., and Ikegami, Y., 2007, "Optimum Design Criteria for an Organic Rankine Cycle Using Low-Temperature Geothermal Heat Sources," Energy, **32**(9), pp. 1698–1706.

[15] Peterseim, J. H., White, S., Tadros, A., and Hellwig, U., 2014, "Concentrating Solar Power Hybrid Plants - Enabling Cost Effective Synergies," Renew. Energy, **67**, pp. 178–185.

[16] Dimarzio, G., Angelini, L., Price, W., Chin, C., and Harris, S., 2015, "The Stillwater Triple Hybrid Power Plant: Integrating Geothermal, Solar Photovoltaic and Solar Thermal Power Generation," *Proceedings World Geothermal Congress 2015*, Melbourne, Australia, pp. 1–5.

[17] Zhu, G., and Turchi, C., 2016, "Solar Field Optical Characterization at Stillwater Geothermal/Solar Hybrid Plant," J. Sol. Energy Eng., **139**(3), p. 031002.

[18] Handal, S., Alvarenga, Y., and Recinos, M., 2007, "Geothermal Steam Production by Solar Energy," *Geothermal Resources Council – Annual Meeting of the Geothermal Resources Council*, pp. 503–510.

[19] Alvarenga Y., Handal S., Recinos, M., 2008, "Solar Steam Booster in the Ahuachapan Geothermal Field," *GRC. Transactions*.

[20] Kim, Y. J., Woo, N. S., Jang, S. C., and Choi, J. J., 2013, "Feasibility Study of a Hybrid Renewable Energy System with Geothermal and Solar Heat Sources for Residential Buildings in South Korea," J. Mech. Sci. Technol., **27**(8), pp. 2513–2521.

[21] Lentz, Á., and Almanza, R., 2006, "Parabolic Troughs to Increase the Geothermal Wells Flow Enthalpy," Sol. Energy, **80**(10), pp. 1290–1295.

[22] Lentz, Á., and Almanza, R., 2006, "Solar-Geothermal Hybrid System," Appl. Therm. Eng., **26**(14–15), pp. 1537–1544.

[23] Astolfi, M., Xodo, L., Romano, M. C., and Macchi, E., 2011, "Technical and Economical Analysis of a Solar-Geothermal Hybrid Plant Based on an Organic Rankine Cycle," Geothermics, **40**(1), pp. 58–68.

[24] Forsberg, C. W., 2012, "Gigawatt-Year Geothermal Energy Storage Coupled to Nuclear Reactors and Large Concentrated Solar Thermal Systems," *Proceedings, Thirty-Seventh Workshop on Geothermal Reservoir Engineering*, Stanford, California, p. SGP-TR-194.

[25] Zhou, C., 2014, "Hybridisation of Solar and Geothermal Energy in Both Subcritical and Supercritical Organic Rankine Cycles," Energy Convers. Manag., **81**, pp. 72–82.

[26] Zhou, C., Doroodchi, E., and Moghtaderi, B., 2013, "An In-Depth Assessment of Hybrid Solar–Geothermal Power Generation," Energy Convers. Manag., **74**, pp. 88–101.

[27]   Ghasemi, H., Paci, M., Tizzanini, A., and Mitsos, A., 2013, "Modeling and Optimization of a Binary Geothermal Power Plant," Energy, **50**, pp. 412–428.

[28]   Sakhrieh, A., Shreim, W., Fakhruldeen, H., and Hasan, H., 2016, "Combined Solar-Geothermal Power Generation Using Organic Rankine Cycle," Jordan J. Mech. Ind. Eng., **10**(1), pp. 1–9.

[29]   Cardemil, J. M., Cortés, F., Díaz, A., and Escobar, R., 2016, "Thermodynamic Evaluation of Solar-Geothermal Hybrid Power Plants in Northern Chile," Energy Convers. Manag., **123**, pp. 348–361.

[30]   Cakici, D. M., Erdogan, A., and Colpan, C. O., 2017, "Thermodynamic Performance Assessment of an Integrated Geothermal Powered Supercritical Regenerative Organic Rankine Cycle and Parabolic Trough Solar Collectors," Energy, **120**, pp. 306–319.

[31]   Heberle, F., Hofer, M., Ürlings, N., Schröder, H., Anderlohr, T., and Brüggemann, D., 2017, "Techno-Economic Analysis of a Solar Thermal Retrofit for an Air-Cooled Geothermal Organic Rankine Cycle Power Plant," Renew. Energy, **113**, pp. 494–502.

[32]   Bonyadi, N., Johnson, E., and Baker, D., 2018, "Technoeconomic and Exergy Analysis of a Solar Geothermal Hybrid Electric Power Plant Using a Novel Combined Cycle," Energy Convers. Manag., **156**(December 2017), pp. 542–554.

[33]   Erdogan, A., Colpan, C. O., and Cakici, D. M., 2017, "Thermal Design and Analysis of a Shell and Tube Heat Exchanger Integrating a Geothermal Based Organic Rankine Cycle and Parabolic Trough Solar Collectors," Renew. Energy, **109**, pp. 372–391.

[34]   Mir, I., Escobar, R., Vergara, J., and Bertrand, J., 2011, "Performance Analysis of a Hybrid Solar-Geothermal Power Plant in Northern Chile," Proc. World Renew. Energy Congr. – Sweden, 8–13 May, 2011, Linköping, Sweden, **57**, pp. 1281–1288.

[35]   Boghossian, J. G., 2011, "Dual-Temperature Kalina Cycle for Geothermal-Solar Hybrid Power Systems By," Massachusetts Institute of Technology.

[36]   Greenhut, A. D., Tester, J. W., Dipippo, R., Field, R., Love, C., Nichols, K., Augustine, C., Batini, F., Price, B., Gigliucci, G., and Fastelli, I., 2010, "Solar-Geothermal Hybrid Cycle Analysis for Low Enthalpy Solar and Geothermal Resources," *Proceedings World Geothermal Congress 2010*, Bali, Indonesia, pp. 25–29.

[37]   Greenhut, A. D., 2010, "Modeling and Analysis of Hybrid Geothermal-Solar Thermal Energy Conversion Systems," Massachusetts Institute of Technology.

[38]   Ayub, M., Mitsos, A., and Ghasemi, H., 2015, "Thermo-Economic Analysis of a Hybrid Solar-Binary Geothermal Power Plant," Energy, **87**, pp. 326–335.

[39]   Jiang, P.-X., Zhang, F.-Z., and Xu, R.-N., 2017, "Thermodynamic Analysis of a Solar–Enhanced Geothermal Hybrid Power Plant Using CO2 as Working Fluid," Appl. Therm. Eng., **116**, pp. 463–472.

[40] Bassetti, M. C., Consoli, D., Manente, G., and Lazzaretto, A., 2017, "Design and Off-Design Models of a Hybrid Geothermal-Solar Power Plant Enhanced by a Thermal Storage," Renew. Energy, pp. 1–13.

[41] Al-Nimr, M. A., Bukhari, M., and Mansour, M., 2017, "A Combined CPV/T and ORC Solar Power Generation System Integrated with Geothermal Cooling and Electrolyser/Fuel Cell Storage Unit," Energy, **133**, pp. 513–524.

[42] Al-Ali, M., and Dincer, I., 2014, "Energetic and Exergetic Studies of a Multigenerational Solar-Geothermal System," Appl. Therm. Eng., **71**(1), pp. 16–23.

[43] Tempesti, D., Manfrida, G., and Fiaschi, D., 2012, "Thermodynamic Analysis of Two Micro CHP Systems Operating with Geothermal and Solar Energy," Appl. Energy, **97**, pp. 609–617.

[44] Tempesti, D., and Fiaschi, D., 2013, "Thermo-Economic Assessment of a Micro CHP System Fuelled by Geothermal and Solar Energy," Energy, **58**, pp. 45–51.

[45] Ruzzenenti, F., Bravi, M., Tempesti, D., Salvatici, E., Manfrida, G., and Basosi, R., 2014, "Evaluation of the Environmental Sustainability of a Micro CHP System Fueled by Low-Temperature Geothermal and Solar Energy," Energy Convers. Manag., **78**, pp. 611–616.

[46] Ghosh, S., and Dincer, I., 2014, "Development and Analysis of a New Integrated Solar-Wind-Geothermal Energy System," Sol. Energy, **107**, pp. 728–745.

[47] Todorović, M. S., and Ličina, D. Ž., 2011, "Parametric Analysis and Thermodynamic Limits of Solar Assisted Geothermal Co-and Tri-Generation Systems," *ASHRAE Transactions*, pp. 22–31.

[48] Calise, F., D'Accadia, M. D., MacAluso, A., Piacentino, A., and Vanoli, L., 2016, "Exergetic and Exergoeconomic Analysis of a Novel Hybrid Solar-Geothermal Polygeneration System Producing Energy and Water," Energy Convers. Manag., **115**, pp. 200–220.

[49] Boyaghchi, F. A., Chavoshi, M., and Sabeti, V., 2015, "Optimization of a Novel Combined Cooling, Heating and Power Cycle Driven by Geothermal and Solar Energies Using the Water/CuO (Copper Oxide) Nanofluid," Energy, **91**, pp. 685–699.

[50] Buonomano, A., Calise, F., Palombo, A., and Vicidomini, M., 2015, "Energy and Economic Analysis of Geothermal-Solar Trigeneration Systems: A Case Study for a Hotel Building in Ischia," Appl. Energy, **138**, pp. 224–241.

[51] Bicer, Y., and Dincer, I., 2016, "Development of a New Solar and Geothermal Based Combined System for Hydrogen Production," Sol. Energy, **127**, pp. 269–284.

[52] Islam, S., and Dincer, I., 2017, "Development, Analysis and Performance Assessment of a Combined Solar and Geothermal Energy-Based Integrated System for Multigeneration," Sol. Energy, **147**, pp. 328–343.

[53]   Boyaghchi, F. A., and Chavoshi, M., 2017, "Multi-Criteria Optimization of a Micro Solar-Geothermal CCHP System Applying Water/CuO Nanofluid Based on Exergy, Exergoeconomic and Exergoenvironmental Concepts," Appl. Therm. Eng., **112**, pp. 660–675.

[54]   Tartière, T., and Astolfi, M., 2017, "A World Overview of the Organic Rankine Cycle Market," Energy Procedia, **129**, pp. 2–9.

[55]   INL, 2006, *The Future of Geothermal Energy: Impact of Enhanced Geothermal Systems (EGS) on the United States in the 21st Century*.

[56]   Bertani, R., 2016, "Geothermal Power Generation in the World 2010-2014 Update Report," Geothermics, **60**, pp. 31–43.

[57]   Zarrouk, S. J., and Moon, H., 2014, "Efficiency of Geothermal Power Plants: A Worldwide Review," Geothermics, **51**, pp. 142–153.

[58]   Barbier, E., 2002, "Geothermal Energy Technology and Current Status: An Overview," Renew. Sustain. Energy Rev., **6**(1–2), pp. 3–65.

[59]   Gewald, D., Karellas, S., Schuster, a., and Spliethoff, H., 2012, "Integrated System Approach for Increase of Engine Combined Cycle Efficiency," Energy Convers. Manag., **60**, pp. 36–44.

[60]   Yamada, N., Mohamad, M. N. A., and Kien, T. T., 2012, "Study on Thermal Efficiency of Low- to Medium-Temperature Organic Rankine Cycles Using HFO-1234yf," Renew. Energy, **41**, pp. 368–375.

[61]   Karellas, S., and Schuster, A., 2008, "Supercritical Fluid Parameters in Organic Rankine Cycle Applications," Int. J. Thermodyn., **11**(3), pp. 101–108.

[62]   Yağli, H., Koç, Y., Koç, A., Görgülü, A., and Tandiroğlu, A., 2016, "Parametric Optimization and Exergetic Analysis Comparison of Subcritical and Supercritical Organic Rankine Cycle (ORC) for Biogas Fuelled Combined Heat and Power (CHP) Engine Exhaust Gas Waste Heat," Energy, **111**, pp. 923–932.

[63]   Chen, H., Goswami, D. Y., Rahman, M. M., and Stefanakos, E. K., 2011, "A Supercritical Rankine Cycle Using Zeotropic Mixture Working Fluids for the Conversion of Low-Grade Heat into Power," Energy, **36**(1), pp. 549–555.

[64]   Li, C., Besarati, S., Goswami, Y., Stefanakos, E., and Chen, H., 2013, "Reverse Osmosis Desalination Driven by Low Temperature Supercritical Organic Rankine Cycle," Appl. Energy, **102**, pp. 1071–1080.

[65]   Glover, S., Douglas, R., De Rosa, M., Zhang, X., and Glover, L., 2015, "Simulation of a Multiple Heat Source Supercritical ORC (Organic Rankine Cycle) for Vehicle Waste Heat Recovery," Energy, **93**, pp. 1568–1580.

[66] Le, V. L., Feidt, M., Kheiri, A., and Pelloux-Prayer, S., 2014, "Performance Optimization of Low-Temperature Power Generation by Supercritical ORCs (Organic Rankine Cycles) Using Low GWP (Global Warming Potential) Working Fluids," Energy, **67**, pp. 513–526.

[67] Toffolo, A., Lazzaretto, A., Manente, G., and Paci, M., 2014, "A Multi-Criteria Approach for the Optimal Selection of Working Fluid and Design Parameters in Organic Rankine Cycle Systems," Appl. Energy, **121**, pp. 219–232.

[68] Astolfi, M., Romano, M. C., Bombarda, P., and Macchi, E., 2014, "Binary ORC (Organic Rankine Cycles) Power Plants for the Exploitation of Medium-Low Temperature Geothermal Sources - Part B: Techno-Economic Optimization," Energy, **66**, pp. 435–446.

[69] Moloney, F., Almatrafi, E., and Goswami, D. Y., 2018, "Working Fluid Parametric Analysis for Recuperative Supercritical Organic Rankine Cycles for Medium Geothermal Reservoir Temperatures," Renew. Energy.

[70] Moloney, F., Almatrafi, E., and Goswami, D. Y., 2017, "Working Fluid Parametric Analysis for Regenerative Supercritical Organic Rankine Cycles for Medium Geothermal Reservoir Temperatures," *Energy Procedia*, Elsevier, pp. 599–606.

[71] Wang, Y.-N., Goh, K., Li, X., Setiawan, L., and Wang, R., 2017, "Membranes and Processes for Forward Osmosis-Based Desalination: Recent Advances and Future Prospects," Desalination, (June), pp. 0–1.

[72] The European Union, 2015, *Guidance for Mobile Air Conditioning (MAC) Sectors Guidance: F Gas and Ozone Regulations*.

[73] Lemmon, E. W., Huber, M. L., and McLinden, M. O., 2013, "NIST Standard Reference Database 23: Reference Fluid Thermodynamic and Transport Properties-REFPROP."

[74] Chaczykowski, M., 2016, "Organic Rankine Cycle for Residual Heat to Power Conversion in Natural Gas Compressor Station. Part I: Modelling and Optimisation Framework," Arch. Min. Sci., **61**(2), pp. 259–274.

[75] Vijayaraghavan, S., and Goswami, D. Y., 2003, "On Evaluating Efficiency of a Combined Power and Cooling Cycle," J. Energy Resour. Technol., **125**(3), p. 221.

[76] Franco, A., and Russo, A., 2002, "Combined Cycle Plant Efficiency Increase Based on the Optimization of the Heat Recovery Steam Generator Operating Parameters," Int. J. Therm. Sci., **41**(9), pp. 843–859.

[77] Yari, M., 2010, "Exergetic Analysis of Various Types of Geothermal Power Plants," Renew. Energy, **35**(1), pp. 112–121.

[78] Goswami, D. Y., Hingorani, S., and Mines, G., 1991, "A Laser-Based Technique for Particle Sizing to Study Two-Phase Expansion in Turbines," J. Sol. Energy Eng., **113**(3), p. 211.

[79] Vidhi, R., Goswami, D. Y., Chen, H., Stefanakos, E., Kuravi, S., and Sabau, A. S., 2011, "Study of Supercritical Carbon Dioxide Power Cycle for Low Grade Heat Conversion," Proc. SCO2 Power Cycle Symp., pp. 0–7.

[80] Chen, H., Goswami, D. Y., and Stefanakos, E. K., 2010, "A Review of Thermodynamic Cycles and Working Fluids for the Conversion of Low-Grade Heat," Renew. Sustain. Energy Rev., **14**(9), pp. 3059–3067.

[81] Dickes, R., 2013, "Design and Fabrication of a Variable Wall Thickness Two-Stage Scroll Expander to Be Integrated in a Micro-Solar Power Plant," University of Liege.

[82] Pacheco, J. E., Moursund, C., Rogers, D., and Wasyluk, D., 2011, "Conceptual Design of a 100 MWe Modular Molten Salt Power Tower Plant," *Eurosun 2006*, p. No. DOE/EE0003595-1.

[83] Dunham, M. T., and Iverson, B. D., 2014, "High-Efficiency Thermodynamic Power Cycles for Concentrated Solar Power Systems," Renew. Sustain. Energy Rev., **30**, pp. 758–770.

[84] Singer, C., Buck, R., Pitz-Paal, R., and Müller-Steinhagen, H., 2010, "Assessment of Solar Power Tower Driven Ultrasupercritical Steam Cycles Applying Tubular Central Receivers With Varied Heat Transfer Media," J. Sol. Energy Eng., **132**(4), p. 041010.

[85] Wang, K., He, Y. L., and Zhu, H. H., 2017, "Integration between Supercritical CO2 Brayton Cycles and Molten Salt Solar Power Towers: A Review and a Comprehensive Comparison of Different Cycle Layouts," Appl. Energy, **195**, pp. 819–836.

[86] Di Maio, D. V., Boccitto, A., and Caruso, G., 2015, "Supercritical Carbon Dioxide Applications for Energy Conversion Systems," Energy Procedia, **82**, pp. 819–824.

[87] Al-Sulaiman, F. A., and Atif, M., 2015, "Performance Comparison of Different Supercritical Carbon Dioxide Brayton Cycles Integrated with a Solar Power Tower," Energy, **82**, pp. 61–71.

[88] Neises, T., and Turchi, C., 2013, "A Comparison of Supercritical Carbon Dioxide Power Cycle Configurations with an Emphasis on CSP Applications," Energy Procedia, **49**, pp. 1187–1196.

[89] Padilla, R. V., Benito, R. G., and Stein, W., 2015, "An Exergy Analysis of Recompression Supercritical CO2 Cycles with and without Reheating," Energy Procedia, **69**, pp. 1181–1191.

[90] Iverson, B. D., Conboy, T. M., Pasch, J. J., and Kruizenga, A. M., 2013, "Supercritical CO2 Brayton Cycles for Solar-Thermal Energy," Appl. Energy, **111**, pp. 957–970.

[91] Forsberg, C. W., Peterson, P. F., and Zhao, H., 2007, "High-Temperature Liquid-Fluoride-Salt Closed-Brayton-Cycle Solar Power Towers," J. Sol. Energy Eng., **129**(2), p. 141.

90

[92] Mabrouk, M. T., Kheiri, A., and Feidt, M., 2018, "A Systematic Procedure to Optimize Integrated Solar Combined Cycle Power Plants (ISCCs)," Appl. Therm. Eng., **136**(March), pp. 97–107.

[93] Buck, R., Tellez, F., Pfänder, M., Bräuning, T., Schwarzbözl, P., and Denk, T., 2002, "Solar-Hybrid Gas Turbine-Based Power Tower Systems (REFOS)," J. Sol. Energy Eng., **124**(1), p. 2.

[94] Kribus, A., Zaibel, R., Carey, D., Segal, A., and Karni, J., 1998, "A Solar-Driven Combined Cycle Power Plant," Sol. Energy, **62**(2), pp. 121–129.

[95] The MathWorks Inc., 2017, "MATLAB."

[96] NIST, 2007, "REFPROP: Reference Fluid Thermodynamic and Transport Properties," Natl. Inst. Stand. Technol., **NIST Stand**.

[97] Sarkar, J., 2009, "Second Law Analysis of Supercritical CO2 Recompression Brayton Cycle," Energy, **34**(9), pp. 1172–1178.

[98] Wagner, M. J., and Kutscher, C., 2011, "The Impact of Hybrid Wet/Dry Cooling on Concentrating Solar Power Plant Performance," *ASME 2010 4th International Conference on Energy Sustainability, Volume 2*, ASME, pp. 675–682.

[99] Besarati, S. M., 2014, "Analysis of Advanced Supercritical Carbon Dioxide Power Cycles for Concentrated Solar Power Applications," University of South Florida Graduate Theses and Dissertations.

[100] Branchini, L., De Pascale, A., and Peretto, A., 2013, "Systematic Comparison of ORC Configurations by Means of Comprehensive Performance Indexes," Appl. Therm. Eng., **61**(2), pp. 129–140.

[101] Ghasemi, H., Sheu, E., Tizzanini, A., Paci, M., and Mitsos, A., 2014, "Hybrid Solar–Geothermal Power Generation: Optimal Retrofitting," Appl. Energy, **131**, pp. 158–170.

[102] Burgaleta, J. I., Arias, S., and Ramirez, D., 2011, "Gemasolar: The First Tower Thermosolar Commercial Plant with Molten Salt Storage System," SolarPACES Int. Conf., (September), pp. 20–23.

[103] Amadei, C. A., Allesina, G., Tartarini, P., and Yuting, W., 2013, "Simulation of GEMASOLAR-Based Solar Tower Plants for the Chinese Energy Market: Influence of Plant Downsizing and Location Change," Renew. Energy, **55**, pp. 366–373.

[104] Astolfi, M., Binotti, M., Mazzola, S., Zanellato, L., and Manzolini, G., 2017, "Heliostat Aiming Point Optimization for External Tower Receiver," Sol. Energy, **157**, pp. 1114–1129.

[105] Boerema, N., Morrison, G., Taylor, R., and Rosengarten, G., 2012, "Liquid Sodium versus Hitec as a Heat Transfer Fluid in Solar Thermal Central Receiver Systems," Sol. Energy, **86**(9), pp. 2293–2305.

[106] NREL, 2016, "National Renewable Energy Lab Geospatial Data Science Maps" [Online]. Available: https://www.nrel.gov/gis/maps.html. [Accessed: 15-Apr-2019].

[107] Blackwell, D., Richards, M., Frone, Z., Batir, J., Williams, M., Ruzo, A., and Dingwall, R., 2011, "SMU Geothermal Laboratory Heat Flow Map of the Conterminous United States," Support. by Google.org [Online]. Available: http://www.smu.edu/geothermal. [Accessed: 15-Apr-2019].

[108] Astolfi, M., Romano, M. C., Bombarda, P., and Macchi, E., 2014, "Binary ORC (Organic Rankine Cycles) Power Plants for the Exploitation of Medium-Low Temperature Geothermal Sources - Part A: Techno-Economic Optimization," Energy, **66**, pp. 435–446.

APPENDIX A: LIST OF SYMBOLS

A.1 Acronyms

CC   combined cycle
CFC   chlorofluorocarbons
CHP   combined heating and power
CSP   concentrating solar power
GWP   global warming potential
HC   hydrocarbons
HCFC   hydrochlorofluorocarbons
HDR   hot dry rock
HFC   hydrofluorocarbons
HFO   hydrofluoroolefins
HTF   heat transfer fluid
HTR   high temperature recuperator
IHE   internal heat exchanger
LCOE   levelized cost of electricity
LTR   low temperature recuperator
MC   main compressor
ODP   ozone depleting potential
ORC   organic Rankine cycle
PHE   primary heat exchanger
PTC   parabolic trough collectors
PV   photovoltaic
RC   recompressor
sCO2   supercritical carbon dioxide
SPT   solar power tower
TES   thermal energy storage

A.2 Variables

A.2.1 Greek Letters

ε   effectiveness
η   efficiency

A.2.2 General

$\dot{E}x$ rate of exergy (kW)

93

$\dot{I}$	exergy destruction (kW)
$\dot{m}$	mass flow (kg/s)
$\dot{Q}$	rate of heat (kW)
$\dot{W}$	power (kW)
x_{fr}	split fraction
h	specific enthalpy (kJ/kg)
s	entropy (kJ/kg)
T	temperature (K)

A.2.3 Subscripts

c	condenser
CC	combined cycle
f	flash
hr	heat rejection
hs	heat source
HTR	hot temperature recuperator
I	first law
II	second law
inc	incremental
m	mechanical
mc	main compressor
o	dead state
ORC	organic Rankine cycle
p	pump
rc	recompressor
s	isentropic
t	turbine
WF	working fluid

APPENDIX B: COPYRIGHT PERMISSIONS

The permission to reuse the published article that contributes to most of Chapter 2, apart from minor changes and an additional section, is shown in the figure below.

Copyright Clearance Center – RightsLink®

Home | Create Account | Help

Title: Working fluid parametric analysis for recuperative supercritical organic Rankine cycles for medium geothermal reservoir temperatures

Author: Francesca Moloney, Eydhah Almatrafi, D.Y. Goswami

Publication: Renewable Energy

Publisher: Elsevier

Date: Available online 10 September 2018

© 2018 Elsevier Ltd. All rights reserved.

LOGIN

If you're a copyright.com user, you can login to RightsLink using your copyright.com credentials.

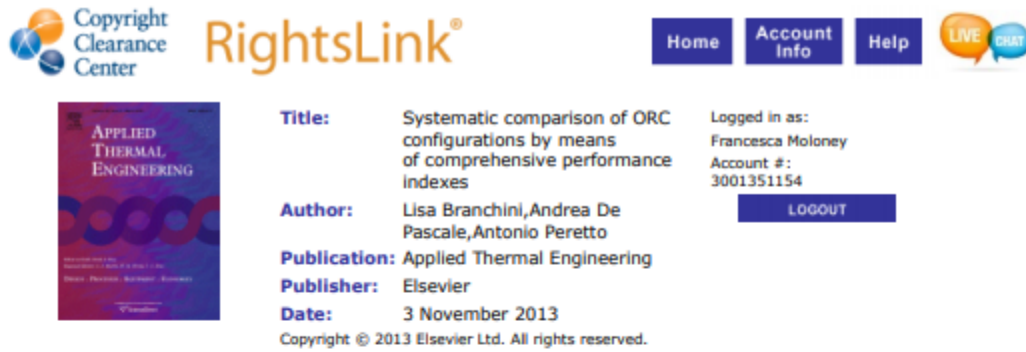Already a RightsLink user or want to learn more?

Please note that, as the author of this Elsevier article, you retain the right to include it in a thesis or dissertation, provided it is not published commercially. Permission is not required, but please ensure that you reference the journal as the original source. For more information on this and on your other retained rights, please visit: https://www.elsevier.com/about/our-business/policies/copyright#Author-rights

BACK | CLOSE WINDOW

The permission to reuse Figure 3-5 from Branchini et al. [100] is shown below.

Copyright Clearance Center **RightsLink®**

Home | Account Info | Help | LIVE CHAT

APPLIED THERMAL ENGINEERING

Title: Systematic comparison of ORC configurations by means of comprehensive performance indexes

Author: Lisa Branchini,Andrea De Pascale,Antonio Peretto

Publication: Applied Thermal Engineering

Publisher: Elsevier

Date: 3 November 2013

Copyright © 2013 Elsevier Ltd. All rights reserved.

Logged in as:
Francesca Moloney
Account #:
3001351154

LOGOUT

Order Completed

Thank you for your order.

This Agreement between Francesca Moloney ("You") and Elsevier ("Elsevier") consists of your license details and the terms and conditions provided by Elsevier and Copyright Clearance Center.

Your confirmation email will contain your order number for future reference.

printable details

License Number	4616450771730
License date	Jun 26, 2019
Licensed Content Publisher	Elsevier
Licensed Content Publication	Applied Thermal Engineering
Licensed Content Title	Systematic comparison of ORC configurations by means of comprehensive performance indexes
Licensed Content Author	Lisa Branchini,Andrea De Pascale,Antonio Peretto
Licensed Content Date	Nov 3, 2013
Licensed Content Volume	61
Licensed Content Issue	2
Licensed Content Pages	12
Type of Use	reuse in a thesis/dissertation
Portion	figures/tables/illustrations
Number of figures/tables/illustrations	1
Format	both print and electronic
Are you the author of this Elsevier article?	No
Will you be translating?	No
Original figure numbers	Fig. 6
Title of your thesis/dissertation	Solar Thermal Geothermal Hybrid System With a Bottoming Supercritical Organic Rankine Cycle
Expected completion date	Aug 2019
Estimated size (number of pages)	110

www.manaraa.com